Field reversed configurations

1988 Nucl. Fusion 28 2033

(http://iopscience.iop.org/0029-5515/28/11/008)

REVIEW PAPER

FIELD REVERSED CONFIGURATIONS

M. TUSZEWSKI
Los Alamos National Laboratory,
University of California,
Los Alamos, New Mexico,
United States of America

ABSTRACT. The review is devoted to field reversed configurations and to the related field reversed mirrors; both are compact toroids with little or no toroidal magnetic field. Experimental and theoretical results on the formation, equilibrium, stability and confinement properties of these plasmas are presented. Although they have been known for about three decades, field reversed configurations have been studied intensively only in recent years. This renewed interest is due to the unusual fusion reactor potential of these high beta plasmas and also to their surprising macroscopic stability. At the present time, field reversed configurations appear to be completely free of gross instabilities and show relatively good confinement. The primary research goal for the near future is to retain these favourable properties in a less kinetic regime. Other important issues include the development of techniques for slow formation and stability, and a clearer assessment of the confinement scaling laws.

1. INTRODUCTION

1.1. Scope and outline of the review

The idea of using magnetic fields from a plasma to help confine this plasma or another one goes back to the earliest days of magnetic fusion research [1–4]. Numerous means have been found to create field reversed plasma states. A common feature is that, although these magnetic field configurations are closed systems, neither coils nor other objects link the plasma toroids. This property led recently [5, 6] to referring to such plasmas as compact toroids or CTs in short. CT plasma configurations generally offer an unusual fusion reactor potential because of their compact geometries and high plasma betas. Accordingly, worldwide, CT research has significantly increased in recent years and remarkable progress has been achieved.

The principal members of the CT family are classified in Table I according to the ratio s of torus minor radius to average ion gyroradius, and also according to the relative magnitudes of their poloidal (B) and toroidal (B_θ) internal magnetic fields. In the more MHD-like ($s > 1$) branch of the CT family, one

TABLE I. THE COMPACT TOROID FAMILY

	s > 1	s < 1
$B \gg B_\theta$	Field reversed configuration (FRC)	
	Field reversed mirror (FRM)	Astron
$B \sim B_\theta$	Spheromak	

distinguishes the field reversed configurations (FRC) with $B \gg B_\theta$ from the spheromaks, which have $B \sim B_\theta$, and from the field reversed mirrors (FRM), which can have either $B \gg B_\theta$ or $B \sim B_\theta$. The scope of this review is mostly FRC research, but it also includes some closely related FRM studies with $B \gg B_\theta$. Spheromaks [1] are the subject of a separate review [7]. Astrons [2] consist of axis encircling ($s < 1$) high energy particles that create a diamagnetic current shell in a magnetic mirror field. They have been recently reviewed by Finn and Sudan [8] and are considered here only as a possible stabilization ingredient when mixed with FRCs.

The FRC is an elongated prolate compact toroid (Fig. 1) that is formed without toroidal field. As seen from Fig. 1, the FRC consists of two distinct regions: a closed-field-line torus inside the separatrix and an open-field-line sheath outside the separatrix. Such plasma configurations appear to have been discovered by accident in the early days of theta pinch research [3, 4], when a bias field was applied in the reversed direction compared with that of the main magnetic field. Accordingly, these configurations have long been known as field reversed theta pinches. In recent years, these plasmas have been named field reversed configurations, an appellation that has gradually gained general acceptance. The intent was to dissociate this plasma configuration from the particular method by which it was formed, recognizing that such toroids could be formed by technical means other than the field reversed theta pinch method. Indeed, FRC formation has been initiated by using either rotating magnetic fields [9] or a coaxial geometry [10]. Conversely, theta pinches with reversed bias magnetic fields have been used to form spheromaks, either by a combination of axial and azimuthal currents [11, 12] or with strongly conical coils [13]. However, the vast majority of the FRC research reviewed here involves theta pinch formation.

In the FRM approach, a CT is formed and sustained by neutral beam injection in a magnetic mirror [14]. Such experiments with $B \gg B_\theta$ have been carried out previously [15], but field reversal was probably not achieved. Later experimental plans have been mostly concerned with spheromaks [16]. The FRM research was reviewed some time ago by Gormezano [17]. Since then, there have been a number of theoretical studies relevant to FRC research; these are included in this review. Possible future directions for FRC research include slow formation and/or sustainment by neutral beam injection [18]. This illustrates the close relationship between FRC and FRM concepts. A field reversed theta pinch has always been regarded as a possible initial source for an FRM, thereby removing the dependence on field reversal by beam injection alone.

This review is organized as follows: The remaining part of the Introduction presents the status of FRC research, its significant reactor potential and its interesting history, which spans thirty years. Sections 2–5 follow the conventional ordering of formation, equilibrium, stability and confinement. In Section 2, the techniques of FRC formation are first presented, followed by the physics of field line connection,

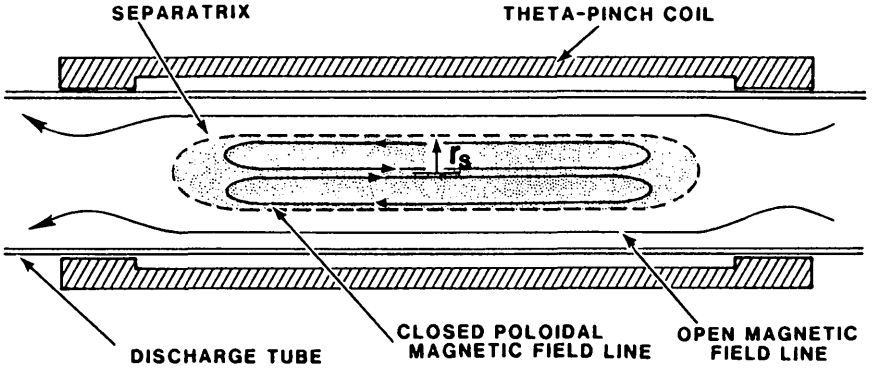

FIG. 1. The field reversed configuration (FRC).

heating and flux trapping. Section 3 begins with a theoretical presentation of FRC equilibria; this is then compared with experimental data. Two ways of modifying equilibria are then discussed: compression and translation. The status of FRC stability is described in Section 4. The various modes predicted theoretically are surveyed, including the now seldom observed tearing instabilities. The substantial work devoted to rotational modes is summarized and the section finishes with a theoretical presentation of tilt instabilities — perhaps the most dangerous modes predicted so far. Section 5 describes the limited present confinement knowledge. Transport mechanisms are first discussed, followed by experimental and theoretical techniques and then by results concerning particle, internal magnetic flux and energy losses.

The reader unfamiliar with CTs in general and FRCs in particular should benefit from the January 1986 issue of Fusion Technology devoted to these plasmas and also from an earlier summary of FRC research [19]. The present review includes many different aspects of FRC and related research, somewhat superficially by necessity. Numerous references are provided to guide the reader towards more detailed descriptions. A list of symbols and acronyms is provided at the end of this review; the reader should refer to it whenever needed, since symbols and acronyms are often defined only once.

1.2. Status of FRC research

1.2.1. Technical achievements

FRC research is actively pursued in the USA, Japan and the USSR, with smaller programmes in Australia, Western Europe, South America and China. Remarkable progress has occurred in recent FRC experiments, resulting in plasmas with good confinement and without gross instabilities.

(a) Values of $n\tau_E \sim 4 \times 10^{11}$ cm^{-3}·s at $T_i = 100$ eV and $n \sim 5 \times 10^{15}$ cm^{-3} have been achieved in the FRX-C device [20]. During translation on the same experiment, values of $n\tau_E \gtrsim 10^{11}$ cm^{-3} at $T_i = 700$ eV and $n \sim 10^{15}$ cm^{-3} have also been obtained [21]. These results were for plasmas with a major radius of only about 7 cm.

(b) The n = 2 rotational instability has been eliminated by application of weak multipole fields after FRC formation [22, 23, 20]. This is particularly significant since it is the only global mode observed experimentally, and it often prematurely terminates the FRC.

(c) Efficient FRC translation has been demonstrated [24–26]. This is one of the most appealing attributes of CTs and, under a number of conditions, FRC translation and trapping has been accomplished without any confinement degradation.

(d) Significant advances in FRC formation have been made: programmed formation has led to improved FRC behaviour [27, 28], and slow formation studies [10] have been initiated that could eventually result in a more attractive technology.

Several important theoretical results have also been recently obtained.

(e) The kinetic theory of the tilt mode [29] is the first promising reconciliation of the observed FRC gross stability with its obviously MHD unstable Z-pinch magnetic field topology.

(f) Two-dimensional MHD numerical work has proved extremely useful in the understanding of FRC equilibrium [30–34] and of FRC formation and translation [35, 36, 26].

1.2.2. Critical issues

At the present time, a number of important FRC research issues have emerged for future investigation:

(a) Gross FRC stability is a major issue, in which kinetic effects, elongation, profile effects and rotation may all play some role. A key parameter for stability (and confinement) is s, the approximate number of ion gyroradii between the field null and the separatrix (the FRC minor radius) [28]. Till now, nearly all FRC experiments have been limited to $s \lesssim 2$, while $s \sim 20$–40 might be required for FRC reactors that use D-T fuel [37, 38]. Preliminary results [29] from a kinetic theory of the tilt mode predict a grossly stable behaviour for present experiments with $s \lesssim 2$ but also a gradual transition to observable unstability for $s > 3$. Hence, the understanding of kinetic and other effects on FRC stability is crucial. The LSX (Large s Experiment) device [39] has been designed to produce FRCs with $s \sim 8$ and to address this issue.

(b) The scaling of FRC confinement as s increases is also a key issue. In present experiments, the determination (and extrapolation) of FRC confinement is highly uncertain. Although typical FRCs exist in a quasi-static equilibrium, they are hardly in a steady state. The configuration lifetimes exceed the Alfvén transit times by at most a factor of 100. Moreover, lifetimes are strongly influenced by formation details [40, 41]. In addition, the intrinsic (closed lines) FRC

confinement is obscured by the edge layer [28]. Increasing s should result in increased plasma lifetime and reduced pressure on the separatrix, thereby allowing a much clearer assessment of FRC confinement properties.

(c) The development of new FRC formation methods is an important issue that is just beginning to be addressed [10]. Slow FRC formation (on resistive rather than the present Alfvén time-scales) leads to a more attractive technology for future FRC sources. Such new techniques may be required to successfully form large-s FRCs (a prerequisite to address issues (a) and (b)) if FRC formation continues to prove increasingly difficult in large-size devices [41].

(d) The studies of thermal conduction and internal flux losses are also important issues for future investigation. There is evidence for some anomalous electron thermal conduction in present FRC experiments and the classical $T_e^{3/2}$ dependence of internal flux decay time is not observed [20]. These observations point to the need for studies of longer lived and higher T_e FRCs. Such plasmas may be produced in future adiabatic compression experiments in the FRX-C/LSM device [42].

1.3. Reactor potential

1.3.1. Reactor advantages

FRCs share with other CTs several significant advantages over most toroidal magnetic confinement concepts; these advantages give promise for the development to an economic fusion reactor system.

(a) CTs allow for a simple cylindrical geometry of the magnet coils, vacuum chamber and blanket and, therefore, for less engineering complexity than systems with complete toroidal symmetry.

(b) The high plasma beta and power density result in systems of potentially small size and unit output power. Furthermore, the necessary successive stages of development can be undertaken without prohibitive financial investment.

(c) The FRC plasma is readily translatable along a cylinder by means of a weak gradient in a solenoidal field. This property permits more efficient adiabatic compression heating and a physical separation of the high technology formation from the burn and quench chambers.

(d) The edge layer structure results in a natural divertor that deposits exhaust plasma conveniently at the ends of a cylindrical system and may perhaps permit direct conversion [18].

In addition, FRCs offer an advantage unique among CTs:

(e) FRCs are among the configurations having the highest plasma beta of all magnetically confined plasmas (volume averaged beta values between 0.5 and 1). This makes the FRC an ideal candidate for possible use of advanced fuels [18].

Clearly, these reactor advantages are only potential, and the usefulness of the FRC as a possible fusion reactor will be determined by its stability and confinement properties [43], which are poorly known at the present time. However, the promise of these very favourable reactor features justifies in itself the ongoing FRC physics research.

1.3.2. Reactor studies

Several FRC reactor studies have been made in recent years. Even though the physics basis of FRCs is the most developed among CTs and has been incorporated in some detail in several reactor designs, these studies remain mostly conceptual. A qualitative description of three categories of reactor concepts is given here: pulsed/translating, pulsed/stationary and steady state.

Pulsed/translating studies exploit all the advantages of FRCs listed above and are the most detailed. They are inspired by the Ion Ring Compressor work of Fleischmann and Kammash [44]. The first such study was CTOR [37], for which Fig. 2 illustrates schematically the separation of functions mentioned previously.

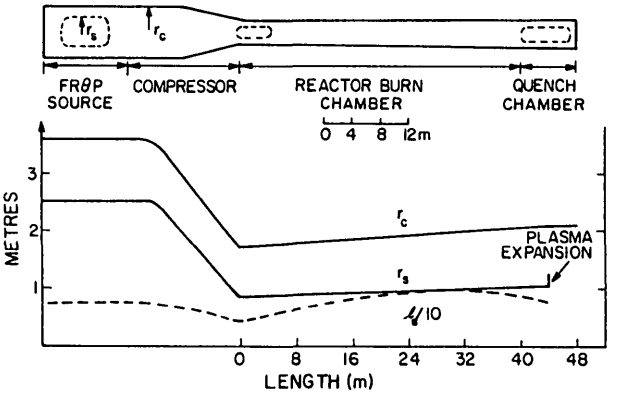

FIG. 2. CTOR: a pulsed, FRC reactor concept based on translation [37].

The FRC is formed in a field reversed theta pinch and heated to ignition by adiabatic compression before injection into and translation through a slightly tapered linear burn chamber that may include liquid metal blankets [45]. The FRC motion terminates in a quench chamber where expansion directly converts internal plasma energy to electrical energy. Recently, the FIREBIRD design [38] extended the CTOR study by incorporating into the physics model the most recent theoretical and experimental confinement results. Both the CTOR and the FIREBIRD studies suggest that attractive FRC reactor designs are possible with burn chamber lengths of 40–100 m and net electrical power of 300–1000 MW(e), depending on the assumed confinement physics. The required FRCs could be formed with as low as 100 MJ plasma energy and values of s in the range of 15–40. Another pulsed reactor concept based on a translating FRC is a medium speed liner (liner velocities around 10^3 m·s^{-1}) that is well separated from the plasma source. This approach is being pursued by Kurtmullaev and co-workers [24] and has also received some attention at Los Alamos [46].

Pulsed/stationary concepts do not take advantage of the FRC translation capability; instead, they aim at smaller reactor size and the associated reduced financial risk. The TRACT approach [47, 48] incorporates the programmed formation techniques and substantial axial shock heating as demonstrated in a small device [5]. Units 9 m in height and 6 m in diameter, producing as little as 10 MW net electrical power, have been identified [48]. FRCs have been considered for the slowly imploding liner (LINUS) reactor concept [49–52]. Such concepts envisage the non-destructive, repetitive and reversible implosion of a liquid metal liner onto FRCs. Details may be found in a comparative reactor study [53] which also includes TRACT and CTOR. The reversed field multiple mirror concept [54] combines the favourable aspects of FRCs and multiple mirrors [55], a symbiosis possibly superior to each concept alone. This approach eliminates the need for strong external mirrors and takes advantage of possible non-adiabatic scattering [56] and improved edge layer confinement [57]. An experiment was proposed [58] but not built, and some related formation studies in the HBQM device have been performed [59]. Finally, the PULSATOR concept has been recently proposed [60]. In this quasi-stationary FRC reactor operating mode, plasmoids are injected and merged, to provide fuelling and magnetic flux sustainment.

Although a detailed steady state FRC reactor study has yet to be made, there is a growing interest in the FRC/FRM international community in that direction. The main motivation is the eventual use of deuterium based advanced fuel cycles. Following the initial SAFFIRE study [61], Miley [62] proposed an experiment that could lead to an advanced fuel FRC reactor. The possibility of sustaining an FRC in steady state via neutral beam injection was also considered by Hirano [63–65]. Finally, a recent workshop at Nagoya [18] reflected the growing interest in advanced fuelled FRCs. The use of D–^{3}He fusion fuels in an FRC may present several advantages over the use of D–T fuel, such as reduction in wall loading, plasma current sustainment by fusion charged particles [66] and operation at possibly reduced s-values (approximately 10 instead of 20–40). The transition from D–T to D–^{3}He fusion burn has also been studied [60, 67]. An important ingredient in steady state FRC reactor studies might be neutral beam injection: it offers several new opportunities for FRCs, such as rotational control [62, 68], fuelling and heating [62], magnetic flux sustainment [63, 18] and stabilization [69]. Such (possibly simultaneous) potential benefits may prove quite valuable for future FRC/FRM research [70].

1.4. History of FRC research

Field reversed theta pinch experiments have been performed in different laboratories since 1958. Most theta pinch experiments have devoted part of their effort to operation with a reversed magnetic field. The principal FRC experiments are listed in Table II, showing the evolution of the experimental characteristics and main physics issues from the earliest days to the near future. The detailed results from the experiments in Table II, as well as from other experiments that have provided important contributions to the FRC community, are mentioned later in the more technical sections of this review. For each device, Table II lists the coil length ℓ_c and inner the diameter d_c, the maximum magnetic field B_M, the fill pressure p_0 and the configuration lifetime τ_ℓ. The main studies with each device are also listed, with a reference number for the listed parameters. The experiments are ordered chronologically according to the year of the quoted reference.

The experiments of Table II are separated into three categories (early, intermediate and modern), showing a progressive evolution to lower radial compression. Most experiments have used values of reversed bias magnetic field of a few kilogauss. However, the early experiments had large values of B_M that resulted in highly compressed plasmas with values of x_s (ratio of separatrix radius to coil radius) in the range of

TABLE II. THE PRINCIPAL FRC EXPERIMENTS

Year	Device	Laboratory	ℓ_c (cm)	d_c	B_M (kG)	p_0 (mtorr)	τ_t (μs)	Main studies	Ref.
(A) Early experiments									
59	—	NRL	10	6	100	100	2	Annihilation	[3]
61	Scylla I	LASL	11	5	55	85	3	Annihilation	[78]
62	Scylla III	LASL	19	8	125	85	4	Rotation	[79]
62	Thetatron	Culham	21	5	86	100	3	Contraction	[87]
62	—	Jülich	10	4	60	230	1	Formation, tearing	[93]
63	—	Culham	30	10	50	50	6	Contraction	[89]
64	θ-P II	Garching	30	5	53	100	1	Tearing, contraction	[99]
(B) Intermediate experiments									
65	Pharos	NRL	180	17	30	60	30	Confinement, rotation	[104]
67	Centaur	Culham	50	19	21	20	15	Confinement, rotation	[110]
67	Julietta	Jülich	128	11	27	50	15	Tearing	[111]
71	E-G	Garching	70	11	28	50	25	Tearing, rotation	[115]
(C) Modern experiments									
75	BN[ab]	Kurchatov	90	21	4.5	2-8	50	Formation	[128]
79	TOR[ab]	Kurchatov	150	30	10	2-5	100	Formation	[5]
79	FRX-A	LASL	100	25	6	4-7	30	Confinement	[130]
81	FRX-B	LANL	100	25	13	9-49	60	Confinement	[19]
82	STP-L	Nagoya	150	12	10	9	30	Rotation	[329]
82	NUCTE	Nihon	200	16	10		60	Confinement, rotation	[325]
82	PIACE	Osaka	100	15	14		60[c]	Rotation	[22]
83	FRX-C[b]	LANL	200	50	8	5-20	300[c]	Confinement	[143]
84	TRX-1[a]	MSNW	100	25	10	5-15	150[c]	Formation, confinement	[28]
84	CTTX	Penn S U	50	12	4	100	40	Confinement	[412]
85	HBQM[a]	U Wash	300	22	5	4-7	30	Formation	[59]
86	OCT[ab]	Osaka	60	22	10		130[c]	Confinement	[25]
86	TRX-2[a]	STI	100	24	13	3-20	100[c]	Formation, confinement	[142]
87	CSS	U Wash	100	45	3	10-60	60	Slow formation	[10]
88	FRXC/LSM[ab]	LANL	200	70	6	2-10	450[c]	Formation, confinement	[411]
90	LSX[a]	STI	500	90	8	2-5		Stability, confinement	[39]

[a] Non-tearing formation.
[b] Translation capability.
[c] Multipole stabilization.

0.2-0.3. Small dimensions and high fill pressures also characterized these early devices, resulting in densities of $n \sim (1\text{-}5) \times 10^{17}$ cm^{-3} and lifetimes τ_t of a few microseconds. Later, the intermediate experiments initiated a trend towards lower compression, with values of $B_M \sim 20\text{-}30$ kG and $x_s \sim 0.3\text{-}0.4$.

Larger dimensions and lower fill pressures yielded $n \sim (1\text{-}5) \times 10^{16}$ cm^{-3} and τ_t of a few tens of microseconds. The modern experiments extended this trend, with typical values of $x_s \sim 0.4\text{-}0.5$, $n \sim (1\text{-}5) \times 10^{15}$ cm^{-3} and τ_t of up to a few hundreds of microseconds. Somewhat lower plasma temperatures

resulted from this evolution. Typical temperatures in modern experiments are $T_e \sim 0.1$–0.2 keV and $T_i \sim 0.1$–1 keV.

The evolution of the experiments just described parallels an evolution of the main physics issues from heating in the early days to confinement in present experiments. In the USA, the early theta pinch experiments at the Naval Research Laboratory (NRL) [3, 71–75] and the Los Alamos Scientific Laboratory (LASL) [76–82] focused on the resistive annihilation of the reversed magnetic field which produced enhanced heating and neutron yields. In Europe, the potential merit of closed-field lines drew early attention [4], and numerous experiments at Culham [83–92], Jülich [93–98] and Garching [99–101] focused on the details of the field reversed configuration. Axial contraction and rotational and tearing instabilities were frequently observed. Techniques were developed for applying the bias magnetic field and for preionization. Later on (intermediate experiments), longer lifetimes were demonstrated at NRL in the PHAROS device [102–106], but these could not be extended in subsequent hard-core experiments [107]. The LASL research with reversed bias [108] was gradually abandoned when substantial heating was also obtained in the zero-bias mode without n=2 rotational instability. In Europe, research continued at Culham [109, 110], Jülich [111–113] and Garching [114, 115]. In these intermediate experiments, the first FRC confinement studies were made. Tearing modes became less frequently observed, and a quiescent period of gross stability was observed before the onset of the n=2 rotational mode. All technical aspects of the standard field reversed theta pinch formation method were developed by then. However, the FRC lifetimes were limited by the n=2 rotation, and interest decreased steadily, in spite of considerable experimental [71–74, 79, 80, 85, 92, 103–107, 112–115] and theoretical [116–127] work devoted to this instability.

Interest in FRC research was revived in the mid-seventies, with interesting results from experiments at the Kurchatov Institute [128, 129, 5]. Lower compression and improved formation techniques produced long-lived FRCs without gross instabilities. Following this work, the FRX series of experiments was initiated at LASL [130, 19]. Rapidly, the FRC concept began to be actively pursued in the USA at the Los Alamos National Laboratory (LANL, formerly LASL) and Spectra Technology, Inc. (STI, formerly MSNW), with smaller programmes at the University of Washington and the Pennsylvania State University. Simultaneously, a strong Japanese research programme produced very significant results in small devices, particularly concerning the n=2 rotation.

It was first discovered on the PIACE device [22] that the n=2 rotation could be completely suppressed by weak multipole fields. Since tearing instabilities are seldom observed in modern FRC experiments, the configuration lifetimes are now limited by confinement, rather than by gross instabilities. The main physics issues naturally evolved to confinement and improved formation, with significant achievements (see Section 1.2.1). In recent years, a consensus emerged in the FRC community that a new regime of FRC confinement and stability could occur at values of s larger than those in present experiments ($s \lesssim 2$). Forming longer lived, grossly stable FRCs with larger s-values is the most crucial issue for FRC research in the near future.

The evolution of the FRC experiments just described in connection with Table II raises a legitimate question: why is low compression in recent devices any better than high compression in early devices? Indeed, it may appear that one merely traded higher densities for somewhat longer lifetimes. The justification for the trend to lower compression comes primarily from stability and confinement considerations. Lower compression was instrumental in eradicating the various gross instabilities such as flutes, tearing and n=2 rotation that plagued early FRCs. This is clear from the evolution of the main studies listed in Table II. Moreover, lower compression is the direction that should logically be taken to reduce radial pressure gradients and hopefully to further improve the FRC confinement (see Section 5).

2. FORMATION

Despite extensive research and relatively good success at forming FRCs, the experimental approach remains largely an empirical process of trial and error. In many cases, and for reasons that have yet to be clarified, the formation phase yields rather irreproducible FRC parameters and confinement properties. The high vulnerability of the FRC during this crucial but only marginally controllable formation phase should be emphasized here. In this section, the techniques of FRC formation are described and then the key physics issues are presented.

2.1. Field reversed theta pinch formation

Up to now, nearly all FRCs have been formed on fast time-scales by the field reversed theta pinch

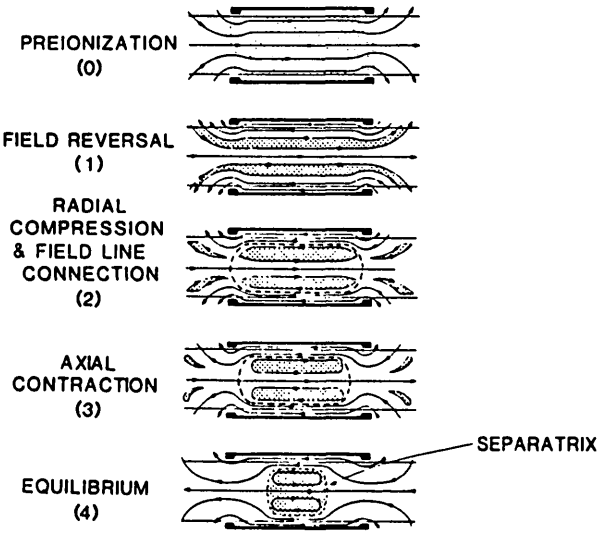

FIG. 3. Stages of FRC formation in a field reversed theta pinch [149].

(FRTP) method. In recent years, several improvements have been made in FRTP formation, resulting in more control and better plasmas.

2.1.1. *The FRC formation sequence*

The various stages of FRC formation in a typical FRTP are illustrated in Fig. 3. First, the discharge tube is filled with neutral gas and a bias magnetic field is applied. The gas is then ionized, freezing the bias field into this cold but sufficiently conducting plasma. Second, the current in the theta pinch coil is quickly reversed, producing a large inductive electric field that causes the plasma and bias field mixture to implode radially. Third, the oppositely directed magnetic field lines connect near the ends of the theta pinch coil, forming a closed-field configuration. Fourth, the magnetic tension at the ends of the configuration generally causes the FRC to contract axially until, finally, equilibrium is reached.

A simplified electrical circuit suitable for the FRTP formation just described is sketched in Fig. 4. A side view of the theta pinch coil and discharge tube is shown, with various capacitor banks and switches connected to the coil. Numerous stray and isolation inductances have been neglected. The first FRC experiments [3, 77, 78, 83–92] operated in the simplest possible manner, with just a main bank ((1) in Fig. 4) discharging into the coil. The first half-cycle of the current discharge provided bias field and preionization. The FRC was then formed and confined during the second half-cycle. Typical charging voltages and ringing periods were 15–100 kV and 10–20 μs, respectively. There was no control of the bias level, except through the gas fill p_0 [83–92]. This method, which can be improved by independent ionization, is still used in modern FRC experiments [5, 131, 132] because of its simplicity and high bias levels.

The usefulness of independently applied bias field and θ-ringing preionization via additional capacitor banks ((2) and (3) in Fig. 4) was recognized early on [74, 78, 93, 94]. Then, the FRC was formed and confined during the first half-cycle of the main bank discharge. Another plasma engineering advance, the 'crowbar' switch ((4) in Fig. 4), soon followed [105, 108] and allowed magnetic field lifetimes of 50–100 μs to be achieved. Even longer lifetimes can be obtained with a power crowbar or by superposing a fast pulsed field on a steady field of opposite direction [133]. Most modern FRC experiments operate in the first half-cycle mode with a crowbar switch. A midplane magnetic field waveform (measured outside the discharge tube but inside the theta pinch coil) from the FRX-B device [19] is shown as a function of time in Fig. 5, to illustrate a typical first half-cycle operation. The magnetic field traces in Fig. 5 are shown for both vacuum and plasma discharges, revealing an FRC configuration lifetime τ_ℓ of $\sim$35 μs. In such an FRC formation, some additional control can be gained by various preionization and field line connection techniques.

2.1.2. *Preionization techniques*

Preionization (PI) is perhaps the most critical and often underestimated phase in FRC formation. Indeed, FRC behaviour after formation has often been found [40, 41] to depend profoundly and inexplicably on the details of preionization, even though it is rather easy to ionize the gas fills of typical FRC experiments. In addition to the second half-cycle and ringing θ-discharge (θ–PI) preionization techniques described in the previous section, many other means have been

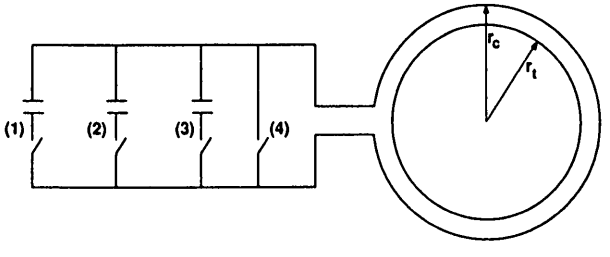

FIG. 4. Simplified field reversed theta pinch electrical circuit.

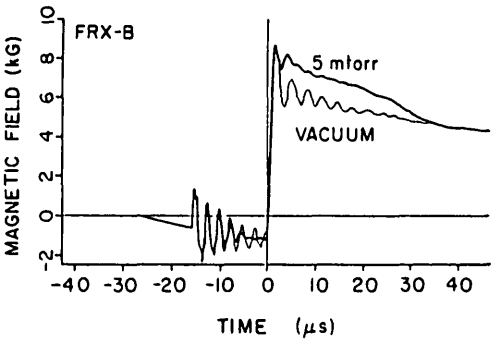

FIG. 5. Typical external field trace from first half-cycle operation of the FRX-B device [19].

conceived over the years. These include axial currents (Z-PI) [134, 131, 135], ringing quadrupoles [5, 136], plasma injection by conical theta pinches at each end of the main coil [22, 137] and laser irradiation of a solid target [138]. The two most popular techniques (θ-PI and Z-PI) are often preceded by seed ionization from some additional system. In such multistage schemes, the seed has been produced by various radio-frequency generators [93, 110, 111, 136], weak discharges along [115, 131] or transverse [139] to the coil axis, ringing quadrupoles [5, 136], octopoles [140], duodecapoles [141] and microwaves [142]. These PI techniques are applied with a variety of amplitudes, timings and bias field waveforms. The gas fills are mostly static, but sometimes they are puffed from the end [5, 26] or from the side to the centre of the coil [139]. All these many factors contribute to a multiplicity of initial conditions for FRC formation.

It is probably fair to say that, even though all of these PI techniques have been proved workable, no one of them is clearly superior to the others. Several schemes used alternately on a given experiment have yielded comparable FRCs [110, 115]. None of the PI techniques listed above are really ideal since they all introduce some axial, radial or azimuthal asymmetry in the preionized plasma. With proper choice of timing and amplitude (a very empirical process), most techniques have yielded FRCs with comparable parameters and confinement properties (within a factor of two or so). However, it must be emphasized that, for a given PI scheme, slight departures from the 'optimum' conditions often lead to very poor FRC formation [20, 40, 41, 142, 143].

2.1.3. *Field line connection techniques*

Until recently, FRCs were formed by plasma tearing of magnetic field lines at the ends of the theta pinch coil. In most cases, this tearing was induced by passive end mirrors, as shown in Fig. 3. The field line connection process is most clearly illustrated by time sequences from 2-D MHD simulations [35] such as those shown in Figs 6–8. Modelling of passive mirror tearing connection is shown in Fig. 6. A nearly complete connection is observed at t = 3 μs, with part of the torn plasma moving away from the coil. For such cases, with given fill pressure, magnetic field waveform and passive mirror geometry, there is no control on the timing of the connection process. Some control can be gained by using independent fast-rising coils beyond the end of the main coil. An example of such triggered connection [5, 131] from the TRX-1 device [131] is given in Fig. 7. Again, tearing is apparent because part of the plasma is lost outside the coil. In this case, the plug coil (furthermost to the left) produces a magnetic field in the same direction as the bias field, which delays connection until it is initiated by the trigger coil (in between the plug coil and the main coil). A suitable connection delay has sometimes been found to maximize FRC heating [5]. Tearing connection (whether passive or triggered) is believed [27, 28, 144] to create axial and azimuthal asymmetries in the FRC and in the connection timing at each end.

Non-tearing connection was first described by Belikov et al. [27] and was further developed in the TRX series of experiments [28, 142]. Such programmed formation is illustrated in Fig. 8 for the same TRX-1 geometry as in Fig. 7. Figure 8 shows three possible modes of non-tearing operation, depending on the timing of the trigger coil. These methods have been named slingshot mode, slow mode and bubble mode [145]. In each case, the plug coil produces a magnetic field opposite to the bias field, hence creating a separatrix. Upon reversal of the main field, this separatrix is drawn in through the discharge tube and defines subsequently the FRC without relying on a tearing connection process. This guarantees a high degree of axial symmetry, in contrast to tearing connection.

One can also achieve a non-tearing formation similar to the slow mode shown in Fig. 8, with just plug coils in addition to the main coil. Historically, devices using fast, independently driven mirrors [19, 25, 146, 147] were probably the first ones to achieve non-tearing connection, provided the mirrors were triggered before the main theta pinch discharge. When the FRX-A device was operated in such a mode, it was noted [19] that a larger particle inventory could be captured in the final FRC, an advantage confirmed later with 2-D

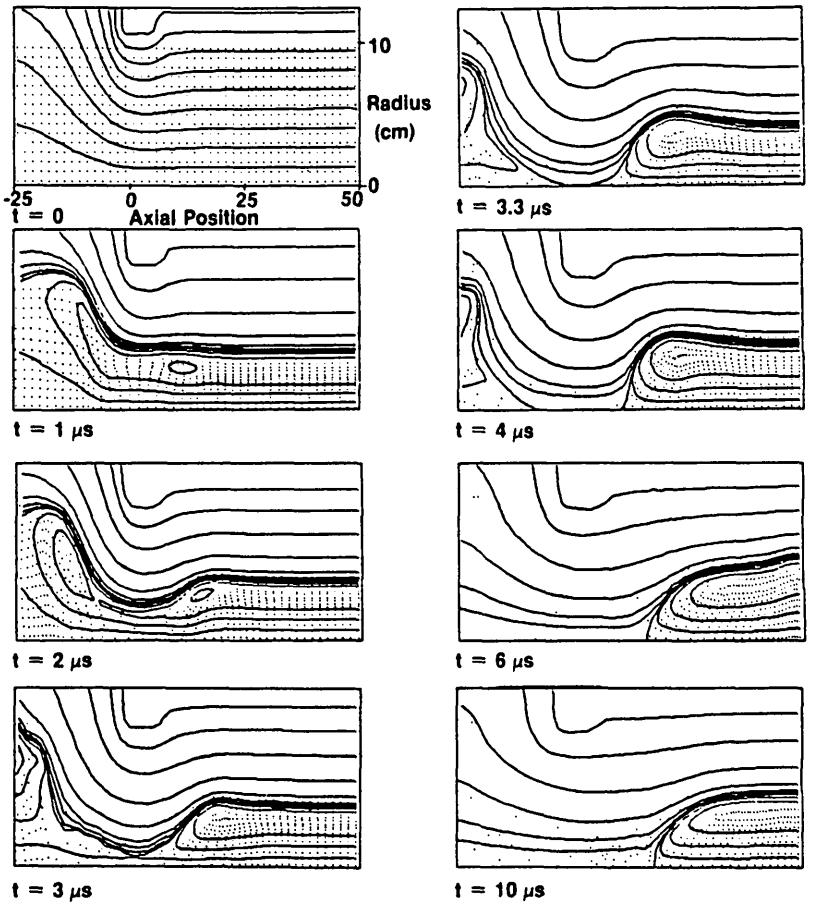

FIG. 6. 2-D MHD simulation of tearing connection induced by passive mirrors in the FRX-B device [35].

MHD simulations [148]. In a large device such as FRX-C/LSM [144], it is technologically less complex to use slow driven mirrors to achieve a non-tearing connection similar to the slow mode of Fig. 8. However, this approach sacrifices the timing control that fast trigger coils can provide.

2.2. Slow FRC formation

The FRTP method just described achieves FRC formation in a time τ_f that is typically a few radial Alfvén transit times τ_A. It would imply high voltages and large amounts of pulsed power when extrapolated to a fusion reactor system. A step in the direction of slower formation has been made with the three-turn TRX-2 theta pinch [149], but by a modest factor over standard FRTPs. Truly slow FRC sources would operate on a resistive diffusion time-scale ($\tau_f \gg \tau_A$) and would permit the use of power from rotating machinery. Four potential candidates have been identified for slow FRC formation: the Coaxial Slow Source, the Rotamak, the Extrap and the FRM.

The Coaxial Slow Source (CSS) produces annular FRCs between concentric coils carrying toroidal currents, as illustrated in Fig. 9 by 2-D MHD simulations [150] of the CSS device [10, 144]. This formation method was first proposed by Phillips [151], on the basis of the unpublished 'Slingshot' experiments conducted at LASL between 1963 and 1965. Similar plasmas have been formed with $\tau_f \sim \tau_A$ in the past [152–156]. The intent here is to slowly form annular plasmas and then to translate them to obtain FRCs. Translation appears feasible [151, 157] since, when the inner coil current reaches its maximum (t = 18 μs frame in Fig. 9), there is no flux linking the two coils. Then, with an additional 'kicker' coil [151], the annular plasmoid could be translated into a flux conserver and coalesced into an FRC. Preliminary results from a small CSS experiment [10, 144] indicate that it is indeed possible to form annular FRCs using low

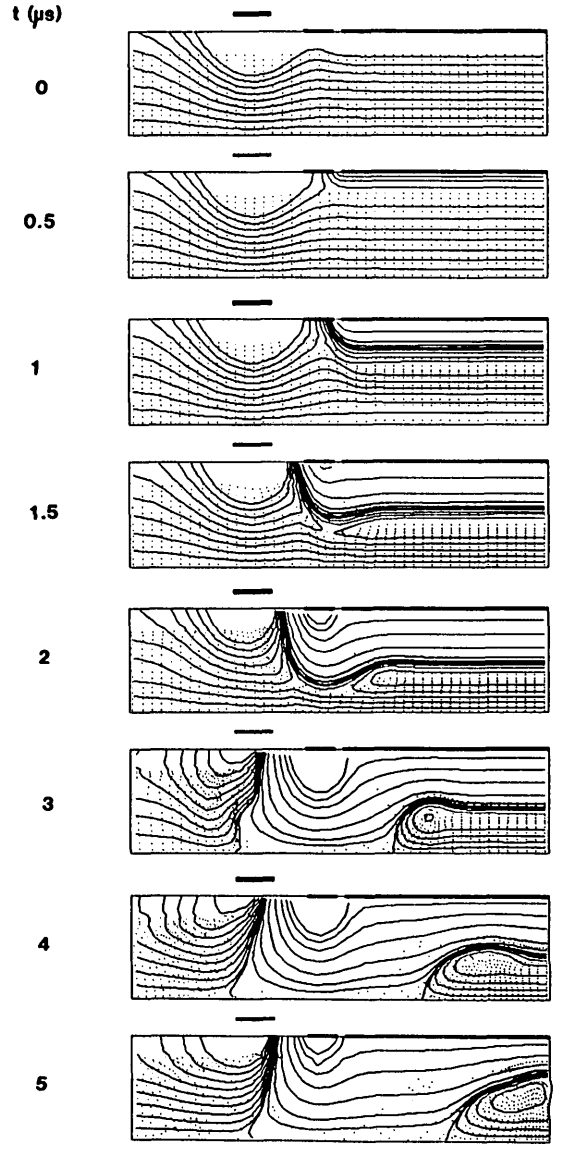

FIG. 7. 2-D MHD simulation of tearing connection induced by trigger coils in the TRX-1 device [148].

voltages and relatively long rise times ($\tau_f/\tau_A \sim 10$). However, plasmas with long flux lifetimes have not yet been produced in those experiments. In the CSS concept, as in most slow FRC formation methods, plasma heating is primarily Ohmic and the Ohmic power is low. Therefore, such FRC sources may be vulnerable to radiation and anomalous energy losses [153], and auxiliary heating may be required in large-size slow devices.

The Rotamak [158, 9] is a CT device in which the rotating magnetic field (RMF) technique [159] is used to drive the toroidal plasma current. Following Blevin and Thonemann [159], recent studies [160] have established that an RMF of appropriate amplitude and rotational frequency will penetrate a plasma and generate a rigid-rotor-like electron current. This efficient current drive technique is most easily understood by analogy to induction motors [161]. However, some experimental observations [162] are not consistent with the above theories [159–161], in cases where a transverse oscillating magnetic field is applied to a plasma. The Rotamak experiments conducted so far have been restricted to low energy plasmas with either high power (1–2 MW) and short duration (~ 20 μs) [9, 163, 164] or intermediate power (a few tens of kW) [9] to low power (a few kW) [9, 163, 165] and long duration (~ 20 ms). A study of an RMF-driven FRC slow source has been made [166]. A conceptual FRC formation by such a technique is sketched in Fig. 10, but an experiment with plasma parameters comparable to those of existing FRCs remains to be done.

The Extrap [167–170] is a magnetic configuration in which a toroidal Z-pinch is immersed in an octopole field. Figure 11 provides a comparison of the FRC and Extrap geometries. Like the FRC, the Extrap has a separatrix between closed and open field lines and is observed to be grossly stable for many Alfvén transit times [168, 169]. This stable behaviour (up to equivalent values of s around 5) may be due to various factors [170], some MHD-like and some related to kinetic effects as for the FRC. For the use of Extrap as a slow FRC source, the Extrap plasma should be formed on resistive time-scales rather than the present dynamic time-scales [168]. The Extrap plasma must also be coalesced into an FRC. A preliminary study of an RMF-driven Extrap experiment [171] suggests that, by a suitable change in the external currents, the toroidal plasma ring of Fig. 11(b) could become an FRC by forcing it out between the external octopole coils and translating it into a flux conserver.

The FRM approach is another possibility for slow FRC formation. In the 2XIIB experiments sketched in Fig. 12, off-axis neutral beams drove ion currents in a mirror-confined plasma target in order to form and sustain an FRM [15]. Field reversal was probably not achieved, for reasons that remain unclear. Possible explanations include insufficient beam power, anomalous losses due to RF fluctuations or to quadrupole resonances, and cancellation of the beam-induced ion current by electrons accelerated by drag. The latter may be prevented by an effective viscosity due to electron orbit effects near the field null [172]. Current cancellation could also be avoided by introducing an impurity ion species [173, 14, 63–65] or by weakly breaking toroidal symmetry with an external multipole

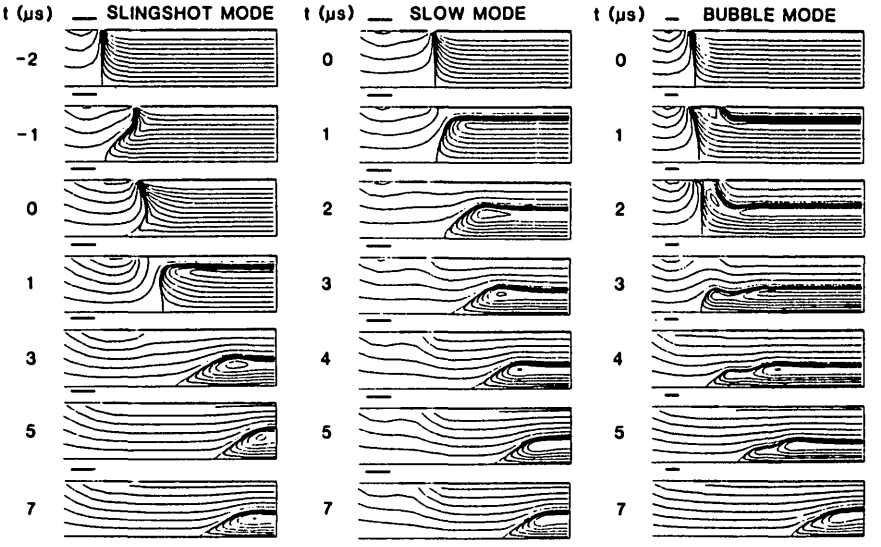

FIG. 8. 2-D MHD simulations of three modes of non-tearing connection in the TRX-1 device [145]: the slingshot mode, the slow mode and the bubble mode.

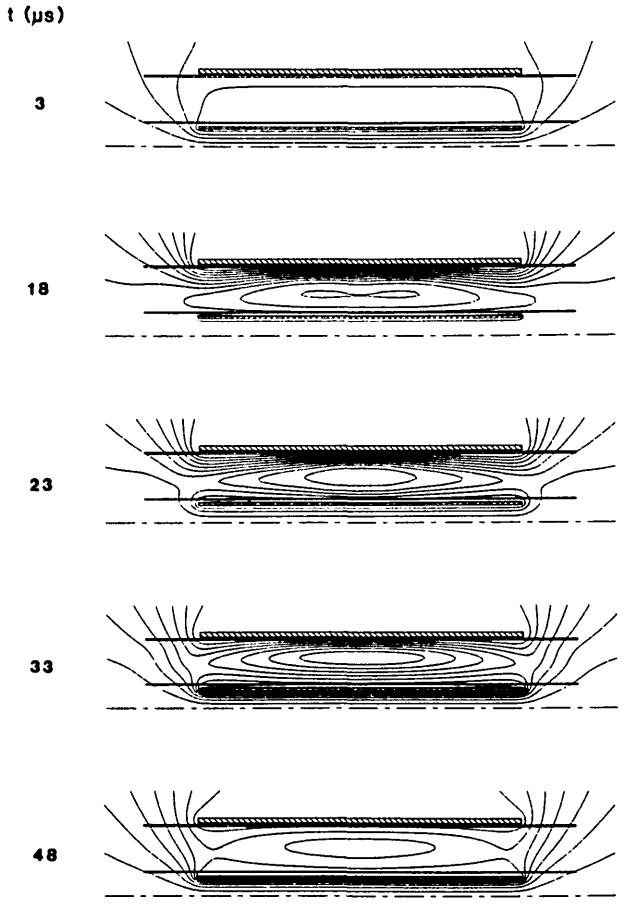

FIG. 9. Flux contours from a 2-D MHD simulation of annular FRC formation in the Coaxial Slow Source device [10].

field [174]. With either method for avoiding current cancellation, one could re-attempt an FRC/FRM slow buildup. One could also drive currents into an FRC target produced by the FRTP method or perhaps by two oppositely directed coaxial sources [175]. The FRC would be translated into a large flux conserver to obtain a low density plasma suitable for side-on neutral beam injection. Such experiments may be initiated in Japan in the near future, with modest initial power ($\lesssim 1$ MW) and pulse duration ($\lesssim 1$ ms) from standard (20–30 keV) neutral beam injectors which are well matched to present FRC parameters [176]. Other high power neutral beam sources are being considered [177].

2.3. Field line connection

The physics of field line connection during the formation of an FRC is not easily grasped because it is a complex phenomenon where geometry, resistivity and kinetic effects mix on dynamic time-scales. Experimentally, it is difficult to probe the neighbourhood of X-points in a non-perturbing way and, theoretically, one has to rely for the most part on numerical simulations with various approximations.

2.3.1. Connection at the ends of the coil

Experimentally, it is known that field lines connect during formation near the ends of the coil, as sketched

in Fig. 3. An indirect proof of connection is the well documented fact that FRC equilibria are formed. Direct experimental evidence came from internal probe measurements, which clearly showed the appearance of X-points [178, 179, 146, 147]. For tearing connection, the importance of passive or independently driven mirrors has been well documented; without mirrors, connection is erratic [115, 180], often delayed for long times [146], or incomplete [147]. Uneven connections, resulting in axial asymmetries and FRC ejection from one end or the other, have been observed [115, 181]. Non-tearing formation ensures a prompt, symmetrical connection, except when it is delayed on purpose, as in the bubble mode of Fig. 8(c). If too long a delay is used, tearing instabilities can occur [27, 146].

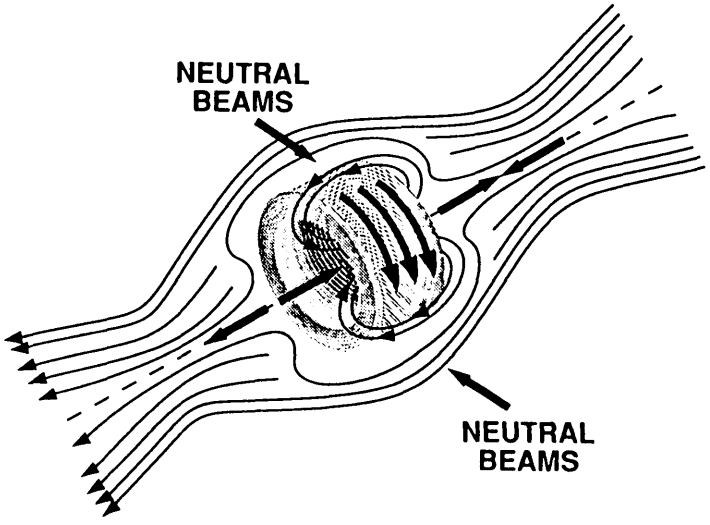

FIG. 12. The field reversed mirror [70].

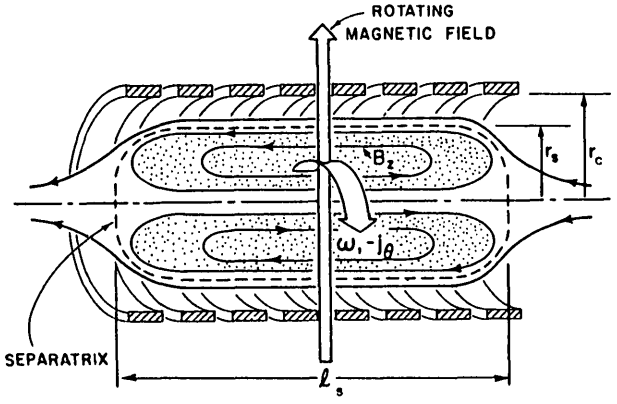

FIG. 10. Conceptual FRC slow source driven by the rotating magnetic field technique [166].

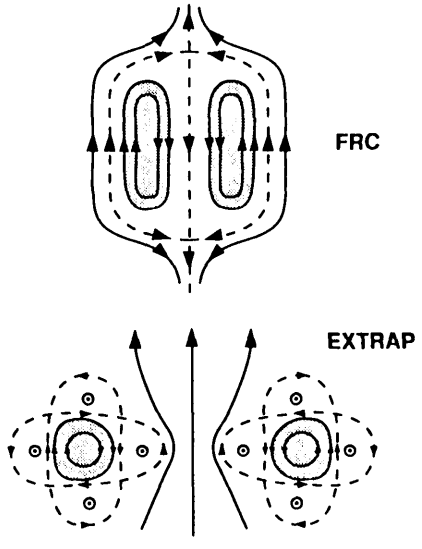

FIG. 11. Comparison of the FRC and Extrap geometries [169].

Plasma resistivity is a necessary ingredient in field line connection. Its influence has been demonstrated by impurity injection at one end of the coil [182], which induced asymmetric connection and FRC translation. In another experiment [147], a clear correlation between the onset of fast connection and high ratios of electron drift to ion sound speed implied that anomalous resistivity driven by microinstabilities may play an important role. The connection process was also observed to proceed slowly at first and then rapidly, with a resistivity at the X-point exceeding the classical one by an order of magnitude [59].

From a theoretical standpoint, the gross features of field line connection during FRC formation have been captured by various 2-D MHD simulations [183–186, 35, 36, 148], in generally good agreement with experiments. Although the role of an anomalous resistivity in initiating connection was recognized [183–185, 35], an important result from such simulations [183, 35] is that connection is a very dynamic process, strongly dependent on plasma motion near the X-points and weakly dependent on the magnitude of the anomalous resistivity. Plasma is continuously evacuated from the X-point, creating along the separatrix sharp field gradients and faster diffusion. Higher resistivities yield gentler gradients — a compensatory effect that explains the weak dependence mentioned previously. Simulations of the FRX-B device confirmed the importance of the end mirror geometry [35]. The connection process has also been shown by computation to proceed slowly at first, and then rapidly because of compressibility [186], which may explain the above data [59].

2.3.2. *Small-scale reconnection*

When field lines are mapped with internal probes, a common observation during radial compression is the rapid formation and subsequent coalescence of small magnetic islands [178, 59, 146, 147]. These islands, formed near the field null, are not observed in 2-D MHD simulations, which suggests the possible importance of kinetic effects. Indeed, with a 2-D hybrid code (fluid electrons, particle ions), Hewett and Seyler [187] have observed such a rapid small-scale reconnection. They explained the island formation as a non-linear consequence of a kinetic version of the Kruskal–Schwarzschild instability. An earlier kinetic analysis of the tearing instability [178] was proposed to explain the same phenomena. However, the Furth–Killeen–Rosenbluth (FKR) resistive MHD model [188] was found to be possibly consistent with observations of island formation in the HBQM device [146], even though the FKR theory does not apply to the shearless FRC case. Hybrid [187] and particle [189] simulations also showed merging of the small-scale islands, presumably by the coalescence instability [190]. Several large islands may remain in the subsequent FRC equilibrium. One cannot deny their possible existence, although internal probe measurements during FRC translation [191, 192] have not clearly revealed such structures.

An unexpected result from the hybrid code [187] was the observation of a spontaneously generated toroidal magnetic field when islands formed. This was also attributed to kinetic effects, but later MHD simulations [193, 194] showed a similar self-generation of B_θ, mostly from the Hall term. Toroidal fields in the end regions can evolve to large magnitude (comparable to the external poloidal field) during the early phases of formation. Later on, as the islands coalesce, the magnitude of B_θ decreases to insignificant levels for a symmetric coil, and there is never a net toroidal flux inside the FRC separatrix [193, 194]. However, larger values of B_θ and a net toroidal flux are possible [122, 194] if a conical theta pinch is used. This may explain in part the experimental observations of B_θ on translated FRCs [191, 192, 195].

2.4. Heating during FRC formation

The FRTP formation method provides substantial heating, primarily to the ions. During preionization, the plasma temperature is typically a few electronvolts. Then radial heating occurs, with a shock followed by a slow compression. Resistive heating also occurs during the radial compression as the reversed field is annihilated. Finally, axial contraction provides additional heating, through shocks and slow compression, before the FRC reaches equilibrium.

FRC heating has been modelled semi-empirically by Siemon and Bartsch [196]. Radial heating was calculated in the zero-bias limit. Slow axial compression was included, but not axial shock and resistive heating. Steinhauer [197] has constructed a more complete model of FRC heating, valid for arbitrary bias field strength. Assuming successive steps of radial shock, thermalization, radial compression, axial shock, and thermalization into equilibrium, the FRC final temperature was calculated with analytical radial profiles and global conservation laws for particles, momentum and energy.

2.4.1. *Radial heating*

This heating is most easily described by first considering the zero-bias limit and then including the effects of a reversed magnetic field. Radial heating in zero-bias theta pinches consists of a kinetic shock (implosion) process, usually followed by a slow compression. The shock process has been quantified by 'snowplow' or 'bounce' models, with comparable results. For example, a bounce model [198] of a sharp-boundary plasma yields a shock temperature equal to $2B_*^2/5\mu_0 n_0$, where n_0 is the fully ionized initial density and $B_* = E_\theta^{1/2}\,(\mu_0 m_i n_0)^{1/4}$ is a reference magnetic field of great importance in FRC formation, first introduced by Green and Newton [109]. In practical units, one has

$$B_* \text{ (kG)} = 1.88\,[E_\theta \text{ (kV}\cdot\text{cm}^{-1})]^{1/2}\,[A_i p_0 \text{ (mtorr)}]^{1/4} \quad (1)$$

where A_i is the ion atomic mass number. One obtains the final ideal implosion temperature, $T_I = T_e + T_i$, by slow radial compression from a magnetic field value of about $1.43B_*$ during the radial shock [197] to the crowbarred field value B_c. With the usual $T \sim B^{4/5}$ scaling [199] appropriate for an adiabatic coefficient of 5/3, one obtains $kT_I = 0.30 B_c^{4/5} B_*^{6/5}/\mu_0 n_0$. Using Eq. (1), T_I can be expressed as

$$T_I \text{ (eV)} = 470\,E_\theta^{3/5} \text{ (kV}\cdot\text{cm}^{-1})\, B_c^{4/5} \text{ (kG)} \times A_i^{3/10}/p_0^{7/10} \text{ (mtorr)} \quad (2)$$

The FRC temperature after radial heating is generally lower than T_I because of the reversed magnetic

field. First, the bounce implosion proceeds in most cases on a magnetized plasma, which lowers the shock temperature by a factor of $\sqrt{3}/2$. An approximate threshold for magnetization is [197] $G_{LO} \gtrsim 0.1$, where $G_{LO} = B_{LO}/B_*$ is the normalized bias field at lift-off time, when radial implosion begins. Second, the radial compression is weakened by a factor $(1 + 1.7G_{LO}^{1.5})^{-1}$, due to the internal magnetic field [149]. Still, radial heating is substantial in most FRC experiments, with values of E_θ in the range 0.3–1 kV·cm^{-1}. However, if the total voltage around the discharge tube is to be kept to technologically reasonable values, future larger devices will have lower values of E_θ and relatively weak radial heating.

2.4.2. *Resistive and axial heating*

The additional plasma heating provided by resistive magnetic field annihilation has been noticed since the earliest FRC experiments [3]. Classical resistive heating is rather low, but FRCs have steep density gradients during radial compression that can drive micro-instabilities and anomalous resistivity [200].

Heating from the axial contraction depends on the effective bias field remaining after field line connection. If more flux is annihilated before the axial contraction, the latter is weaker, so that the sum of resistive and axial heating is relatively constant at a given bias field strength. Detailed studies of the axial contraction were performed in early Culham work [86–92]. More recent Russian studies [5, 201, 27] pointed out the potential advantages of collisionless axial shock heating. Strong axial shocks can provide high temperatures, enhanced stability by keeping the plasma close to conducting boundaries, and a more efficient use of the external magnetic energy. Furthermore, substantial axial heating eliminates the requirement for high voltages that characterize radial heating. Experimentally, some evidence was provided [5, 201, 27] for increased temperatures from axial shocks, but for low fill pressure cases with final temperatures (1–1.5 keV) that did not exceed T_I by more than about a factor of two.

Axial shock heating was evaluated by Bodin et al. [86] using a sharp boundary fluid model, an analysis generalized later by Steinhauer [197]. The contributions from combined resistive and axial heating can be most easily calculated [149] by invoking global energy conservation for the final FRC equilibrium after radial implosion. The incremental temperature increase is $4B_{LO}^{6/5} B_c^{4/5} f_P/5\mu_0 n_0$, where f_P is a factor [149] that depends on flux dissipation. For most FRC experiments, f_P varies in a narrow range (0.9–1.1), which illustrates the compensating effect between resistive and axial heating mentioned previously. Assuming $f_P = 1$ and adding the contribution of radial heating, one obtains [202] the final equilibrium temperature T as

$$T = T_I [(\sqrt{3}/2)/(1 + 1.7G_{LO}^{1.5}) + 2.7G_{LO}^{1.2}] \quad (3)$$

This expression is valid for a magnetized bounce radial implosion with $G_{LO} \gtrsim 0.1$. For $G_{LO} \to 0$, the correct limit is just $T \to T_I$.

The ratio T/T_I from Eq. (3) is shown in Fig. 13 (solid line) as a function of G_{LO}. This curve is in good agreement with the one given by Steinhauer [197]. The respective contributions of radial heating and of combined resistive and axial heating (first and second terms on the right-hand side of Eq. (3), respectively) are indicated by dashed lines in Fig. 13. Some experimental data points are also plotted for cases where G_{LO} was estimated. The correspondence between symbols and devices is given in Table III. From Fig. 13 it can be seen that the FRC total temperatures calculated from Eq. (3) are in reasonable agreement with the available experimental data. They are also in good agreement with results from 2-D MHD simulations [35]. Resistive and axial heating are small for

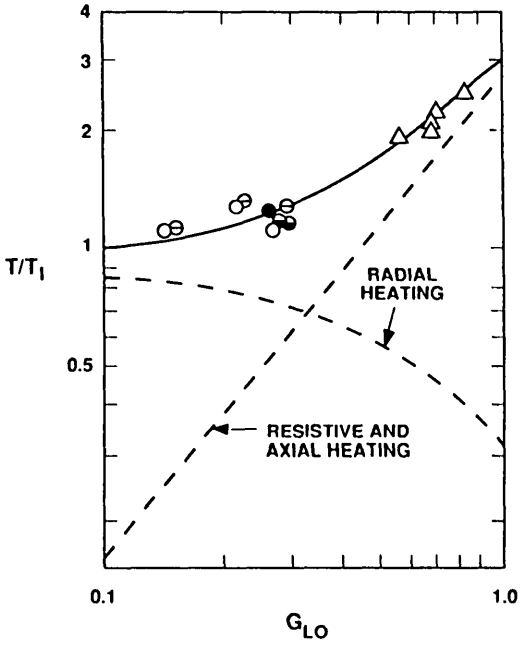

FIG. 13. Ratio of total FRC temperature T after formation to the ideal implosion temperature T_I as a function of G_{LO} [202]. Some experimental data are indicated by the symbols explained in Table III.

TABLE III. SYMBOLS USED TO REFER TO VARIOUS FRC EXPERIMENTS

Device	Nominal B_e	Reduced B_e
Centaur	○	
E-G	*	
FRX-A	□	
FRX-B	×	
STP-L	■	
NUCTE	+	
PIACE	◇	
FRX-C	●	◒
TRX-1	▲	
OCT	▽	▼
TRX-2	△	▲
FRX-C/LSM	○	⊖

$G_{LO} \lesssim 0.3$ but are substantial for the TRX-2 data with $G_{LO} \sim 0.7$. For the latter data, high temperatures were obtained with a relatively small E_θ of 0.13 $kV \cdot cm^{-1}$, a step towards slow FRC formation. However, formation with $\tau_f \gg \tau_A$ would require values of G_{LO} well in excess of unity, since $\tau_f/\tau_A \sim (B_c/B_*)\, G_{LO}$ for a FRTP and since typical values of B_c/B_* are in the range of 2–10.

2.5. Flux trapping efficiency

One of the most important aspects of FRC formation is the maximization of the poloidal flux ϕ contained within the configuration. Since no external magnetic circuit threads the toroid, the ultimate FRC lifetime depends on the magnitude and rate of decay of ϕ. In this section, the flux trapping limitations of FRTP formation are discussed.

2.5.1. Internal flux history

A typical FRC formation is shown in Fig. 14, for the same sequence as in Fig. 3. The evolution of ϕ is shown by a dashed line in Fig. 14, starting at a value ϕ_0 at t = 0 when the main bank discharges and decreasing to a value ϕ_e as the FRC equilibrium is reached. Also shown in Fig. 14 are the external magnetic field waveform B_e and the diamagnetism $\Delta\phi$. These two traces are obtained at the coil midplane from a diagnostic essential in FRC research — the excluded flux array [88]; combining the signals from a flux loop and a B_z magnetic probe at a radius r_ℓ intermediate between r_c and r_t, the diamagnetism is defined as

$$\Delta\phi = \pi r_\ell^2 B_e - \int_0^{r_\ell} B_z\, 2\pi\, r\, dr \qquad (4)$$

The diamagnetism $\Delta\phi$ is useful for following the time history of ϕ during FRC formation. It is convenient to approximate the plasma as a thin annulus of radius r_p separating the internal magnetic field B_i from the external magnetic field B_e [84, 97, 203, 204]. In the following analysis, B_i is negative and $\phi = -\pi r_p^2 B_i$ is positive. With such a model, Eq. (4) reduces to $\Delta\phi = \pi r_p^2 (B_e - B_i)$. At t = 0, $B_e = B_i = -B_0$ and $\Delta\phi = 0$. At zero-crossing time, $\Delta\phi = \phi_{zc}$ since $B_e = 0$ [109, 131]. At lift-off time t_{LO}, $r_p = r_t$, $B_e = -B_i = B_{LO}$, $\Delta\phi = 2\phi_{LO}$, and the radial implosion begins. $\Delta\phi$ soon reaches a maximum and starts to drop as the decrease in plasma area πr_p^2 overcomes the increasing B_e ($\Delta\phi = \pi r_p^2 B_e + \phi$, with ϕ approximately constant). During radial compression, the plasma motion becomes oscillatory [97], from overcompressed with $B_i^2 > B_e^2$ to undercompressed with $B_i^2 > B_e^2$. During that stage, as can be seen in Fig. 14, $\Delta\phi$ varies little around an equilibrium level, $\Delta\phi_a$ ($B_e = -B_i$), until field line connection is complete. Then $\Delta\phi$ increases

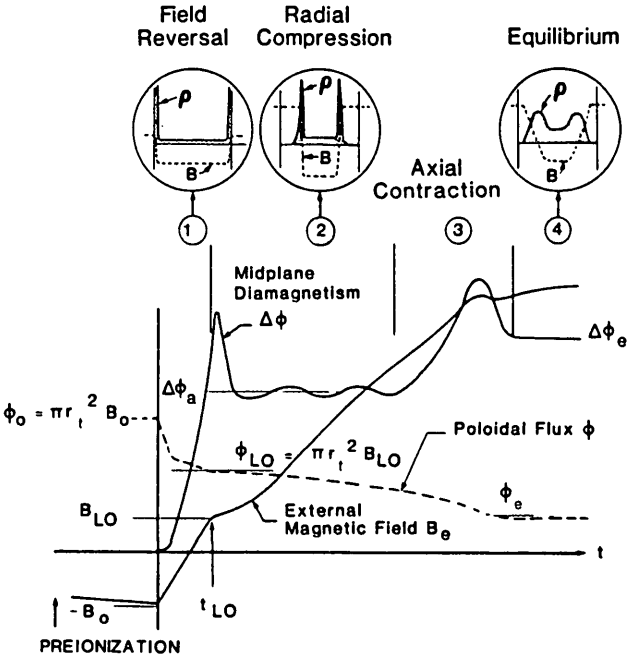

FIG. 14. Time history of the internal magnetic flux during FRC formation [149].

as the plasma contracts axially and expands radially outwards. After peak axial compression, the plasma rebounds (drop of $\Delta\phi$) and reaches equilibrium ($\Delta\phi = \Delta\phi_e$).

The initial value ϕ_0 generally differs from the bias magnetic flux $\phi_b = \pi r_t^2 B_b$, depending on when and how the preionization is achieved. This is especially true with ringing θ-PI, for which values ϕ_0/ϕ_b of about 0.5 [203], 0.7 [205], or even greater than unity [206] have been reported. The important quantity $B_{LO} = \phi_{LO}/\pi r_t^2$ can be measured directly at lift-off time by using Eq. (4), or it can be estimated as $B_{LO} \sim \Delta\phi_a/2\pi r_t^2$ assuming plasma energy and flux conservation during the radial compression [27, 149]. The zero-crossing effective bias $B_{zc} = \phi_{zc}/\pi r_t^2$ provides a useful reference, intermediate between B_0 and B_{LO}. The determination of ϕ after lift-off is difficult and requires various assumptions [207]. When equilibrium is reached, ϕ_e can be inferred from models described in Section 3.

2.5.2. *Flux loss during reversal*

Field reversal occurs during the time interval in which B_e changes from $-B_0$ to $+B_{LO}$. During this time, the plasma and internal magnetic flux expand towards the discharge tube, with possible substantial flux loss. Green and Newton [109] proposed a model for convective flux loss at the Alfvén speed. Instantaneous particle and flux losses were assumed when the plasma contacted the tube. Therefore, the reversal time $\tau_r \sim 2B_0/\dot{B}$ must be less than the radial Alfvén time $\tau_A = r_t/v_A$ of the preionized plasma to avoid substantial flux loss. The relation $\tau_r \leq \tau_A$ can be rewritten as $B_0 \leq B_*$, where B_* is the Green-Newton field of Eq. (1). This flux loss model yields approximately

$$B_{LO}/B_0 = 1 - (B_0/B_*)^2 \qquad (5)$$

Equation (5) describes fairly well the flux loss during reversal for $B_0/B_* \lesssim 0.5$ [131]. For example, in the HBQM device [205], fair agreement with Eq. (5) was obtained and up to 75% of the initial flux could be retained through reversal. To reduce flux losses during reversal, pulsed multipole fields have been used on some experiments to avoid plasma-wall contact [208, 5, 209, 131].

Recent data showed that Eq. (5) significantly overestimates the flux loss during reversal for $B_0/B_* \gtrsim 0.5$ [210, 131]. To explain the observed good flux trapping, it was postulated that a thin pressure bearing plasma sheath forms at the discharge tube during reversal (see Fig. 14). This sheath is highly conducting and modifies the flux loss from an inertial process to a slower resistive process. Kutuzov et al. [210] found good agreement with their experimental results by using a simple quasi-steady model for a fully ionized plasma. Later on, extensive computations were made [211] with a 1-D MHD code that included diffusion of neutrals relative to ions. One important conclusion from this work was that the flux trapping efficiency B_{LO}/B_0 is independent of the device size for a given applied voltage around the discharge tube. Good agreement between this numerical work and data from the TRX-1 device [131] was found. More recently, Steinhauer showed with a quasi-steady flow model similar to the one of Vekstein [212] that the flux loss during reversal also depends on the transfer efficiency η_t of the external circuit [213]. One obtains approximately

$$B_{LO}/B_0 = [1 + 1.7\,(B_0/B_*)(N_*/N_0)^{1/4}\,(1-\eta_t)^{2/5}]^{-1} \qquad (6)$$

where $N_0 = \pi r_t^2 n_0$ is the initial line density and $N_* = 2\pi\, m_i/\mu_0 e^2$ is the critical line density [197]. Steinhauer [213] also showed that high values of B_{LO} can result in substantial temperature rises of the discharge tube. This could cause impurity influx and fast annihilation of the reversed flux [214, 215]. These considerations lead to a practical limit of $G_{LO} \lesssim 1$-2 for most devices. So far, FRCs have been produced with G_{LO} values up to unity [149].

2.5.3. *Flux loss during radial compression*

As illustrated in Fig. 14, the radial compression is an antiparallel field configuration that is highly susceptible to tearing. These instabilities can develop if field line connection is not completed rapidly enough [149, 27, 146]. To avoid tearing instabilities that grow on time-scales of the order of τ_A, one presumably has to operate with $\tau_r \lesssim \tau_A$. This would limit FRC formation to values of G_{LO} less than unity.

Experimentally, flux loss during the FRC radial compression has been inferred from internal probe measurements. In early small-size experiments [76, 77, 95, 99-101, 113, 115], rapid flux annihilation was observed. In some modern experiments [180, 205, 146, 216], the loss of a large fraction (60-90%) of the initial flux ϕ_0 was reported. Flux loss during radial compression has also been inferred in the TRX-2 device by controlling the timing of the axial contraction [207]. The trapped flux does not decrease monotonically during the radial compression but displays

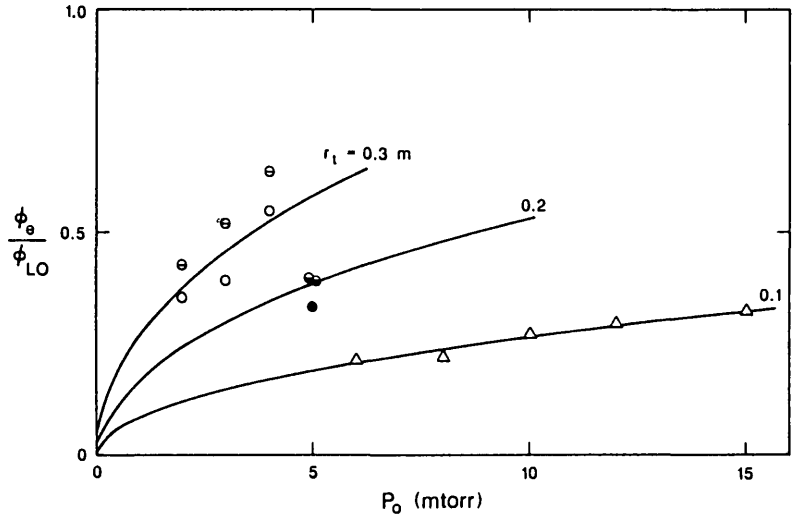

FIG. 15. Comparison of experimental and calculated values of the flux retention factor after lift-off [202]. The symbols are explained in Table III.

oscillations [180, 205, 146, 216]. These are not clearly understood but have been attributed in one case [216] to large off-diagonal terms in the ion pressure tensor. The observed flux loss during radial compression implies an anomalous resistivity, enhanced by about an order of magnitude over the classical value [146, 200, 207].

This is consistent with microinstabilities driven by sharp pressure gradients. Such modes may produce a growing resistivity [217] and a broadening of the pressure gradients to a few ion gyroradii. Then, the micro-instabilities would subside and the anomalous transport would drop to a low level [218]. Similar current sheath broadening during the radial implosion of zero-bias theta pinches has been observed and successfully modelled [219] with a 1-D hybrid simulation including Chodura anomalous resistivity [220]. This empirical resistivity has also been found useful in modelling flux loss during FRC radial compression [200, 207].

A possible explanation for the observed flux loss is that the plasma undergoes rapid turbulent relaxation until the ion drift parameter v_D/v_i ($v_D = (dp_i/dr)/neB$ and $v_i = (T_i/m_i)^{1/2}$) at the magnetic axis diminishes to a certain level ν. Steinhauer [197] has calculated the flux loss by invoking such a relaxation criterion. Assuming some radial pressure profile to compute the equilibrium flux ϕ_e just after formation, the flux retention factor after lift-off, ϕ_e/ϕ_{LO}, can be expressed as a function of ν. The best fit to the available TRX-2 data yields $\nu \sim 0.35$ [149] and one obtains for most cases [202]

$$\phi_e/\phi_{LO} = 0.85\ r_t(m)\ p_0^{1/2}\ (mtorr) \qquad (7)$$

Figure 15 gives a comparison of this expression with the available experimental data. The experimental values of ϕ_e/ϕ_{LO} are obtained from the same data and with the same symbols as in Fig. 13 and the solid lines correspond to Eq. (7). The good agreement for $r_t = 0.1$ m is not surprising since ν was chosen to fit the TRX-2 data [149]. Values of ϕ_e/ϕ_{LO} consistent with the $r_t = 0.1$ m data of Fig. 15 can also be inferred from the FRX-B [180] and HBQM [146, 205] devices, where $\phi_e/\phi_b \sim 0.1$–0.2 and $\phi_b/\phi_{LO} \sim 2$ were reported.

Interestingly, one notes from Fig. 15 that Eq. (7) describes quite well the data from larger-size devices. The data reveal a small B_c dependence not included in Eq. (7) but physically understandable since reduced B_c results in larger gradient lengths. At sufficiently high fill pressures, lower values of ϕ_e/ϕ_{LO} than predicted by Eq. (7) are generally obtained. This may indicate a breakdown of the relaxation criterion for collisional plasmas. Nonetheless, for most FRC cases of interest, Eq. (7) seems to provide a good estimate of ϕ_e/ϕ_{LO}, unlike the prediction of constant ϕ_e/ϕ_0 from a turbulent relaxation theory [221]. As seen in Fig. 15, up to 60% of the lift-off flux has been retained after formation in the FRX-C/LSM device. This is obviously a favourable result, but it has possibly a negative aspect, as discussed in the next section: resistive heating is less and less effective as the size of the device increases.

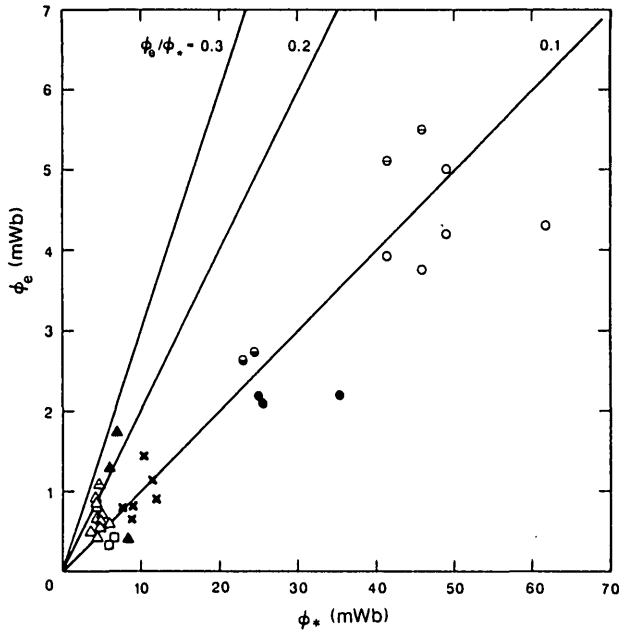

FIG. 16. Experimental values of the equilibrium flux just after formation for long lived FRCs from various devices [202]. The symbols are explained in Table III.

2.5.4. *Flux limitations*

During axial contraction, the flux loss rate is observed to be lower than during radial compression [149, 207] because radial magnetic field gradients are presumably reduced by a simultaneous radial expansion of the FRC [207]. Hence, flux loss during axial contraction probably contributes little to ϕ_e/ϕ_{LO} in Eq. (7). However, in large-size experiments, strong axial implosions appear to cause a deterioration of the FRC confinement after formation [41]. So far, this deterioration limits the values of ϕ_e that can be usefully obtained by restricting FRC formation to bias field values sufficiently low to avoid strong axial implosions.

This flux limitation can be appreciated by considering the experimental values of ϕ_e, plotted in Fig. 16 against their corresponding values of $\phi_* = \pi r_t^2 B_*$. The symbols are those of Table III and the values of ϕ_e are averages of the best data for given conditions. Most values of ϕ_e/ϕ_* are in the range 0.1–0.2 and do not exceed ~0.1 for the larger FRX-C and FRX-C/LSM devices. Since $\phi_e/\phi_* = (\phi_e/\phi_{LO})G_{LO}$, these data imply lower values of G_{LO} because larger values of ϕ_e/ϕ_{LO} are achieved in large-size devices. One should note that, in Fig. 16, it is not the value of B_{LO} that can be trapped but rather the value of B_{LO} that can be tolerated which limits ϕ_e. The low values of G_{LO} obtained in the FRX-C and FRX-C/LSM devices are only about 20–30% larger than those corresponding to the onset of axial contractions, as can be determined analytically [202]. Hence, these experimental G_{LO} values correspond to moderate axial contractions. Higher values of G_{LO} consistently yield strong axial implosions and a deterioration of the FRC confinement after formation [41].

What happens during strong axial implosions is not understood, in spite of numerous observations. In early experiments, an abrupt disappearance of the reverse field was noted at peak axial contraction [87, 89, 91, 92, 112], and lower bias fields led to weaker contractions and longer-lived structures [89, 112]. In modern experiments, one sometimes observes destruction of the FRC [27, 28, 222, 223], confinement degradation [41] and flux dumps [207]. End-on luminosity has suggested sausage instabilities [77, 224, 225], other gross azimuthal asymmetries [207] and transient contact with the discharge tube [226] around peak contraction time. Side-on luminosity indicated tearing [91, 112] or tilting instabilities [227, 228]. Internal probes indicated transverse magnetic fields during axial shocks, also possibly consistent with tilting instabilities [223, 226].

Whether FRCs can survive strong axial implosions is an open but crucial question at the present time. Techniques employing non-tearing field line connection [27, 5, 222, 28, 142, 145, 223] and substantial parallel classical viscosity [207] may be helpful. However, recent FRX-C/LSM data with non-tearing formation and high viscosity still showed a rapid confinement degradation whenever strong axial implosions occurred [41]. Longer coils could be helpful if there is a lower limit on the transient FRC elongation $\ell_s/2r_s$ [228]. If FRCs cannot survive axial shocks, future large-size devices would be limited to values of G_{LO} and ϕ_e/ϕ_* of about 0.1 [202]. Increasing s over present values would then require large values of ϕ_* [229], and FRTP heating would be essentially radial. Of course, formation methods other than the FRTP may not be subject to strong axial implosions, which provides added incentive for their development.

Finally, one should mention some other limitations that can also occur during FRC formation in FRTPs. Excessive radial compression results in shorter-lived FRCs, so that the ratio B_e/B_{LO} should be less than about 10–20 [202]. Preionization becomes increasingly difficult at very low fill pressures [230]. At high fill pressures, the FRC length may exceed the coil length [196, 230] or lean on the end mirrors, and the plasma collisionality may be excessive. Difficulties yet to be clarified are often encountered when a toroidal field is deliberately introduced during FRC formation

[107, 128, 231-233, 12]. Finally, impurities can prevent the formation of long-lived FRCs [98-100, 130, 19].

3. EQUILIBRIUM

This is probably the area of FRC physics that is relatively the most understood theoretically and experimentally. Theoretical results are first presented, with simple analytical results of great usefulness, followed by more detailed numerical work. Surprisingly, these results derived in the MHD limit agree quite well with present experimental FRC equilibria that have $s \lesssim 2$. Data that give clear evidence of high beta toroidal equilibria are presented. Finally, two important ways of modifying FRC equilibria are discussed: adiabatic compression and translation.

3.1. Theoretical results

3.1.1. General properties

Considerable insight can be gained by considering axisymmetric elongated FRC equilibria inside a cylindrical flux conserver. Such equilibria (with no B_θ) closely describe most experimental cases similar to Fig. 1. Since an FRC is a torus of very low aspect ratio, cylindrical geometry is required for accurate modelling, although useful qualitative properties have been obtained with conformal mapping techniques [234]. Sharp-boundary FRC equilibria in cylindrical geometry have been studied in the past [235, 236], but more general results can be obtained for arbitrary diffuse plasma profiles [237, 19, 30]. First, assuming straight field lines near the coil midplane and neglecting rotational effects, radial pressure balance can be written as

$$p_M = p + \frac{B_z^2}{2\mu_0} = \frac{B_e^2}{2\mu_0} \tag{8}$$

Assuming that the plasma pressure p is only a function of the poloidal flux variable

$$\psi = \int_0^r B_z \, r dr$$

the relation $d\psi/B_Z = r dr$ becomes $\pm d\psi/\sqrt{2\mu_0 (p_M - p(\psi))} = r dr$ when Eq. (8) is used. This expression implies that ψ is a symmetric function of $r^2 - R^2$. Hence, all equilibrium quantities that are functions of ψ only are also symmetric functions of $r^2 - R^2$. Since ψ varies from 0 on axis and at the separatrix to a maximum value ψ_M at the field null, integration of the above differential expression from 0 to R and from R to r_s yields

$$r_s = \sqrt{2}R \tag{9}$$

Another profile independent result is obtained by considering axial equilibrium. Neglecting pressure outside the separatrix and assuming a sufficiently long flux conserver so that there is a vacuum end-plane region of straight field lines, one can integrate the equilibrium equations over the volume bounded by the midplane, the conducting wall of radius r_c and the end-plane to obtain the axial force balance between field-line tension and plasma pressure [19]. Then, combining this axial condition with Eqs (8) and (9), one obtains

$$\langle\beta\rangle = 1 - x_s^2/2 \tag{10}$$

where

$$\langle\beta\rangle = (2/r_s^2) \int_0^{r_s} (p/p_M) \, r dr$$

is the volume average of β within the separatrix, and where $x_s = r_s/r_c$. Equation (10) was first derived by Barnes et al. [237] and is perhaps the most useful relation in FRC physics. It implies radial pressure profiles that are peaked when x_s approaches unity and that are broad for small values of x_s. Many useful analytic estimates are facilitated by Eq. (10) because it allows the physics of elongated FRCs to be studied in one (radial) dimension.

An important corollary of Eq. (10) is that the poloidal flux $\phi = 2\pi\psi_M$ contained in an elongated FRC is bounded by two values [238-240]. Using

$$\phi = \int_R^{r_s} B \, 2\pi \, r dr,$$

Schwartz inequality, and Eqs (8) and (10), one obtains $(x_s/\sqrt{2})^2 \leq \phi/\pi R^2 B_e \leq x_s/\sqrt{2}$ [239]. The limiting cases are two sharp-boundary profiles with lowest (LFSB) and highest (HFSB) fluxes; these are illustrated in Fig. 17 for $x_s = 0.5$. The above inequalities allow ϕ to be written as

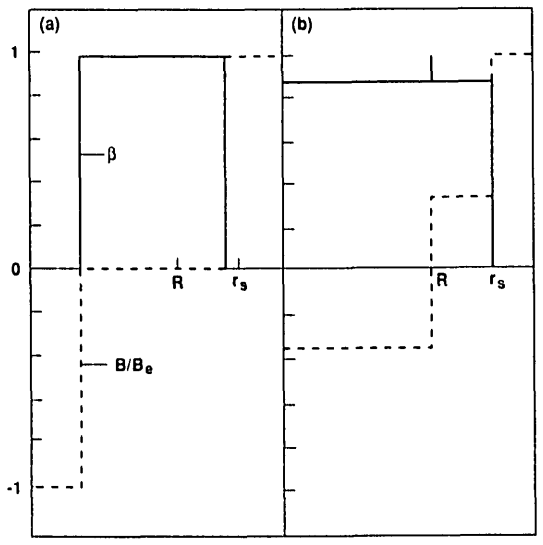

FIG. 17. Limiting sharp-boundary FRC radial profiles: (a) the low-flux sharp boundary and (b) the high-flux sharp boundary. The normalized pressure β is shown by solid lines and the magnetic field B/B_e by dotted lines.

$$\phi = \pi r_c^2 B_e \left(\frac{x_s}{\sqrt{2}}\right)^{3+\epsilon} \tag{11}$$

where ϵ is a parameter in the range 0 to 1 [241]. The parameter s has been defined [28] as

$$s = \int_R^{r_s} r dr / r_s \rho_i$$

This parameter is related in an approximate way to the number of ion gyroradii between R and r_s. Assuming a radially uniform ion temperature, one can write

$$s = \frac{\phi}{2\pi\, r_s\, \rho_{ie}\, B_e} \tag{12}$$

where ρ_{ie} is the external ion gyroradius. Hence, s is also bounded by the above inequalities. Defining $S = R/\rho_{ie}$, one obtains $Sx_s^2/4\sqrt{2} \leq s \leq Sx_s/4$.

These bounds on s and ϕ leave room for substantial uncertainty and, to obtain a better estimate within these limits, one must either measure B(r) or rely on some transport model. An often used radial pressure profile that approximates well present strongly viscous FRCs (except in the vicinity of the separatrix) is the shearless rigid rotor [19], for which $B = B_e \tanh [K(r^2/R^2 - 1)]$. With the constant K chosen to satisfy Eq. (10), this profile yields values of ϕ close to those of the HFSB profile.

3.1.2. Computation of equilibria

Most numerical calculations of FRC equilibria have been restricted to the MHD model. Some kinetic FRC equilibria have been recently computed [242, 243]. As for other axisymmetric toroidal equilibria, the numerical procedure involves solving the Grad-Shafranov equation, which assumes a scalar plasma pressure. For the FRC case, one seeks a solution to this equation in cylindrical co-ordinates with a flux-conserving boundary at $r = r_c$ and assuming no toroidal field.

Two approaches have been adopted in computing FRC equilibria: either an entropy variable μ [244-246, 32, 34] or the plasma pressure p [247, 31, 33, 248, 249] is specified as a function of ψ. The entropy method has the advantages [34] of using the experimentally estimated value ψ_M as an input quantity, of allowing easy adiabatic compression and of automatically providing small grid spacing near the separatrix where pressure gradients are steep. Furthermore, computing an elongated FRC with a desired separatrix length is straightforward since ℓ_s is proportional to the integral $\int_0^{\psi_M} \mu d\psi$ [34]. On the other hand, the computation of an elongated FRC is quite difficult when $p(\psi)$ is specified because of bifurcated solutions [247, 250], and obtaining a desired value of ℓ_s requires a global constraint such as the total current [31] or the poloidal separatrix area [33]. However, specifying $p(\psi)$ avoids the singularities in p and $dp/d\psi$ at the separatrix inherent in the entropy method whenever there is finite pressure on the separatrix [248].

The entropy codes have large currents at the separatrix as a result of those singularities. Surprisingly, such current spikes appear necessary (within the MHD model) to obtain rather elliptical separatrices, inside which flux surfaces are gradually distributed axially. This may explain why codes that specify smooth $p(\psi)$ functionals yield very racetrack-like separatrices, unless a current spike is imposed near the separatrix [248]. Computed examples of elliptical and racetrack FRC equilibria are shown in Fig. 18. The issue of separatrix shape comes up naturally when numerical equilibria are compared with the experimental data; it is also of some importance for FRC stability.

One important result from the computations is that, for a given value of x_s, no equilibria are possible if the plasma pressure on the separatrix is too high [31, 251]. Recently, Spencer et al. [252] showed that this occurs whenever the separatrix pressure exceeds the downstream vacuum magnetic pressure. This implies that 2-D FRC equilibria must satisfy $\beta_s \leq (1-x_s^2)^2$, in good

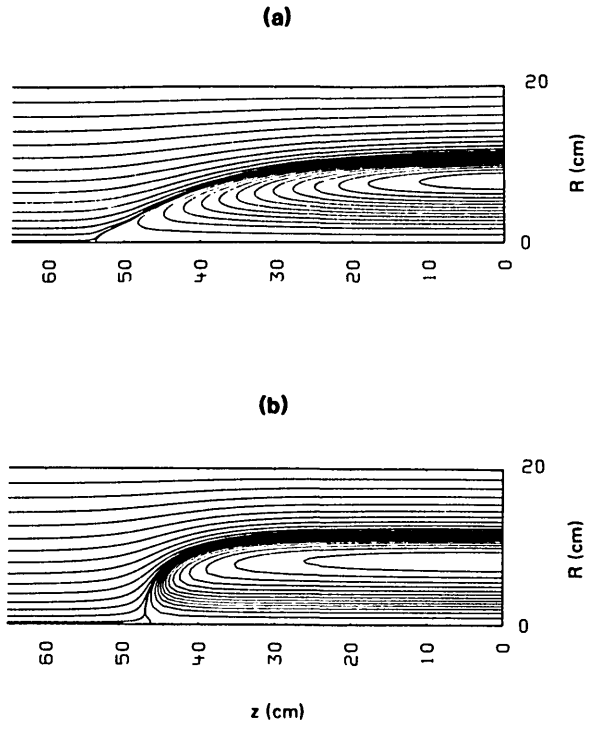

FIG. 18. Two numerical FRC equilibria inside a flux conserver: (a) elliptical and (b) racetrack equilibria from an entropy code [34].

agreement with previous empirical numerical results [31]. A consequence of this relation is that the HFSB profile of Fig. 17 cannot exist in two dimensions [252] since $(1-x_s^2)^2 \leq 1-x_s^2/2$. Therefore, it is likely that an upper bound on ϕ exists which is slightly lower than the flux of the HFSB profile.

Numerical FRC equilibria yield values of $\langle\beta\rangle$ that are very close to the simple result of Eq. (10). This justifies a posteriori the various assumptions made in deriving this expression. Various corrections to Eq. (10) have been estimated by a combination of analytical and numerical work. Kinetic effects [57] and typical plasma rotations bring small corrective terms, of the order of $1/S^2$ (most experimental values of S are in the range 10–30). Plasma pressure on open field lines is a negligible effect [248] (typically less than 1%). The thrust force in the exhaust plasma could also yield a small correction. The possible presence of a toroidal field lowers $\langle\beta\rangle$ by the volume average midplane value of $(B_\theta/B_e)^2$ [248], a 2–3% effect according to measurements on translated FRCs [20, 192]. Curvature effects lower $\langle\beta\rangle$ by generally small factors, of the order of $(r_s/\ell_s)^2$ for elliptical separatrices [249]. The most important correction to Eq. (10) seems to arise when FRCs are confined axially by mirror fields [248, 33]. For such cases, $\langle\beta\rangle$ can increase by a few per cent, which lowers ϕ significantly and causes a deterioration of the FRC confinement when $\langle\beta\rangle$ approaches unity [248, 253]. If one considers pressure profiles all with the same value of $\langle\beta\rangle$, mirror corrections in Eq. (10) imply increases in x_s [33].

3.1.3. Other equilibrium studies

Field reversed equilibria relevant to FRMs and FRCs have been considered analytically and numerically. These axisymmetric MHD equilibria are not generally consistent with an external cylindrical flux conserver. One notable exception is the spherical Hill's vortex [254], which matches to a uniform magnetic field far from the field reversed plasma and therefore accommodates a straight flux conserving boundary condition for small values of x_s [247, 249, 255]. The analytical Hill's vortex solution has often been used to study FRM particle orbits [70, 256] and to gain insight into FRC equilibrium [247, 249, 250, 257]. For the latter cases, separatrices of arbitrary ellipticity have been considered: oblate separatrices match in the external vacuum region to mirror-like magnetic fields and are similar to the FRM equilibria obtained with the SUPERLAYER particle code [258]. Conversely, prolate separatrices match to complex antimirror-like magnetic fields, especially for large elongations [247, 257].

More general analytical solutions than the Hill's vortex have been obtained [255]. These include racetrack separatrices with arbitrarily low midplane curvature that have been used as input to 2-D MHD equilibrium and stability codes such as CYLEQ [259]. Other 2-D MHD numerical equilibria have been computed without a flux conserving boundary to study convective stability [260]. Analytical 2-D equilibria with arbitrary plasma rotation have been identified [261, 262]. Periodic 2-D FRC equilibria relevant to the reversed field multiple mirror concept [54] have also been considered [263].

Finally, 2-D (r,θ) non-axisymmetric FRC equilibria in the presence of multipole fields have been analysed to study rotational stability [174, 264–266]. These studies reveal that two rotating MHD equilibria are possible for a long FRC in a multipole field: viewed from the end, one is nearly circular [264, 266], while the other is cusp-shaped [174, 265, 266]. The latter equilibria are usually obtained in experiments and hybrid simulations.

TABLE IV. THE PRINCIPAL FRC DIAGNOSTICS

Diagnostic	Information obtained
1. Excluded flux array	B_e, $r_s(z)$
2. Interferometry (side-on)	$\int$ ndr, n(r), end loss mapping
3. Framing camera (end-on) streak camera (side-on)	Gross plasma geometry and symmetry
4. Internal probes	B(r)
5. Monochromator	Impurity line intensities, T_e
6. Polychromator	T_i, rotational velocity
7. Neutron emission	T_i
8. Thomson scattering	$T_e(r)$, n(r)
9. Holography (end-on)	$\int$ ndz, particle inventory
10. Bolometry	Radiated power
11. B_θ and B_r probes	Symmetry
12. Pressure probe	End loss mapping
13. CO_2 laser scattering	Fluctuations

3.2. Experimental characterization

3.2.1. Plasma parameters and diagnostics

After formation, FRC equilibria of up to 100 μs duration have been observed before the onset of the n = 2 rotational instability. When this mode is stabilized by external multipole fields [22, 23, 20], the observation time of FRC equilibria can be extended to a few hundreds of microseconds. In modern FRC experiments, the typical parameters during the equilibrium phase are: $n \sim (1\text{–}5) \times 10^{15}$ cm^{-3}, $B_e \sim 5\text{–}10$ kG, $T_e \sim 0.1\text{–}0.2$ keV and $T_i \sim 0.1\text{–}1$ keV. The separatrices have radii $r_s \sim 5\text{–}20$ cm and elongations $\ell_s/2r_s \sim 3\text{–}10$. Typical values of x_s are in the range 0.4–0.6, although values as high as 0.9 have been achieved [132]. Well formed FRCs have values of ϕ of up to 6 mWb, as shown in Fig. 16, corresponding to values of s in the range 1–2.

The principal diagnostics used to characterize FRC equilibria are listed in Table IV. An attempt has been made in this table to arrange these diagnostics by frequency of use. The excluded flux array is probably the most useful diagnostic in studying FRC equilibrium as well as FRC formation: it usually consists of external B_z magnetic probes and flux loops that measure the FRC diamagnetism. The array can be simplified [267] by using a single flux loop, or even no flux loop at all when a vacuum region exists within the flux conserver. This simple, non-perturbing diagnostic is particularly suited to the very high beta FRC equilibria and has been used since the earliest days of FRC research [88]. The excluded flux radius $r_{\Delta\phi}$ is defined by $(\Delta\phi/\pi B_e)^{1/2}$, where $\Delta\phi$ is given by Eq. (4). In the vicinity of the axial midplane, $r_{\Delta\phi}$ approximates r_s quite well for elongated FRC equilibria [19, 268, 30]. Furthermore, the $r_{\Delta\phi}(z)$ profiles follow fairly closely the separatrix shapes $r_s(z)$ as long as their axial variations are sufficiently weak [268, 30]. The excluded flux array permits one to infer ϕ (and therefore τ_ϕ) by using Eq. (11) and assuming some constant value of ϵ (see Eq. (11)) [269, 241, 20]. The latter assumption was found good in some cases [241, 34], but it could cause significant errors in ϕ and τ_ϕ if ϵ varies monotonically during the FRC equilibrium phase [252]. The excluded flux array also allows one to infer the FRC energy confinement times τ_E [270]. Obtaining so much information from this simple measurement is a privilege of the high beta, elongated FRC equilibria.

Another relatively simple diagnostic that proved quite useful in studying FRC equilibria is side-on interferometry. This is because the density is fairly uniform inside the separatrix and rapidly becomes negligible on open field lines, which allows the path length to be defined as $2r_{\Delta\phi}$ for a single pass. With a chord aligned along a diameter, one can define the average density as $\langle n\rangle = \int ndr/2r_{\Delta\phi}$ and, to a good approximation [271], the maximum density at the field null as $n_M = \langle n\rangle/\langle\beta\rangle$ ($\langle\beta\rangle$ is obtained from Eq. (10) with $x_s = r_{\Delta\phi}/r_c$). For typical FRC experiments, a convenient laser wavelength for side-on interferometry is the 3.39 μm helium-neon line. Vibrations cause few problems, owing to the short configuration lifetimes, but the time variations of $\int$ ndr can be quite severe during formation. Combined with an excluded flux array, a single chord of side-on interferometry provides a good estimate of the separatrix particle inventory N and of the particle confinement time τ_N. Assuming radial equilibrium, the same combination permits estimation of the total temperature $T_e + T_i$. Multichord measurements at the coil midplane yield valuable density profile information [271, 253, 272].

The other diagnostics listed in Table IV have all proved quite useful. They will not be discussed further in this review because they are not as specific to FRC physics as the excluded flux array and side-on interferometry. Virtually all FRC experiments use diagnostics 1 and 2, most of them use diagnostics 3 and 5, the other diagnostics being used occasionally when the value of a specific parameter is desired.

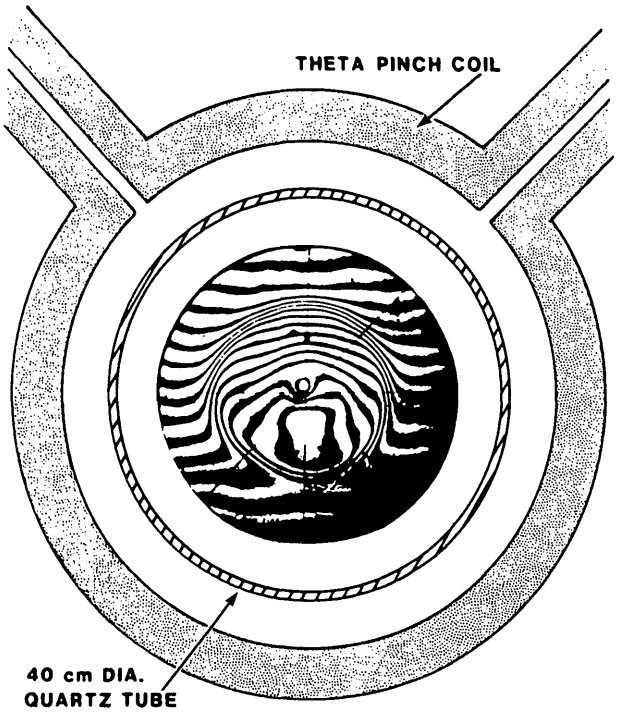

FIG. 19. End-on FRC hologram for the equilibrium phase [20].

3.2.2. *Experimental results*

Evidence for a high beta closed field line configuration comes from various measurements. First, internal probes have revealed the existence of a reversed magnetic field [76, 77, 95, 99, 100, 113] in early experiments. More recently, with reduced plasma pressure and larger dimensions, such measurements were extended through the entire FRC equilibrium phase [130, 132, 137]. This allowed the magnetic field radial profiles to be determined either at the midplane [140] or at all axial locations on translated FRCs [191, 192]. Second, end-on holograms from the FRX-C device [273] provided a strikingly graphic evidence of FRC equilibria. Such a hologram is shown in Fig. 19: sharp density gradients are clearly seen near the separatrix (its location agrees well with $r_{\Delta\phi}$ measurements), separating a fairly uniform high density inner region from a near-vacuum exterior region. Third, axial profiles of excluded flux radius and line integrated density gave further evidence of high beta FRC equilibria. Such profiles, shown in Fig. 20, present large drops in $r_{\Delta\phi}$ and $\int$ ndr near the end of the coil that suggest a closed field structure.

Measurements of midplane FRC radial density profiles have been made. Multichord $\int$ ndr data [271, 253, 272] were best fitted by the radial density profiles shown in Fig. 21. Similar density profiles were obtained from Thomson scattering data [19] and inferred from end-on luminosity [74, 111, 112] and holography [274]. These profiles are characterized by a central density hole and steep gradients near the separatrix. Typical values of n_s/n_M are in the range 0.5–0.6 [19, 271, 253, 272]. The density hole is not easily observed in end-on holograms such as in Fig. 19 because of the presence of open field line plasma beyond the ends of the FRC [274]. The parameter w shown in Fig. 21 has been defined [57] as the ratio of separatrix density gradient length δ to external gyroradius ρ_{ie}, evaluated with $v_i = (kT_i/m_i)^{1/2}$. Values of w of order unity were inferred early on [104, 19] and more accurate recent data [23, 273, 271, 275, 253, 272] suggest w values in the range 2–4.

Midplane radial profiles of electron temperature have been obtained over many discharges by single-point Thomson scattering measurements [19, 276]. The $T_e(r)$ profiles appear essentially uniform inside the separatrix and drop substantially on open field lines, with gradient lengths comparable to those of the density. A $T_e(r)$ profile obtained in the FRX-C device [276] at 5 mtorr fill pressure is shown in Fig. 22. Radial ion temperature profiles have not been determined experimentally, except for some Doppler profiles of carbon V line radiation [131] that suggested uniform T_i inside the separatrix. Such uniform profiles are almost ensured in present FRCs, with only about one gyro-orbit from the field null to the separatrix. With both temperatures essentially uniform radially, the midplane radial pressure profiles can be approxi-

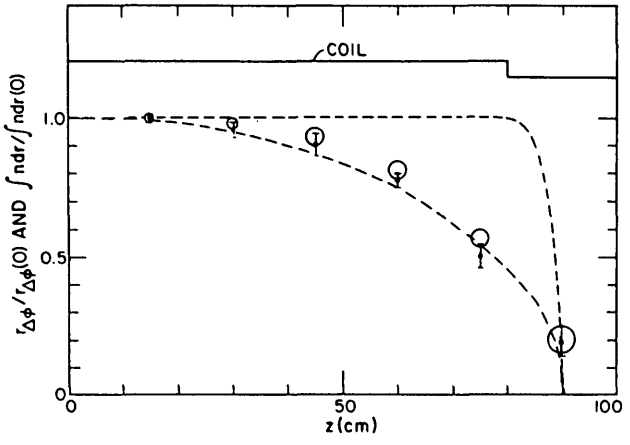

FIG. 20. Axial profiles of the line-integrated density $\int$ ndr and of the excluded flux radius $r_{\Delta\phi}$ during FRC equilibrium [271]. The open and solid circles are $\int$ ndr and $r_{\Delta\phi}$ data, respectively. The dashed curves are elliptical and racetrack contours.

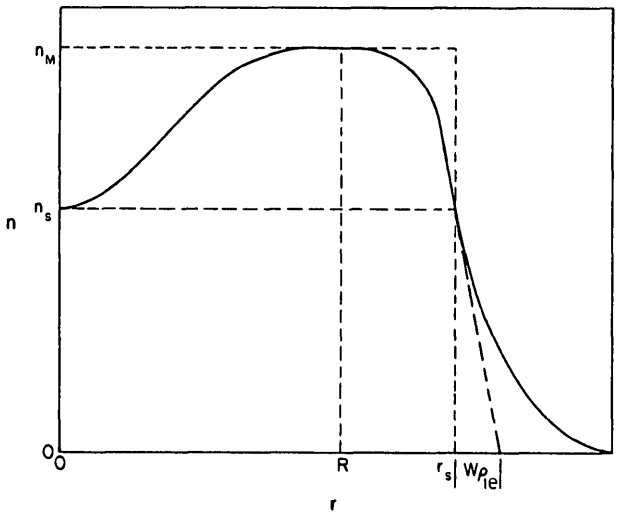

FIG. 21. Model of midplane radial density profile that fits best some FRC ∫ ndr data during the equilibrium phase [271].

mated by the density profiles of Fig. 21. In particular, one can write $\beta = n/n_M$.

The general properties of elongated FRCs inside a flux conserver, discussed in Section 3.1.1, have been verified within experimental errors. Radial pressure balance (Eq. (8)) has been checked within 50% by independent measurements of ∫ ndr, T_e, T_i and B_e [19]. For very collisional FRCs, where $T_e \sim T_i$ could be safely assumed, Eq. (8) has also been verified within 10–20% on FRX-C [276]. These FRX-C data are shown in Fig. 23. The relation $r_s = \sqrt{2}R$ (Eq. (9)) has been checked experimentally, by combining $r_{\Delta\phi}$ and end-on luminosity measurements [19], by internal magnetic probes [140, 191], and by combined $r_{\Delta\phi}$ and side-on interferometry measurements [271, 253, 272]. The axial condition $\langle\beta\rangle = 1-x_s^2/2$ (Eq. (10)) has been confirmed by radial density profile information [271, 253, 272], with the assumption $\beta = n/n_M$ mentioned previously. Finally, ϕ has been evaluated from internal probe data on translated FRCs [191, 192] and found consistent with the value predicted by Eq. (11) with $\epsilon = 0.25$.

Some data [19] have suggested that the shape of FRC separatrices is that of a racetrack, as in Fig. 1. However, recent measurements show that the separatrices are close to ellipses [271], as appears clearly in Fig. 20. The near-elliptical separatrix shape is also an essential ingredient in understanding the radial profiles of end-on holograms [274] and can be seen in every FRC translating past a fixed chord of side-on interferometry [21]. The ∫ ndr and $r_{\Delta\phi}$ axial profiles of Fig. 20 are similar, implying fairly uniform average density along the FRC length. To match these data, it was found necessary [248, 34] to compute 2-D equilibria with internal flux surfaces that have a gradual axial distribution.

During the FRC equilibrium phase, there is plasma on open field lines, as shown in Fig. 21, presumably from the continual leakage of particles from the separatrix volume. This plasma flows axially beyond the end of the separatrix, forming an exhaust region called the 'jet' [19, 271]. Such plasma end-flow was mapped with a piezo-electric pressure probe on the FRX-A device [19]. These data indicated a jet radius of 3–4 cm, an axial flow velocity comparable to the sound speed and a distribution outside the coil that approximately followed vacuum flux surfaces. Recent density measurements in the end region have confirmed this jet geometry [271].

3.3. Adiabatic compression and translation

3.3.1. Adiabatic compression

As demonstrated in many other magnetically confined plasmas, adiabatic compression provides large input

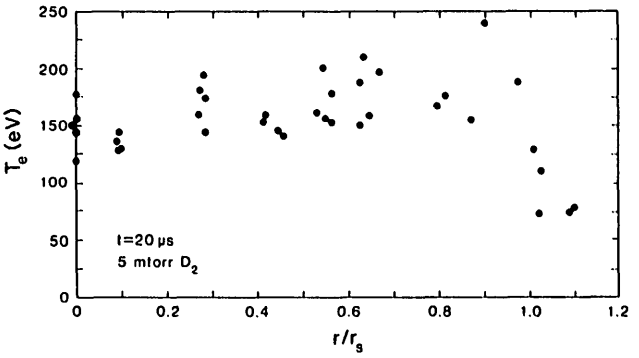

FIG. 22. Radial profile of the equilibrium FRC electron temperature measured by single-point Thomson scattering in the FRX-C device [276].

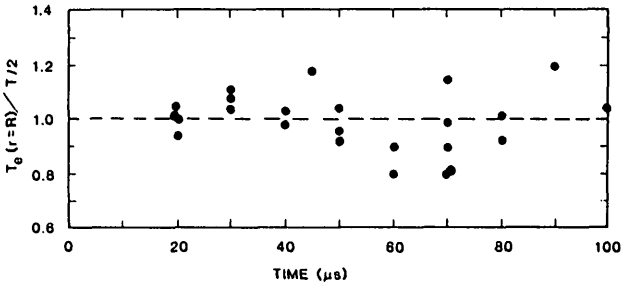

FIG. 23. Ratio of measured electron temperature T_e to the calculated half-pressure balance temperature T/2 as a function of time [276].

TABLE V. ADIABATIC COMPRESSION LAWS OF ELONGATED FRCs

Plasma quantity	Adiabatic scaling[a,b,c]
ℓ_s	$x_s^{2(4+3\epsilon)/5} \langle\beta\rangle^{-(3+2\epsilon)/5} r_c^{2/5}$
T	$x_s^{-4(3+\epsilon)/5} \langle\beta\rangle^{2(1-\epsilon)/5} r_c^{-8/5}$
n_M	$x_s^{-6(3+\epsilon)/5} \langle\beta\rangle^{-2(1-\epsilon)/5} r_c^{-12/5}$
B_e	$x_s^{-(3+\epsilon)} r_c^{-2}$

[a] $\langle\beta\rangle = 1-x_s^2/2$.
[b] Adiabatic coefficient of 5/3.
[c] ϵ is a profile parameter in the range 0–1.

power to the plasma in a fairly efficient and controlled manner. Adiabatic compression has been proposed in near-term FRC heating experiments [42] as well as in most FRC reactor concepts. It also occurs in present FRC experiments during formation, during the equilibrium phase (decompression) as B_e decays and during translation. Adiabatic compression here implies compression times that are long compared to collision times but short compared to confinement times. Approximate laws for adiabatic compression of elongated FRCs can be easily obtained by neglecting profile effects and considering radial equilibrium, $nT \sim B_e^2$, conservation of particles, $nV \sim$ const., and the adiabatic relation $nT \sim V^{-5/3}$. From these, one obtains $T \sim B_e^{4/5}$ and $n \sim B_e^{6/5}$. Then, ϕ conservation in Eq. (11) and $V \sim r_s^2 \ell_s \sim B_e^{-6/5}$ yield $\ell_s \sim r_c^{2/5} x_s^{2(4+3\epsilon)/5}$, assuming ϵ is constant during compression.

Analytical laws for the adiabatic compression of elongated FRCs have been obtained [241] that include profile effects. These laws are given in Table V, as functions of x_s and r_c for an adiabatic coefficient of 5/3. These laws are not much different from the simple relations derived in the previous paragraph. There are two types of adiabatic compression: flux and wall compressions governed by changes in x_s and r_c, respectively. The laws of Table V were derived by assuming that ϵ is constant during flux compression — an approximation that is suggested by some numerical modelling [241, 34]. These computations indicate that values of ϵ in the range 0.1–0.3 are appropriate for present FRX-C data. One can recover from Table V for $\epsilon = 0$ and 1 results derived directly with the limiting sharp-boundary profiles [235, 236, 19, 238]. The laws of Table V are in good agreement with 2-D numerical studies of FRC adiabatic compression [244, 245, 30, 241, 34] as long as the FRC remains elongated. This is the case for wall compression, since $\ell_s \sim r_c^{2/5}$ and the FRC elongation $\ell_s/2r_s$ actually increases as r_c decreases. However, the FRC length shrinks rapidly during flux compression and the FRC elongation diminishes with x_s. For quasi-spherical separatrices, flux compression proceeds essentially in one dimension [245, 236, 30], and the laws of Table V do not apply.

Experimentally, wall compression has been performed in the Tor-liner device [195, 24]. In these medium-speed liner experiments, substantial FRC heating was achieved, with a total neutron yield of about 2×10^8. Zero-dimensional modelling [277] indicated that this neutron yield is consistent with volume compression ratios in the range 700–6000 and plasma temperatures of 1.5–3.5 keV, depending on whether Bohm transport or classical transport is assumed. Such large compression ratios were achieved by shaping the liner wall to obtain a near 3-D compression [24], for which global efficiencies of about 80% can be realized [278].

Flux decompression can sometimes be tested inside a theta pinch coil by reducing B_c. The main limitation here is that the FRC length should remain smaller than the coil length. In Fig. 24, the results of such decompression experiments in the FRX-C device [20] are compared with the limiting predictions of Table V. The theory is seen to be in reasonable agreement with the experimental data. Flux compression alone is a quite inefficient heating mechanism because x_s decreases and most of the input energy ends up in the large volume of external magnetic field. Net heating efficiencies are a few per cent, comparable to those of FRC formation in most FRTPs. This is in contrast to wall compression, for which x_s remains constant and high efficiencies can be obtained. Therefore, proposals for FRC heating by adiabatic compression usually combine flux and wall compressions [37, 38, 229, 25, 42] in a passive liner approach allowed by FRC translation. A perhaps even more efficient way to achieve adiabatic compression has been conceived by Bellan [279]: a travelling magnetic mirror permits a 3-D compression at constant magnetic energy. This concept has not yet been tested on a compact toroid.

The heating of FRCs after formation can also be achieved by other means: high energy particle injection is a possibility, in particular with neutral beams. Radio-frequency heating has been considered for high beta plasmas [280, 281]. These studies of magneto-acoustic oscillations suggest that the wave can penetrate the plasma and should couple to the ions. For the theta pinch geometry, enhanced plasma heating was found with a reversed field trapped inside the plasma [281].

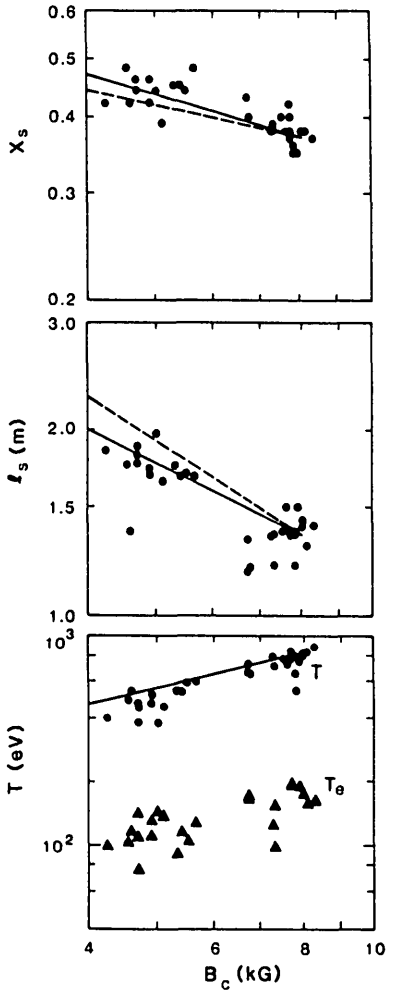

FIG. 24. Variations of x_s, separatrix length ℓ_s, pressure balance temperature and electron temperature as functions of the crowbar field B_c for 5 mtorr FRX-C data [20]. The limiting predictions of adiabatic theory (Table V) are indicated by dashed lines for $\epsilon = 0$ and solid lines for $\epsilon = 1$.

Laser heating, possibly relevant to FRC formation, has also been considered [282].

3.3.2. *Translation*

There is considerable motivation for FRC translation [5, 26]. First, it permits a more efficient use of adiabatic compression to heat FRCs, as mentioned above. Second, it eliminates the need for some expensive power crowbar system to prevent B_e decay in the source. Third, it permits straightforward use of vacuum-coupled diagnostics, yields axial profiles at times when an FRC transits past a diagnostic's field of view, and it may permit a novel fuelling method by translating the FRC onto a pellet [283]. Fourth, translation onto a pellet or into a flux conserver of smaller radius may provide some increase in the parameter s. Fifth, translation is a key ingredient in many FRC reactor studies because it allows the high technology formation region to be separated from the burn and quench chambers.

Successful FRC translation has been achieved in several experiments. FRC motion is most often initiated by using uneven driven magnetic mirrors at the ends of the theta pinch coil [19, 284, 25, 5, 285]. One can induce an asymmetric field line connection by a magnetic plunger inserted at one end of the coil [231] or by impurity blow-off [182]. A slightly conical theta pinch coil in FRX-C/T has also provided successful FRC translation [26]. An example from the FRX-C/T device is shown in Fig. 25, with $r_{\Delta\phi}(z)$ profiles as functions of time. An FRC is formed with 5 mtorr fill pressure inside the 2 m long coil of 1.4° cone angle (the coil midplane is at z = 0) and is accelerated in about 20 μs into a 5 m long flux conserver. From Fig. 25 it can be seen that the FRC reflects three times from magnetic mirrors and is trapped after a total trajectory of about 16 m. Confinement analysis of such translated FRCs [21] revealed that, in most cases, translation does not alter the FRC confinement, in spite of considerable deformation of the separatrix and translation velocities approaching Alfvén velocities. The main features of FRC translations such as in Fig. 25 have been found to be in good overall agreement with 2-D numerical modelling [26].

FRC translation can be most easily understood by assuming equilibrium at all times. It is useful to consider the total energy E_T inside the entire flux conserving volume (source and translation region). This energy consists of plasma thermal and kinetic energies and magnetic field energy. Using Eqs (8–10), one obtains (see Refs [139, 26]):

$$E_T = \frac{5}{2} NkT + \frac{1}{2} Nm_i v_z^2 + E_{BV} \qquad (13)$$

where N is the ion inventory, T is the total (ion + electron) plasma temperature, v_z is the axial translation velocity and E_{BV} is the vacuum magnetic energy (in the absence of plasma and assuming the same magnetic flux at the coil wall). Neglecting possible small changes in E_{BV} and N, Eq. (13) yields the FRC axial velocity in the translation region $v_z = (5k\Delta T/m_i)^{1/2}$, where $\Delta T = T_1 - T_2$ is the change in T from the source ($v_z = 0$) to the translation vessel predicted by the adiabatic theory. The translation velocity can be conveniently adjusted by changes in the

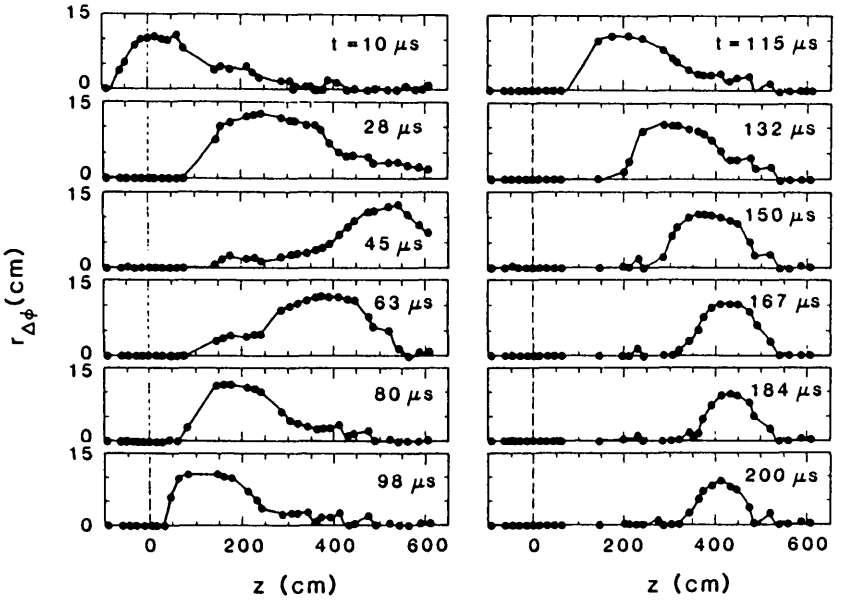

FIG. 25. Excluded flux radius profiles as functions of time for a translated FRC from the FRX-C/T device [26].

DC vacuum guide field strength B_0 of the translation region. Reducing B_0 causes the FRC to cool, so that ΔT and v_z increase.

Experimentally, one observes values of ΔT somewhat smaller than predicted by the adiabatic law of Table V: the plasma expands more and cools less in the experiment, presumably because the translation times are comparable to the ion-ion collision times, which violates the reversible adiabatic assumptions. Indeed, higher values of T_2 are predicted by collisionless models [284, 286], which may be more appropriate for these data. The measured velocities v_z are shown in Fig. 26 as function of B_0 for 5 mtorr data from the FRX-C device [26, 20]. The predictions of the adiabatic law (with $\epsilon = 0.25$) of Table V are shown in Fig. 26 as a dashed curve. One observes reasonable agreement between theory and experiment for the largest values of B_0. However, for small values of B_0, v_z appears to saturate as it approaches the ion thermal speed of about 20 cm·μs^{-1}. These results are consistent with the departure from adiabatic theory mentioned previously, which increases at higher values of v_z.

When a translating FRC reflects off a magnetic mirror, its axial kinetic energy is reduced [284, 139, 287, 26]. This effect is also seen in 2-D MHD simulations [26] and provides an easy way of trapping the FRC inside the translation vessel without pulsed gate magnet coils. The measured ratio of reflected to incident speeds for FRX-C/T data [26] is shown in Fig. 27 as a function of B_0. These data indicate that the magnitude of v_z is reduced by 20–50%. Similar values have been reported on other experiments [284, 139]. The largest losses in axial kinetic energy (about 75%) appear to occur for the fastest moving plasmas. This inelasticity of magnetic mirror reflection is observed to be independent of the mirror ratio. However, substantial confinement degradation has been reported [139, 287, 21] when FRCs interact with strong mirrors whose magnetic scale lengths are much

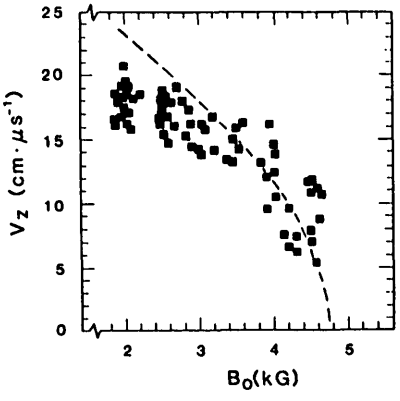

FIG. 26. Axial velocities of translated FRCs in the FRX-C/T device as functions of the guide field in the translation vessel [20]. The dashed curve is the prediction of adiabatic theory.

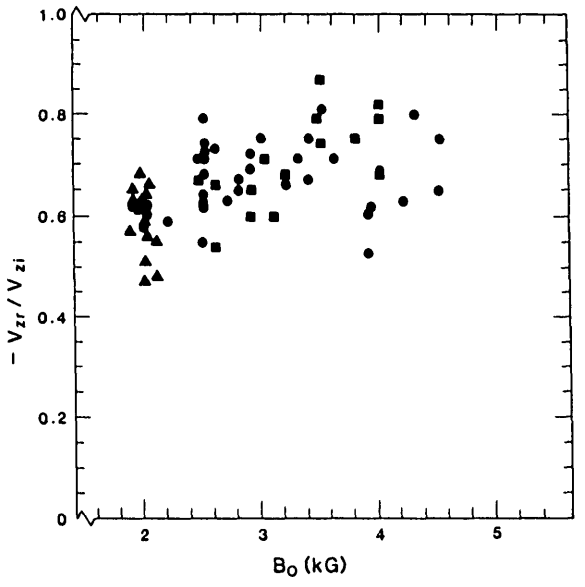

FIG. 27. Ratio of reflected to incident axial velocities as a function of the translation guide field, for FRCs reflecting off a magnetic mirror in the FRX-C/T device [26]. The symbols are for different mirror ratios.

shorter than the FRC lengths. This indicates that there are limits to the otherwise extreme robustness of translating FRCs.

Interestingly, in some cases the kinetic energy lost during a mirror reflection does not appear to thermalize into the plasma [287, 26]. If thermalization occurred without change in E_{BV}, Eq. (13) would predict equal values of T from initial to final states with $v_z = 0$ [139]. This was approximately observed in one case [139] and the increase in ion temperature after reflection was clearly measured [288]. For some other cases, the kinetic energy appears to be lost by processes that are not understood. It has been proposed [287, 192, 26] that this energy might be stored inside the FRC separatrix as plasma oscillations, but there is no experimental or numerical evidence of such effects. Reactor studies involving FRC translation [37, 38] consider axial velocities that are much smaller than the thermal velocities. For such cases, the issue of kinetic energy thermalization is purely academic and FRC translation should be in good agreement with the reversible adiabatic theory of Table V.

In present experiments, the relatively short FRC confinement times force compression and/or translation time-scales that are too short to satisfy the reversible adiabatic assumptions. In a sense, present data have demonstrated successful and efficient FRC translation in the most difficult conditions. Finally, FRC translation in a vessel that does not conserve flux has been analysed [289]. This case is of interest when adiabatic flux compression follows FRC translation [229, 42]. Such translation requires higher values of B_0 and produces lower values of T relative to translation into a flux conserver.

4. STABILITY

This section includes only FRC macrostability (microstability is reviewed in Section 5). Gross FRC stability is an intriguing issue: while many modes are predicted, FRC lifetimes are not limited by any instabilities at the present time, although the difficulty in FRC formation at larger sizes, discussed in Section 2.5.4, may perhaps be related to a reduction in stabilizing factors. This situation is in contrast to early experiments that were plagued by various tearing and rotational modes. It is possible, as will be discussed here, that stability might become again a limiting factor in future, more MHD-like, FRC experiments.

4.1. Theory versus experiment

4.1.1. General picture

At this point, most plasma physicists would probably conclude that FRCs should be inherently unstable. This is a natural conclusion based on the MHD model that applies to most magnetized plasma configurations: indeed, as seen in Fig. 1, the FRC topology is similar to some elongated, low aspect ratio, toroidal version of the Z-pinch. As was soon evident experimentally in the earliest days of fusion research, the Z-pinch is quite unstable to kink and sausage modes in the absence of toroidal field.

The principal instabilities predicted for the FRC are listed in Table VI, and it is indicated for each mode whether there has been an observation. The tokamak nomenclature has been adopted here, with n and m being the toroidal and poloidal mode numbers, respectively (the theta pinch convention of m and k_z for toroidal and axial mode numbers, respectively, is also frequently used in the FRC literature). Since the FRC poloidal cross-section is not circular, the meaning of a poloidal mode number m is not precise. Therefore, the poloidal mode character is also specified in Table VI as mostly radial or axial.

Various local and global non-rotating ideal MHD modes are listed in Table VI, but these modes have not been observed so far. Incidently, finite-n interchanges and n = 1, m = 1 tilt instabilities for the

TABLE VI. FRC STABILITY: MHD THEORY VERSUS EXPERIMENT

n (toroidal)	m (poloidal)	Mode character	Mode name	Experimental observation
1. Local ideal modes				
∞	0		Interchange	no
∞	1,2	Axial or radial	Co-interchange (ballooning)	no
2. Global ideal modes				
2(a) No rotation				
0	1	Axial	Roman candle	no
1	1	Radial	Sideway shift	no
≥1	1	Axial	Tilt	no
2(b) Rotation				
1	1	Radial	Wobble	yes[a]
2	1	Radial	n=2	yes[b]
>2	1	Radial	n>2	no
3. Resistive modes				
0	2	Radial and axial	Tearing	yes[c]

[a] Saturates at finite amplitude.
[b] Stabilized by multipole fields.
[c] Disappeared in modern experiments.

FRC correspond respectively to sausages and kinks for the Z-pinch. Two global ideal modes driven by rotation have been predicted and observed experimentally: the n = 1 'wobble', of little concern since it saturates at low amplitude, and the n = 2 rotational instability, which prematurely destroyed most FRCs until its recent suppression by external multipole fields [22, 23, 20]. Higher-order (n > 2) rotational modes have also been predicted, but these modes have not been clearly observed experimentally. Resistive tearing modes have also been identified: they were frequent in early FRC experiments but are seldom seen nowadays. Hence, present FRCs appear stable — a somewhat surprising fact from the MHD point of view. However, many FRC studies have identified various features that promote stability:

(a) The FRC has little toroidal field (none ideally) so that it has nearly closed field lines and the compressive energy of the high-beta plasma is a stabilizing factor [290, 291]. This effect is absent in plasma configurations with toroidal field for which the field lines are not closed.

(b) The low-beta open-field-line region outside the FRC separatrix is MHD stable because of the good curvature in the low-field end regions. External modes should be damped and possible internal modes may be more constrained. The axial plasma flow in the edge layer may also be stabilizing, in a similar way as in some mirror machines [292].

(c) The presence of a nearby conducting boundary is important for the stability of several modes listed in Table VI. This may explain in part the improved stability properties of modern FRC experiments which have lower radial compression of the plasma.

(d) The FRC flux surfaces are axially elongated (unlike the circular flux surfaces of a Z-pinch), which ensures a reduction in most MHD growth rates. Low pressure gradients around the field null and high pressures on the separatrix are also stabilizing [291].

(e) Toroidal rotation and Hall effects, which occur naturally, are stabilizing factors for the tearing and tilt instabilities.

(f) Kinetic effects are extremely important for present FRCs with values of s in the range of 1-2 and

may account by themselves for the observed FRC stability. Finite Larmor Radius (FLR) effects provide a reduction of the MHD growth rates and may stabilize all but the lowest mode numbers.

4.1.2. *Ideal MHD modes*

Local MHD modes have large toroidal mode numbers ($n \to \infty$), as indicated in Table VI. Although FLR effects probably reduce their growth rates or even stabilize them, the analysis of local modes is a good way to start because they have the largest ideal-MHD growth rates and because well known methods such as the energy principle [293] have been developed for their study. Among local modes, the interchanges (flutes), which have $m = 0$, are distinguished from the co-interchanges (ballooning), where m is a small non-zero integer. Interchanges can be unstable [291, 294, 295], but compressibility, low aspect ratio, large elongation and high separatrix beta may stabilize them. These effects are significant in present FRCs, but most of them should be reduced in future FRCs with large values of s and x_s.

Co-interchanges are incompressible modes (i.e. not changing the volume of a flux tube) and therefore they do not benefit from the stabilizing effect of compressibility. They are always found to be unstable for the FRC [296–300]. The most dangerous mode is the $m = 1$ kink [296, 298–300]; the $m = 2$ modes are marginally stable and the $m > 2$ modes are stable [296, 299, 300]. The growth rates γ_{MHD} of co-interchange modes are approximately $2v_A/\ell_s$. Hence, FLR effects may be quite important for elongated FRCs since MHD theory breaks down when γ_{MHD} is less than the ion diamagnetic frequency [299]. Dimensional analysis shows that this is the case if $s \lesssim e_s/2$ for the $m = 1$ mode ($e_s = \ell_s/2r_s$ is the FRC elongation). Similar values of γ_{MHD} have been found for racetracks and for elliptical separatrices [297].

If all local modes can be stable, global stability is ensured. This gives incentive to search for some sufficient condition for local stability. However, it is quite difficult to find a sufficient condition with a small gap between its requirements and the known necessary conditions, so that this approach tends to be overly pessimistic. This work is progressing [301] towards more optimistic sufficient conditions.

The lowest order global modes are not easily stabilized by FLR effects. For the FRC, the 'Roman candle' instability [54] is an $m = 1$, $n = 0$ axial shift that could eject the plasma out of the confining region. However, this mode is stabilized by a conducting boundary or by external end mirrors [291]. The latter ought not be too strong; otherwise they could destabilize another global mode, the $n = 1$, $m = 1$ radial shift, which could drive the FRC rapidly to the wall [291]. Under normal experimental conditions, both modes are stable. However, without a conducting boundary, either the axial or the radial shift modes are unstable.

As seen from Table VI, there are other non-rotating global modes: the $n \geq 1$, $m = 1$ tilt instabilities. Since FLR effects would probably influence the $n > 1$ modes most, the $n = 1$, $m = 1$ axial tilt is considered to be the most dangerous ideal-MHD mode for FRCs. Furthermore, the tilting of internal flux surfaces of an elongated FRC does not appear to be stabilized by conducting walls, external field shaping, or profile effects. Most of the theoretical effort on FRC stability has focused on the internal tilt mode (see Section 4.3), but this instability has not yet been observed. Finally, considerable theoretical and experimental work has been devoted to the global ideal modes driven by rotation, in particular the $n = 2$ rotational instability. This extensive work is discussed in Section 4.2.

4.1.3. *Tearing instabilities*

Many early FRCs tore spontaneously into several fragments along the coil axis. The physics of this phenomenon is, on a larger scale, similar to that of spontaneous field line reconnection near the field null described in Section 2.3.2. Tearing instabilities were only observed during FRC formation [91, 100, 101, 111–113, 152, 115]. They often occurred during axial contraction, with high bias fields and fill pressures [91, 111, 113, 115, 181]. They have also been correlated with weak [111, 115] or axially non-uniform [302] preionizations. The latter effect has also been noticed in 2-D MHD simulations [148]. Impurities [100, 130] and external perturbations, such as probe ports and side pockets on the discharge tube [100], or coil slots [115], can also induce tearing instabilities. Finally, these instabilities occurred less frequently with reduced radial compression [111, 5, 181].

Considerable research in the 1960s was devoted to the understanding and control of tearing, in particular as the FKR theory [188] was developed. Many experiments tried to correlate the experimentally observed tearing growth rates which the predictions of the FKR theory, sometimes finding agreement [91, 111, 113], sometimes finding significantly lower growth rates than predicted [101, 152, 115]. In most of the intermediate FRC experiments listed in Table II, tearing became

infrequent [110, 115] and a large discrepancy between experiments and FKR theory was noted [115].

These observations strongly suggest that, although the FRC is vulnerable to tearing instabilities during the highly dynamic formation phase, these modes can be avoided with proper care. This illustrates once more the importance of a good, uniform and clean preionization, the need to minimize violent axial contractions or expansions (the latter can occur with poor crowbar of the external magnetic field), and the likely benefit of lower radial compression in intermediate and modern FRC experiments.

Once FRCs survive the formation phase, their subsequent equilibria appear quite stable to tearing. This is reasonably understood, since many stabilizing factors have been identified, most of them discussed by Eberhagen and Grossman [115]. First, a nearby conducting boundary can stabilize resistive tearing modes [303–305]. This conducting boundary may be relatively far from the FRC separatrix for flux-excluding radial pressure profiles [305]. Second, tearing modes can be stabilized by non-linear effects in a collisionless plasma, provided that the initial perturbation is sufficiently small [306]. This may explain why careful formation proves effective in preventing tearing instabilities and why these modes are seldom observed after formation. Third, plasma rotation is a stabilizing factor for tearing instabilities [115, 307, 304], in particular for low enough initial perturbation [115]. Finally, for a rotating FRC, Hall terms also have a stabilizing influence on tearing modes [307, 304].

4.2. Rotational instabilities

4.2.1. Instabilities of a rotating FRC

In most cases, the FRC current just after formation is primarily carried by electrons, while ions are approximately at rest. However, as in zero-bias theta pinches, most FRC experiments show that the ions soon begin to rotate in the ion diamagnetic direction. This rotation often reaches a sufficiently high level to cause instabilities. The origin of the rotation is not yet completely understood (it is discussed in Section 4.2.2). On the other hand, given the rotation, the conditions for instabilities are fairly well understood.

In many theta pinches with zero bias, a rotating n = 1 'wobble' is observed to grow and to saturate at finite amplitude. In most FRC experiments, it is a destructive n = 2 mode that grows after a stable period τ_s. This is illustrated in Fig. 28(a), where the n = 2 instability appears as a growing modulation of

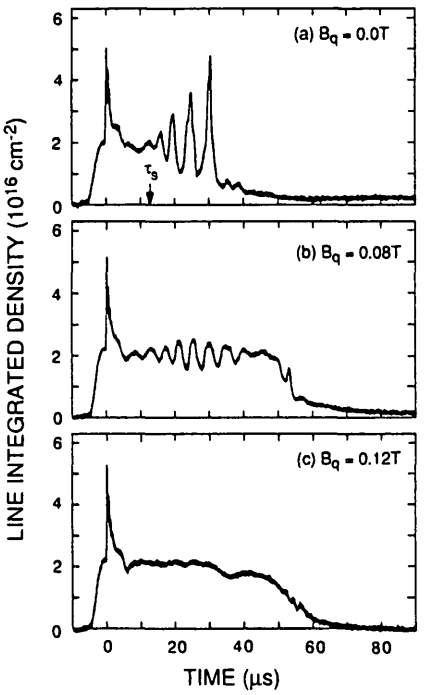

FIG. 28. Stabilization of the n=2 rotational instability by external quadrupole fields in the PIACE device [22]. Traces of side-on interferometry are given as functions of time for (a) B_q = 0, (b) B_q = 0.08 T and (c) B_q = 0.12 T. B_q is the maximum quadrupole field strength at the separatrix.

the line integrated density at $\tau_s \sim 13$ μs. This modulation corresponds to an area preserving [271], elliptical deformation of the plasma cross-section. When the major radius of the ellipse equals r_t, the FRC quickly disrupts, as is seen at about 25 μs in Fig. 28(a). This troublesome instability almost put an end to FRC research in the 1960s, in favour of zero-bias theta pinches [108].

In the MHD limit, theta pinches are marginally stable to the n = 1 rotational mode and unstable to n ≥ 2 modes. For $k_z = 0$, the growth rate is $\sqrt{n-1}\Omega$, where Ω is the plasma rotational frequency. However, when kinetic effects are included, unstable modes are only found beyond some threshold in Ω [116]. Using a linearized fluid model with FLR corrections, Freidberg and Pearlstein [308] found that an n = 1 mode with finite k_z first develops, in agreement with experimental data [309]. The stability threshold was expressed in terms of a parameter α

$$\alpha = \Omega/\Omega_{Di} \tag{14}$$

where Ω_{Di} is the ion diamagnetic drift frequency. The threshold for the n = 1 mode was α = 1, and an n = 2 mode could also grow for α greater than

1.2–1.4. For FRCs, the n = 2 mode was predicted to grow first, with a threshold value $\alpha \gtrsim 1.6$ for some data from the FRX-B device [130]. This result was suspect because the FLR expansion breaks down near the field null for the FRC case. However, a similar threshold, $\alpha \sim 1.3$–1.5, was found by Seyler [310] with the exact Vlasov fluid equations. Seyler also predicted $\omega_r/\Omega_{Di} \sim 1.7$ (ω_r is the real part of the mode frequency). These kinetic results imply $\omega_r > \Omega$, while MHD theory including FLR corrections would predict $\omega_r = \Omega$ [116, 118, 310]. The fastest n = 2 growth was found for $k_z = 0$. Finite values of k_z led to lower growth rates because of field line bending effects [310]. The n = 1 mode was also predicted for the FRC case, with lower growth rate and higher threshold than for the n = 2 mode.

The n = 2 rotational instability has also been observed in 3-D ideal MHD simulations [311]. With a 2-D hybrid code, Harned [312] observed the instability for very low values of α. The discrepancy with the Vlasov fluid prediction of Seyler [310] was tentatively attributed to resonant ions. Interestingly, Harned also found some modes with n = 3, 4 and 5, for cases with reduced pressure on the separatrix. Presumably, these modes are FLR stabilized in present FRC experiments. Non-linearly, both the real and imaginary parts of the n = 2 modal frequency were observed to saturate or even to decrease in time.

These theoretical results are in fair agreement with the available data. The values of Ω can be estimated by end-on luminosity [110, 115], side-on interferometry [271] or visible light measurements [25, 135, 313], Doppler broadening of impurity lines [114, 130, 19, 20] and neutral beam spectroscopy [288]. Doppler broadening measurements on the FRX-B device yielded values of α around 0.4 [130]. More recent measurements suggest threshold values of α in the range 1–2. There are large uncertainties because Ω_{Di} is usually inferred to have a rigid rotor profile and because most measurements require the n = 2 mode to be well into a non-linear regime or because they assume equal impurity and plasma rotations [130, 19]. The most reliable technique to date is presumably neutral beam spectroscopy, which yielded a threshold value of $\alpha \sim 1$–1.2 for the n = 2 mode [288].

FRCs are observed to rotate in the ion diamagnetic direction ($\alpha > 0$ in Eq. (14)) and simultaneous measurements at various axial locations show that the n = 2 instability has $k_z \simeq 0$. The stabilizing influence of finite k_z may explain why the n = 2 mode was not observed for a nearly spherical FRC [314]. An n = 1 'wobble' of finite amplitude has also been observed [271, 23, 253, 272]. Saturation or decrease in time of the n = 2 non-linear growth rate and real frequency have been observed in several experiments. Finally, recent measurements [288] indicate $\omega_r > \Omega$, which may be the first experimental evidence of ion kinetic effects.

4.2.2. *Origin of the rotation*

Over three decades, many theories have been proposed to explain the origin of the plasma rotation in theta pinches. Most of these studies rely on Hall currents or on off-diagonal ion pressure tensor terms; they have been reviewed by Haines [125]. Several models assume that the plasma column does not acquire angular momentum as a whole, but that it separates into distinct fragments rotating in opposite directions: the separation could be radial [123, 125] or axial [122]. Various schemes involving contact of the plasma with the discharge tube have been conceived [118, 120, 125]. Thermoelectric effects have been invoked as a possible source of plasma rotation [121]. Transverse fields from external multipole conductors or field errors can induce plasma rotation [119, 104, 114, 124, 127]. End-shorting of the electric field on open field lines has been proposed as a spin-up mechanism [87, 92, 315, 126, 316–318]. Finally, particle loss has also been identified as a possible source of plasma rotation [115, 319, 237, 320–322].

Most of the above theories do not really account for the experimentally observed rotation rates. There has been no evidence for oppositely rotating plasma fragments in FRC experiments. Some of the theories involving wall contact or thermoelectric effects have been found incorrect [125]. Transverse fields can explain the plasma rotation in experiments with external multipoles [102–107, 114], but in experiments without multipoles the existence of small field errors has to be taken into account [104]. When such errors are known to be quite small, one cannot account for the observed spin-up [315]. While several of the above effects could contribute to the FRC rotation, the two most promising mechanisms that have been considered so far are probably particle loss and end-shorting.

Particle loss can induce a plasma rotation in the ion diamagnetic direction. Indeed, examination of particle orbits reveals [256, 323] that particles lost out of the FRC separatrix have a preferred sign (negative) of their angular momentum. Therefore, as they leave, the remaining plasma gradually acquires a net (positive) rotational motion. Lost particles could include a class of particles unconfined in velocity space [322] and

particles lost by radial diffusive transport [115, 319, 237], possibly driven by some microinstability [320]. For present FRC parameters, a loss of about half the particle inventory would result in a rotation with $\alpha = 1$ [237, 238, 321], which suggests comparable values of τ_s and τ_N. Particle loss in 2-D hybrid simulations [321] led to a localized rotation near the separatrix; this rotation suddenly relaxed, allowing the bulk of the plasma to rotate sufficiently to drive the n=2 instability. The relaxation did not require collisional viscosity and suggested the presence of some instability driven by velocity shear such as the Kelvin-Helmoltz instability [324].

End-shorting of the radial electric field on open field lines causes this region of the plasma to rotate in the ion diamagnetic direction. This can be seen from the radial component of the ion fluid equilibrium equation, which reduces to $\alpha = 1$ for zero electric field. End-shorting explains fairly well the rotation in zero-bias theta pinches where all field lines are open [316, 309]. For the FRC, a two-step process has to be invoked: first, end-shorting causes the edge layer to rotate and, second, viscous friction spins up the separatrix volume. This two-step process has been analysed by Steinhauer [318], who found three regimes, depending on the relative importance of the spin-up time ℓ_c/v_A of the open field lines compared with the viscous transfer time to the closed field lines. For most FRC experiments with moderate values of x_s, plasma pressure and viscosity are high at the separatrix and τ_s scales as ℓ_c/v_A. For high values of x_s and low values of β_s, the separatrix viscosity is low and $\tau_s \gg \ell_c/v_A$. There is also an intermediate viscosity regime.

Experimentally, it has not been possible so far to make a definitive case for particle loss or end-shorting [135]. Comparable values of τ_s and τ_N have sometimes been obtained, as is appropriate considering particle loss. Two empirical scaling laws based on particle transport were found to be consistent with the τ_s data available at the time; the first law, $\tau_s \sim n r_s \ell_c \ell_s$, comes from an estimate of the FRC particle confinement time τ_N based on open-field-line axial flow [325]. The second law, $\tau_s \sim \tau_N \sim R^2/\rho_{ie}$, was proposed [19, 326] following the numerical work of Hamasaki and Krall [327]. To test the particle loss theory of FRC rotation, it has recently been proposed to put a divertor on the separatrix, thereby losing most particles without a preferred value of angular momentum [328]. Several observations are consistent with the end-shorting theory [318], such as increased values of τ_s for larger coil lengths [72, 73, 80, 115, 19, 329, 313] and fill pressures [92, 130, 114]. On the STP-L device, direct

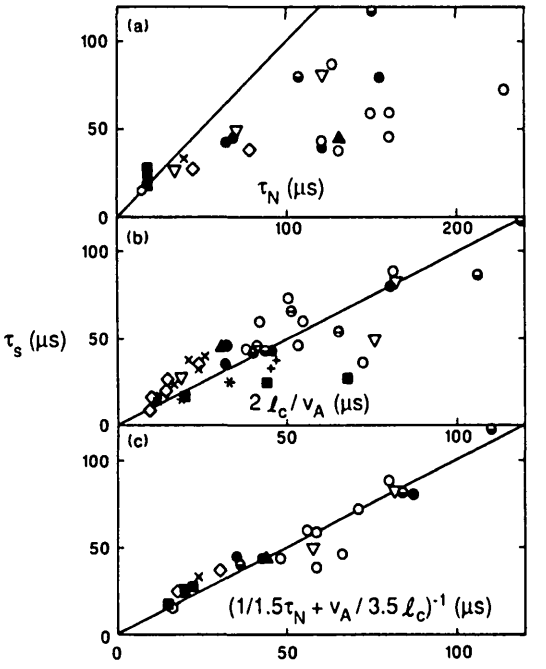

FIG. 29. Comparison of several scaling laws for the observed stable periods τ_s of various FRC experiments [331]. The symbols are explained in Table III.

measurements of edge layer rotation and of the delay in τ_s with guide fields at the ends of the theta pinch coil give partial support for the end-shorting process [329] and also for particle transport [330].

A recent survey of the available τ_s data suggests that neither particle loss nor end-shorting account by themselves for all experimental results [331], as illustrated in Figs 29(a) and 29(b). However, the assumption that both processes contribute to the plasma rotation is consistent with nearly all data, as shown in Fig. 29(c). In most experiments, end-shorting dominates the spin-up process, with a τ_s scaling similar to the one of Fig. 29(b), as long as FRCs retain high viscosity.

It should be noted that no spin-up mechanism is required to achieve $\alpha > 1$ by itself because several processes could be simultaneously active, because the n = 2 mode can grow with $\alpha < 1$ [312, 321], and because many effects can cause a gradual increase of α for a given acquired angular momentum [19]. The latter effects include internal flux loss [116, 117, 73, 75, 92], equipartition of electron and ion temperatures [92, 116, 19], and radial compression [19]. They may also explain in part the absence of observable n = 2 instability in several experiments [5, 132]: for example, a rapid B_e decrease would lower α substantially. In addition, the n = 2 mode may be delayed or even suppressed in those experiments by large values of x_s

because of reduced particle loss and low viscosity. The latter may cause τ_s to exceed τ_ℓ and may also cause velocity shear stabilization [332].

4.2.3. *Multipole stabilization*

The influence of external multipole fields on FRC rotation was noticed in some early experiments [80, 102, 114]. The onset of the n = 2 instability was delayed and plasma centring did improve with added hexapoles [80, 102]. However, transverse fields were also identified as a potential cause of plasma spin-up, theoretically [125] and experimentally [114]. These somewhat conflicting observations left some doubt about whether multipole fields were actually helpful or harmful, and their use in FRC experiments was forgotten until recently.

Suppression of the n = 2 instability by applied multipole fields was first clearly demonstrated in the PIACE device [22]. These results are shown in Fig. 28: for given FRC conditions, the destructive n = 2 instability of Fig. 28(a) is controlled in Fig. 28(b) and suppressed in Fig. 28(c), with increasing quadrupole strength. Similar results with octopoles [23] and quadrupoles [20] were reported soon after the first demonstration and multipoles became widely used. At first, it was believed that multipoles had to be applied just after FRC formation [22], but the stabilization was found to be insensitive to quadrupole field timing (over the range -2 to +40 μs) in the FRX-C device [20]. Multipole stabilization is clearly illustrated by end-viewing holograms such as those presented in Fig. 30: the n = 2 distortion, present at late times without quadrupoles, is suppressed with quadrupoles, leaving the FRC plasma with a nearly square cross-section [20]. This cross-section is displaced by about 45° from what one could expect with Bernoulli's law [266]. This displacement is also observed in numerical simulations [265] and can be explained in terms of cusp-like equilibria [266].

Multipole stabilization was first studied theoretically by Ishimura [264] with an MHD model. Assuming that the FRC cross-section remains nearly circular and that the multipole fields are excluded from the separatrix volume, he predicted stability of the n = 2 mode for sufficient multipole field strength. The threshold is

$$B_{th} = r_s \frac{\Omega}{2} \left(\frac{\mu_0 n_M m_i}{\ell - 1} \right)^{1/2} \qquad (15)$$

where 2ℓ is the order of the multipole field. B_{th} in Eq. (15) refers to the maximum multipole strength at the separatrix, without plasma or nearby conducting boundaries. When the presence of the FRC and of the coil are taken into account, the separatrix multipole field is approximately doubled [22, 313].

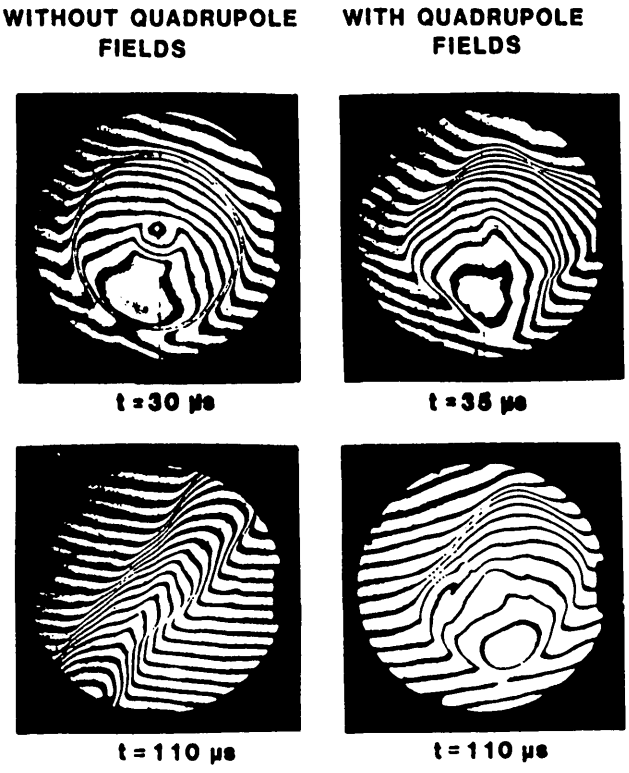

FIG. 30. End-on FRC holograms illustrating multipole stabilization of the n=2 rotational instability [20].

Equation (15) indicates that stability is achieved when the average multipole field pressure at the separatrix equals the centrifugal pressure of the rotating plasma. This result looks quite robust, but it is more pessimistic than experimental observations: Eq. (15) overestimates the required field strengths by about a factor of four for quadrupoles [22, 20, 313] and by a factor of two for octopoles [23, 288]. Numerical modelling of quadrupole stabilization with a 2-D hybrid code [265, 313] reduced to one-half the discrepancy between theory and experiment and suggested that kinetic effects are important. The rather large discrepancy between experiments and the MHD analysis [264] is also caused in part by several assumptions: first, the mode coupling between the n = 2 perturbation and the n = 2ℓ pressure modulation caused by the multipoles was neglected, which proved correct for higher-order multipoles but not for quadrupoles [264, 266]. Second, the equilibrium plasma cross-section in the presence of the multipole fields

was assumed to be circular: this is a good approximation for higher-order multipoles but not for quadrupoles, since a nearly square equilibrium is observed in experiments [20], in numerical simulations [265] and also in equilibrium analysis [266]. Square equilibria may be more stable than circular ones [266]. Finally, stabilizing field line bending effects [310] associated with finite plasma length were neglected [264]. A modified MHD analysis [333] that considers finite plasma length yields smaller values of B_{th} than those predicted by Eq. (15), in better agreement with experimental data.

In general, the applied multipole fields do not suppress the plasma rotation but merely prevent the n = 2 deformation from growing. This is clearly shown by a residual modulation on various diagnostics [20, 23, 135, 288], when the multipole strength is insufficient to completely suppress the instability (see Fig. 28(b)). The elliptical deformation also reappeared as soon as translated FRCs entered a region without multipoles [313]. Plasma rotation in the presence of multipoles has also been noted in 2-D hybrid simulations [265]. However, some impurity measurements have suggested that the FRC rotation can be suppressed when multipole fields are applied [20, 334], sometimes in conflict with hydrogen rotation data [334].

A sustained FRC rotation in the presence of multipole fields can prove beneficial, for several reasons. First, plasma rotation may help stabilize tearing and tilting modes. Second, rotation limits the penetration of external multipoles past the FRC separatrix to a small skin depth. This may minimize possible deleterious effects of field line opening [174, 335] and may explain why FRC confinement does not appear to be appreciably degraded by applied multipole fields [20, 23, 313], at least for field strengths smaller than B_{th} [313]. Whether multipoles will remain effective and harmless on the longer time-scales expected in future FRC experiments remains to be seen. Other stabilization techniques that involve neutral beams have been considered [62, 68].

Helical multipole fields have also been found useful in suppressing the n = 2 rotational instability [25, 135, 313, 334]. In one experiment, lower thresholds for stabilization of the n = 2 mode were reported for helical quadrupoles than for straight quadrupoles [135]. However, comparable thresholds were found in another experiment [313]. A recent extension of the MHD analysis [264] to helical multipoles reconciles these data, showing them to be a result of differences in helical pitch [333]. Independently of their efficiency in stabilizing the n = 2 mode, helical multipoles offer some potential advantages over straight multipoles: closed magnetic flux surfaces might be retained after penetration of the helical field to the inside of the FRC [336] and may also be present outside the separatrix [266].

4.3. Tilt instabilities

Tilt instabilities are probably the most dangerous global modes for FRCs. Most of the theoretical work has focused on the n = 1 instability, although modes with n > 1 have been found even more unstable [19]. So far, none of these instabilities has yet been observed. One likely explanation is that the growth times are longer than predicted by MHD theory and that present FRC lifetimes do not exceed a few growth times. One must also recognize that it is difficult to detect internal modes. External magnetic measurements might prove ineffective or too insensitive if no or little perturbation exists outside the separatrix. Internal magnetic probe measurements are possible, in particular on translated FRCs, but they yield reliable information for only short times. A side-on Faraday rotation chord along a diameter might reveal the internal tilt mode by finite signals near the ends of the FRC [337], but no measurement has yet been attempted. For small elongations, the FRC may also be unstable to the n = 1, m = 1 external tilt mode which, in the simplest picture, produces a flip in the plasma axis [228]. This mode may have been observed during FRC formation, around the peak of violent axial shocks, with luminosity [227] and internal probe [223] measurements.

4.3.1. MHD predictions

The tilt mode was first found to be unstable for prolate CTs by Rosenbluth and Bussac [338]. They used a modified energy principle and assumed nearly spherical, pressureless equilibria with toroidal field. Conducting walls, while limiting the separatrix motion, could not prevent the tilting of internal flux surfaces unless the wall was uncomfortably close to the separatrix. This result was later confirmed for more general separatrix shapes and arbitrary plasma pressures [339]. Rosenbluth and Bussac speculated that the tilt mode should also be present in FRCs. However, if this mode was indeed observed for prolate spheromaks [340], it was not detected in FRC experiments.

The first predictions of the internal tilt mode for the FRC geometry [237, 341] soon followed the analysis

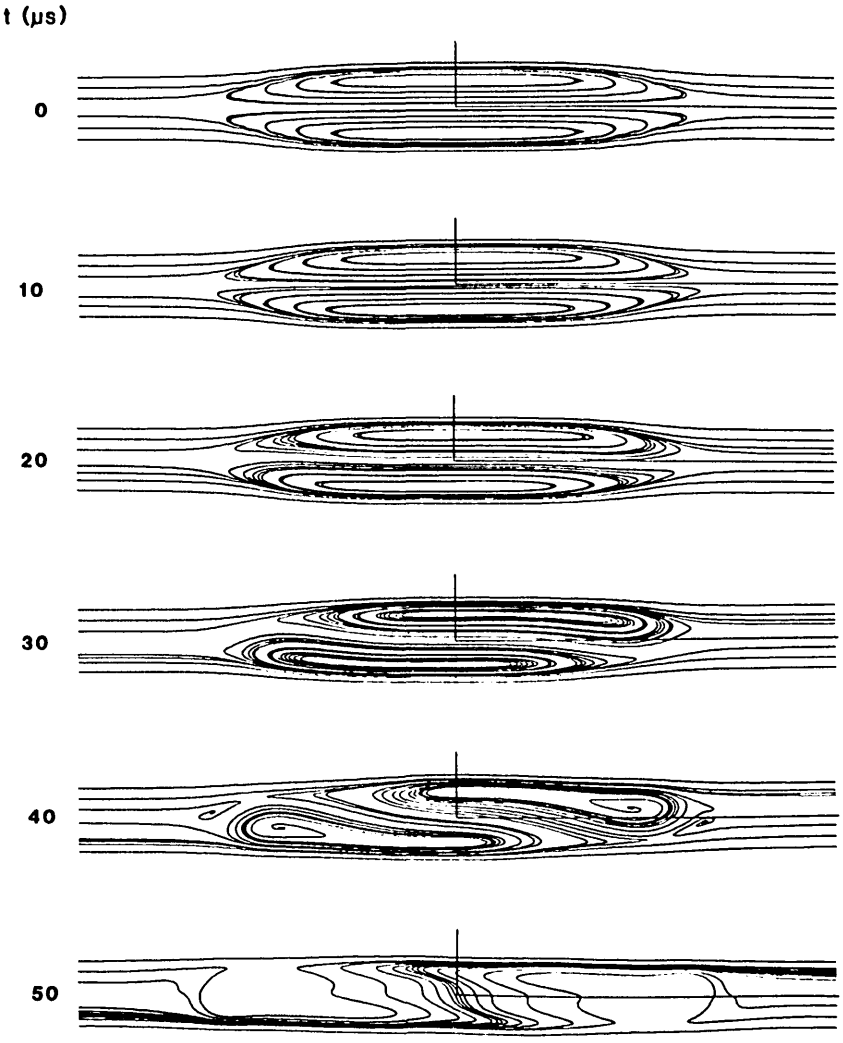

FIG. 31. Time sequence of magnetic field lines from 3-D MHD simulations illustrating the internal tilt instability [346].

of Rosenbluth and Bussac [338]. This mode is not easily stabilized by profile effects or by a conducting boundary, as shown analytically [342, 343] and numerically [344]. In the latter work, a trial function approach and a time-dependent linearized MHD code were used: both calculations yielded comparable results and indicated that the tilt should be unstable for various separatrix shapes and pressure profiles.

The linearized MHD growth rates of the internal tilt mode are similar to those of co-interchanges and can be written as $\gamma_{MHD} \sim 2v_A/\ell_s$ [342–344], where $v_A = B_e/(\mu_0 n_M m_i)^{1/2}$. Most FRC experiments have values of $\gamma_{MHD}\,\tau_\ell$ in the range of 30–60, which should be sufficient to observe the instability if its growth rate γ is comparable to γ_{MHD}. The observed FRC stability could be explained if the tilt mode saturated non-linearly at low amplitude. However, 3-D MHD simulations [345, 346], a 2 1/2-D MHD particle code [347] and a qualitative analysis [348] indicate that the instability continues to grow non-linearly until the FRC is destroyed by rapid field line reconnection. This is illustrated in Fig. 31, which gives a time sequence of computed magnetic field lines [346].

4.3.2. Rotational and Hall effects

Several fluid calculations have included an azimuthal plasma rotation, as naturally occurs in FRC experiments. Clemente and Milovich [349] have first studied the influence of plasma rotation on internal tilt mode stability for an analytical, rigidly rotating MHD equilibrium [261]. They used a trial function displacement in the Frieman and Rotenberg energy principle

[350] and found that Mach numbers (ratio of separatrix ion velocity to plasma sound speed) somewhat larger than unity are required for stability. Their conclusion was that plasma rotation should not contribute significantly to the observed gross FRC stability since present FRC experiments have Mach numbers well below unity. A two-fluid calculation [351], with a Hill's Vortex equilibrium and a trial function approach, also indicated that stability can be obtained for Mach numbers somewhat greater than unity. Rotation has also been included in recent 3-D MHD simulations [346]; although still incomplete, these computations suggest that rotation has little effect on internal tilt mode stability, but that a gross distortion of the separatrix may occur for Mach numbers greater than about unity. Therefore, it appears that much larger rotation rates than in present experiments would be required to provide a stabilizing influence in future FRCs. A scheme to induce such rotations was proposed [352]: hot electron rings would generate a radial electric field in the edge layer and make it spin. This rotation would then be transferred to the FRC via viscous effects.

The two-fluid calculation [351] indicates that Hall effects are another stabilizing factor for the FRC internal tilt mode. Stability is found for sufficiently large values of FRC elongation e_s. For the Hill's Vortex model of that calculation, the stability threshold is approximately $s \lesssim e_s/3$. This result is quite similar to the FLR estimate $s \lesssim e_s/2$ discussed in Section 4.1.2. This may perhaps be understood by the fact that, for FRCs, the Hall terms in Ohm's law are of the order of $\rho_i/L_\perp$ ($L_\perp$ is a characteristic radial scale length) and are therefore corrective terms to the MHD model, being of similar order and scaling as FLR terms. For future FRCs, both rotation and Hall effects do not appear sufficient to ensure gross stability against the tilt mode by themselves. However, together with other stabilizing factors, they could still influence FRC stability.

4.3.3. Kinetic effects

Seyler and Barnes [353] developed an FLR model from the Vlasov fluid equations [354] using a variational dispersion functional. These equations accurately account for the arbitrarily large orbits of collisionless ions and assume cold and massless electrons. Unfortunately, the FLR approximation proved inadequate for the FRC geometry [355] because of field-null singularities and because the magnetic moment is not conserved at the tips of the flux surfaces [355, 356, 337]. An FLR stability theory [357] applied so far to mirror plasmas may perhaps be extended to the FRC case in the near future.

Several kinetic studies, related in some way to the FRC, have been made. Morse and Miley [358] investigated FRM stability with an energy principle derived from the Vlasov equations. They identified the possibility of n = 1 and 2 unstable modes by using trial functions in a sufficient stability condition, but could not go further in the stability analysis. Finn [359] analysed the effect of axis encircling particles on the stability of local modes in FRMs. The ion population was approximated as a beam of axis encircling particles plus a thermal small-orbit background. The contribution of the beam ions was derived from the Finn and Sudan [360] Vlasov dispersion functional while a fluid model was used for the thermal ions. Stability was found for $\rho_i/L_\perp \gtrsim 3$ (i.e. approximately $s \lesssim 3$), provided the plasma was not too elongated. Kim [361] studied the stability of a Z-pinch with elliptical cross-section (a geometry similar to the FRC) by using trial functions in a similar dispersion functional: kinetic ions could stabilize modes with large k_z but not those with small k_z.

The first kinetic calculation dedicated to the internal FRC tilt instability was performed by Barnes et al. [29]. Eigenfrequencies were calculated from a Vlasov fluid dispersion functional [362] separated into fluid and kinetic portions. To evaluate the latter, a Monte Carlo method was used to follow a sample of equilibrium orbits from a 2-D MHD numerical FRC equilibrium [31]. A trial function was used to compute the eigenfrequencies. The main result from this work is illustrated in Fig. 32, where the growth rate γ from

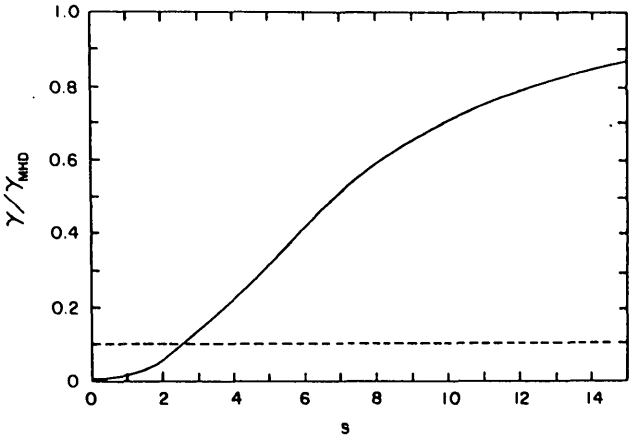

FIG. 32. Variation with s of the growth rate for the internal tilt mode predicted by kinetic theory, normalized by the MHD growth rate [29, 20]. The dashed line is the approximate threshold for the mode that can be observed in present experiments.

the kinetic calculation (normalized to the MHD growth rate γ_{MHD}) is plotted as function of s. It can be seen that γ is reduced from γ_{MHD} by more than an order of magnitude for the values $s \lesssim 2$ of present FRC experiments. This could perhaps explain why the internal tilt instability has not yet been observed. However, assuming a relationship between γ and s as in Fig. 32, recent TRX data with initial values of s greater than 4 showed no evidence of tilt instability in spite of values of $\int \gamma dt$ in excess of 20 [141].

The detailed quantitative result shown in Fig. 32 should not be regarded as generally applicable to experiments, for many reasons. So far, only one FRC equilibrium has been considered; thus, geometrical and profile effects have not yet been assessed. The Vlasov fluid formalism assumes collisionless ions, zero-temperature electrons, and no plasma rotation. There is no guarantee that the assumed trial function is reasonably close to the true eigenfunction and further calculations with self-consistent tilt displacements are required. The linear stability theory cannot predict the time required for the tilt to develop to an observable level. Such a time could be comparable to the observed confinement times, which may cause some ambiguity in the interpretation of the data. Hence, additional studies are necessary for a more quantitative answer.

Since the data presented in Fig. 32 were obtained, the kinetic calculations [29] have been extended so as to determine the kinetic eigenmode self-consistently with the eigenfrequency [363]. These computations generally confirmed the results of Fig. 32, but still used the rigid-axial-shift approximation for the displacement field. This approximation will be removed in further near-term calculations [364]. These calculations will also explore the influence of the FRC elongation e_s and study the stability of large-s FRCs, with a hot ion component added to the thermal component.

Recently, several other kinetic results have been obtained. First, a linearized hybrid code [365] was used to study the FRC internal tilt mode by an initial value approach, with the same FRC equilibrium as used previously [29]: for $s = 7$, γ agreed well [366] with the value shown in Fig. 32. Second, a 3-D hybrid particle code was used to study FRC stability [337]. This rather formidable tool required 50 hours of CRAY-2 computer resource time for each run of about three MHD growth times. The internal tilt mode was observed to grow with $\gamma \sim \gamma_{MHD}$ for an FRC case with $s = 12$. In a second run with $s = 1.6$, no clear instability was detected. Although quite preliminary, these results confirm that the internal tilt is probably the mode to look for experimentally and theoretically, since it was observed without initial perturbation and trial function. It should be noted that the initial equilibrium studied with the 3-D hybrid code [242] differed considerably from that used previously [29, 366].

4.3.4. Possible stabilization

Future large size FRCs may require some additional means of stabilizing the internal tilt mode because of conflicting requirements between confinement and stability. Present understanding of FRC confinement (see Section 5) projects values of s in the range of 20–40 for reactor conditions [37, 38]. On the other hand, small values of s appear desirable for FRC stability because most stabilizing factors mentioned in Section 4.1.1 lose importance for FRCs with large values of s. These conflicting requirements may not permit a working compromise without invoking some additional stabilization mechanisms.

The most effective way of maintaining gross FRC stability at large values of s is probably to retain substantial kinetic effects via high energy particles [29]. The kinetic term in the Vlasov fluid dispersion functional shows a fourth power dependence on particle velocity. Hence, although quantitative numbers have not yet been determined, gross FRC stability might be achieved by maintaining some high energy tail on the ion population. This could occur naturally, once ignition is reached, with large-orbit charged fusion products [66]. High energy particles could also be produced either by some radiofrequency heating scheme or by high energy particle injection from neutral beams (FRM approach) or from large-orbit ion rings (Astron approach). The latter are tilt stable in most cases, provided the beam circulation frequency exceeds the betatron frequency (inverse ion transit time through the ring width) [367, 69]. An ion ring could perhaps be combined with an FRC to achieve a stable mixed-CT configuration [368, 369]. Ion ring experiments at Cornell University are progressing towards near-future FRC stabilization experiments [370].

Some important issues have to be resolved in the mixed-CT concept. The required ring strength for possible FRC tilt stabilization is unknown. Several related studies suggest ratios of beam current to plasma current in the range 0.25–1 for stabilization [371], although ratios of a few per cent have been found sufficient for stabilization of an external tilt perturbation [69]. The stability of the ring itself, in the presence of the FRC plasma, must be assessed. Ion

rings of sufficient proton number and energy have to be generated with a technology compatible with FRC formation. Once formed, the ring must be guided and merged into the FRC. When the ring is merged, its slowing-down time must be longer than or comparable to the FRC lifetime. Some theoretical [372] and experimental [370] studies of ring trapping in a magnetized plasma by Alfvén wave generation have been performed.

5. CONFINEMENT

This area of FRC physics remains largely obscure. Understanding of FRC transport properties is not expected at the present time because of limited diagnostics and database. In addition, other factors affect present FRC confinement studies: the discharges are unsteady and of short duration, there is a large scatter of data because of intrinsic variations in the marginally controlled formation process, and the edge layer obscures the intrinsic closed-line confinement.

5.1. Transport mechanisms

5.1.1. General picture

As shown in Fig. 1, the inside of the FRC separatrix consists of elongated closed field lines. Therefore, radial diffusion presumably dominates energy losses. This view has sometimes been challenged because of the X-points at the ends of the FRC: particles and heat could conceivably escape axially as in magnetic cusps. This does not appear to be the case, for several reasons. First, Auerbach and Condit [373] have shown that X-points on axis have no deleterious effect on transport, unlike off-axis X-points. Although derived for an elliptical Hill's Vortex geometry and for classical transport, this conclusion holds for any transport model. Second, if particles are mostly leaking through some fixed area around the X-points, the global FRC particle confinement time τ_N would be proportional to the separatrix length ℓ_s. However, most FRC experiments show little or no dependence of τ_N on ℓ_s. Another result from Auerbach and Condit [373] is that a one-dimensional radial transport approximation is justified for elliptical FRC separatrices of elongations e_s greater than about 3.

Most FRCs with values of x_s in the range 0.4 to 0.6 are well removed from cold radial material boundaries, as shown in Fig. 1. Plasma particles and heat lost from the separatrix are diverted axially in the edge layer. Therefore, one might expect impurity influx and radial ion thermal conduction to be small. This may not apply to FRCs with x_s close to unity.

Present FRC radial pressure profiles at the axial midplane are similar to the density profile shown in Fig. 21. This profile is characterized by a broad maximum around the field null and by steep gradients near the separatrix. These features result in characteristic radial transport scale lengths $L_\perp$ smaller than $r_s - R$ and probably cause relatively short confinement times. For example, an FRC formed within a 50 cm diameter coil has typically $r_s \sim 10$ cm, $L_\perp \sim 2$–3 cm, and confinement times of about 100 μs.

Finally, within the ideal picture of Fig. 1, there is a single field null at $z = 0$ and $r = R$. At this point, the internal flux ϕ decays by resistive annihiliation of the positive ($r > R$) and negative ($r < R$) magnetic fields. An assessment of flux loss requires knowledge of the FRC resistivity and also of the magnetic field structure near the field null.

5.1.2. Microinstabilities

At the present time, it is well established that the FRC confinement is anomalous, i.e. non-classical. Anomalies have been clearly identified in particle [374, 57], flux [269] and energy [375] confinements. Within the FRC separatrix, there may be electrostatic and electromagnetic microinstabilities that could cause an anomalously high plasma resistivity. Numerous electrostatic modes have been identified for the theta pinch geometry and the plasma parameters were reviewed by Davidson and Krall [376]; they were also reviewed by Carlson [377] for the FRC. The ion drift parameter v_D/v_i has typical values of 0.2–0.8 near the separatrix; for such cases, the most important mode is probably the lower hybrid drift (LHD) instability. Other possible modes include the ion cyclotron drift, the universal drift and the ion cyclotron electron density drift instabilities [377]. However, it is believed that these modes either produce less anomalous resistivity than the LHD or are stabilized by finite beta and length effects.

The LHD instability is a flute-like mode driven primarily by density gradients. Its linear theory is fairly well understood and predicts growth rates comparable to the hybrid gyrofrequency and wavelengths comparable to the electron gyroradius. These predictions have been verified by many numerical simulations [378–380] and by some density fluctuation measurements [381]. However, the non-linear evolution of the LHD, its saturation level and associated transport, possible stabilization factors, electromagnetic

and non-local effects (including cylindrical geometry) are still poorly understood at the present time. Non-local LHD effects [382] appear to result in transport coefficients quite similar to those obtained with a local theory. Many saturation mechanisms have been proposed; the most probable appear to be mode coupling and ion trapping [377]. Interestingly, most mechanisms lead to resistivity estimates similar to the widely used wave-energy-bound resistivity [378], $\eta_{LHD} \propto (B/n)(v_D/v_i)^2$. For $v_D/v_i = 1$, this resistivity is similar in scaling and magnitude to Bohm resistivity [142].

The quadratic scaling $\eta_{LHD} \sim (v_D/v_i)^2$ implies an anomalous resistivity profile strongly peaked near the separatrix and suggests no anomaly at the field null. However, recent numerical work [383] indicates that the latter may not be true. Experimentally, density fluctuations in good agreement with the LHD instability have been measured by CO_2 laser scattering on the zero-bias INTEREX theta pinch [381]. On the other hand, similar measurements on the TRX-2 device did not reveal any LHD-like density fluctuations [377]; the LHD mode was either grossly altered or it was stabilized by some mechanism (electron collisionality was identified as the most likely possibility), or some entirely different processes were responsible for the observed anomalous particle loss rates in that experiment. Clearly, further experimental and theoretical studies are required to clarify the possible impact of the LHD and other microinstabilities on FRC transport.

Since most of the FRC plasma is high beta, one can also expect some electromagnetic modes to be active. Such modes would create magnetic fluctuations that disrupt flux tubes and might cause substantial anomalous resistivity in the FRC interior [384, 385]. Recently, Krall [385] identified several low frequency instabilities for a slab geometry similar to the FRC. In the long central region of straight magnetic field lines, a high beta version of the drift dissipative instability may be active. In the curved end-regions, electromagnetic and electrostatic trapped particle modes are possible. These low frequency drift modes may perhaps stabilize the LHD in FRC experiments by three-wave coupling [386]. Interestingly, this coupling appears to be more unlikely for the lower beta INTEREX plasmas where LHD fluctuations have been detected [381]. Another electromagnetic instability suggested for the FRC [19] is the ∇T_e-driven microtearing mode [387]. However, aside from a dimensional estimate [388], a microtearing transport study for the FRC case remains to be done. Finally, a high frequency mode has been identified near the field null in an early study [389].

Another mode that could play an important role in FRC transport is the Kelvin-Helmholtz instability [324]. It could occur in present FRCs if the plasma rotation has sufficient shear. Then, vortices would cause plasma mixing and anomalous viscosity. The Kelvin-Helmholtz instability could also be driven by charged fusion products [324] in future FRCs with advanced fuels [66]. A self-consistent calculation for the FRC is needed.

To assess possible anomalies in present FRC experiments, one needs to estimate classical losses accurately. However, such a benchmark does not yet exist for FRC particle transport because classical losses are not only diffusive but also include some unconfined particles ; these have been identified by Miley and co-workers [390, 62, 322]; particles within a certain velocity sphere can be lost from the separatrix volume, in a similar way as particles in the loss cone escape from a simple magnetic mirror. Classical (and possibly anomalous) collisions continually feed the velocity sphere with particles that are promptly lost. The size of the velocity sphere depends on spatial location and is greatest near the separatrix, where substantial losses could occur for present FRCs with large separatrix densities. A definitive particle loss calculation based on this velocity space loss sphere (VSLS) model should include self-consistent electric fields. Such a calculation is being developed [391].

5.1.3. Influence of the edge layer

The edge layer strongly influences the confinement properties of present FRCs. This important point, inspired by several studies [392, 393], is detailed below for particle transport only, but it can be generalized to other energy losses. Assuming an equilibrium radial diffusive flow of particles out of an elongated FRC, one can equate the number of particles per second that leave the separatrix radially to the number of particles per second that leave the edge layer axially: one obtains $\delta = (D_\perp \tau_\parallel)^{1/2}$, where δ is the length of the separatrix density gradient, $D_\perp$ is the closed-line diffusion coefficient and $\tau_\parallel$ is the characteristic loss time of the edge layer [110, 394]. Leaving aside numerical factors for simplicity, the particle confinement time, $\tau_N = N/2\pi r_s \ell_s (D_\perp n_s/\delta)$, can then be expressed as $\tau_N \sim (\tau_\perp \tau_\parallel)^{1/2}/\beta_s$, where $\tau_\perp \sim r_s^2/D_\perp$.

To proceed further, let us consider the density (pressure) radial profile of Fig. 33. This profile was obtained from a particle transport numerical model [57] for the design case of the LSX device [39]. The characteristic density gradient length $L_\perp$ shown in Fig. 33

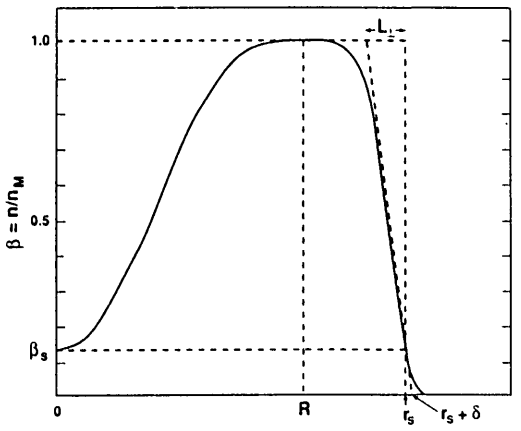

FIG. 33. Calculated radial density profile [57] for the LSX design case, with $x_s = 0.6$ and $s = 8$.

is approximately related to δ and β_s by $\beta_s/(1 - \beta_s) = \delta/L_\perp$. The internal flux ϕ can be approximated by $2\pi r_s L_\perp B_e$ and, using Eq. (12), one obtains $s/w \sim L_\perp/\delta$. One can now contrast present and future FRC cases:

(a) Present FRC experiments with low values of s ($\sim$w) are characterized by $L_\perp \sim \delta$ and $\beta_s \sim 1/2$, as shown for example in Fig. 21. For such cases, $\tau_N \sim (\tau_\parallel \tau_\perp)^{1/2}$, which shows coupling of the intrinsic transport properties of the closed-line and open-line regions. Furthermore, the ion drift parameter $v_D/v_i \sim \beta_s/\beta w$ is approximately equal to 1/w everywhere through the FRC density gradient. Since typical values of w are in the range 2–4, electrostatic microinstabilities could be active through most of the FRC interior. Electromagnetic modes could also be active within the entire separatrix volume because the values of beta are high everywhere.

(b) Future FRC experiments with high values of s ($\gg$w) may be characterized by $L_\perp \gg \delta$ and $\beta_s \ll 1$, as shown for example in Fig. 33. For such cases, $\tau_N \sim \tau_\perp$ since $\beta_s \sim (\tau_\parallel/\tau_\perp)^{1/2}$, and one recovers the intrinsic confinement of the closed-field-line region. Furthermore, the ion drift parameter is small everywhere, except near the separatrix where it is still about equal to 1/w. Hence, electrostatic microinstabilities would be localized near the separatrix. Electromagnetic modes could still be active through most of the FRC interior, but they may be stable in the low-beta region near the separatrix.

The above arguments clearly show that definitive transport studies require FRCs with large values of s. These would offer not only a much clearer assessment of the intrinsic FRC confinement properties but also a qualitatively different transport regime, where microinstabilities may become more localized rather than spread through the entire separatrix volume. The LSX device [39] has been designed to access this new confinement regime. Of course, the above discussion implicitly assumes that FRCs with large values of s will remain MHD stable. Local modes such as interchanges may become unstable near the separatrix and relatively high values of β_s may persist as a consequence of MHD activity. Moreover, it may be desirable to have high values of β_s in order to reduce MHD activity; this might be achieved by improving the edge layer confinement. If this is the case, FRC confinement will remain in the present regime (a).

The above arguments also show that the physics of the edge layer is of great importance for present experimental confinement studies and their theoretical modelling. However, at the present time, relatively little effort has been devoted to experimentally characterize the edge layer or to describe it accurately in transport models. One example is the crude estimate of $\tau_\parallel$ as a free streaming time $\tau_\parallel = \ell_s/2(T/m_i)^{1/2}$, which results in calculated values of δ significantly smaller than those measured (e.g. $w \sim 1$ instead of $w \sim 3$). This effect and other inconsistencies compared with the free-streaming model have led Steinhauer [275] to propose that self-generated electrostatic potentials govern the axial flow in the edge layer, as often occurs in magnetic mirror and cusp plasmas. This theory is supported by some related numerical work [395]. An alternative view is that particle losses may be dominated by the VSLS process rather than by radial diffusion. These issues require further studies.

5.2. Transport techniques

5.2.1. Experimental methods

FRC particle loss can be measured experimentally with reasonable accuracy. One defines τ_N as $-N/(dN/dt)$, where N is the particle inventory within the FRC separatrix. This assumes that possible sources of particles are negligible, a good assumption for most FRCs because the initial gas fills are nearly fully ionized: typical values of N account for about 2/3 of the initial gas inventory within the coil length [19, 274, 20]. The remaining neutrals probably do not have enough time to reach the FRC separatrix and would be ionized in the FRC edge layer [396]. Finally, a possible electron source from impurity ionization appears negligible (see Section 5.3.3).

The time history of N is often followed by combining interferometry and excluded flux measurements.

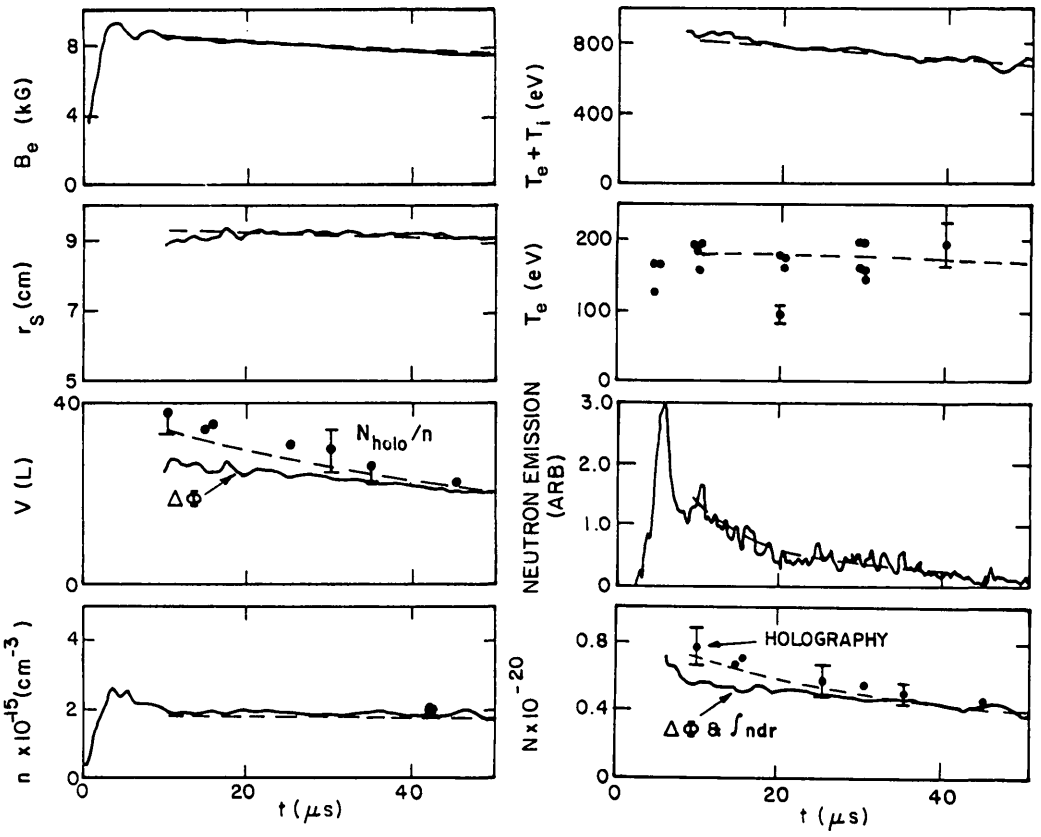

FIG. 34. Time evolution of various measured and inferred quantities for 5 mtorr data from the FRX-C device [20]. The dashed lines result from a zero-dimensional modelling.

N is estimated as the product of the separatrix volume V and the average density n, as illustrated in Fig. 34 for some 5 mtorr data from the FRX-C device [20]. A variant of this method is possible during FRC translation past a chord of side-on interferometry [21]. Occasionally, end-on interferometry is used to measure N: the area integral of the fringe shift, in holograms such as the one presented in Fig. 19, yields the total electron inventory in the field of view. This inventory approximates N well because density corrections beyond the FRC ends are usually small [274]. N is measured at various times, on different discharges, as shown in Fig. 34. For these data, the holograms yielded $\tau_N = 67 \pm 25$ μs, while the combined $\Delta\phi$ and $\int$ ndr measurements gave $\tau_N = 100 \pm 20$ μs. This is probably the largest discrepancy noticed so far between the two methods. The biggest source of error comes from the usually small time interval during which the decay of N can be estimated. Therefore, reliable values of τ_N always require statistical averages, from many discharges taken under similar conditions.

A direct measurement of the FRC internal flux decay requires non-perturbing internal magnetic field measurements. To date, no such measurement has been performed with the necessary accuracy level. Therefore, ϕ is inferred from Eq. (11), with B_e and x_s obtained from the excluded flux array and with some choice for ϵ in the range 0–0.3. Some internal probe measurements during FRC translation roughly support this method of inferring ϕ [191]. Then, the flux confinement time $\tau_\phi = -\phi/(d\phi/dt)$ is inferred from the time history of ϕ. Errors in estimating τ_ϕ can also occur because of the short observation times and, possibly, from the assumption of constant ϵ [252].

The estimate of the field-null resistivity, once τ_ϕ is inferred, has an additional uncertainty, associated with the magnetic field gradient at r = R. For an elongated FRC, one can combine the Ohm, Ampere and Faraday laws and obtain [269, 239, 40, 253]

$$\eta_\perp(R) = \frac{\mu_0 \phi}{2\pi R \tau_\phi \dfrac{dB}{dr}(R)} \qquad (16)$$

One can infer ϕ and dB/dr(R) from some global pressure profile constrained by Eq. (10). Then, values

of $\eta_\perp(R)(\tau_\phi/\mu_0 r_s^2)$ in the range 16 to 18 are usually obtained from Eq. (16).

The major energy losses other than particle transport are radiation and thermal conduction. Radiation losses can be measured fairly accurately by calorimetry [192, 20]. The concentrations of various impurities such as oxygen and carbon can be estimated by spectroscopy, with a calibration from controlled impurity seeding [192]. Thermal conduction losses have not been experimentally measured, but they can be inferred by subtracting from the total energy losses the contributions of particle and radiation losses.

The total energy losses can be inferred with reasonable accuracy, by assuming the simple properties of elongated FRC equilibria described in Section 3.1.1. By itself, the excluded flux array permits inference of the global energy confinement time τ_E that includes the Ohmic and compressional input powers [270]. One can also obtain the value of $-E_p/(dE_p/dt)$ that does not include those input powers and that is larger than τ_E by a factor typically in the range 1.2–1.6. If the time history of T_e is available, one can estimate the contributions of the electron and ion thermal losses (for cases with $T_i > T_e$) by fitting the time histories of B_e, r_s, V, n, T, T_e and N with some transport model. For the example of Fig. 34, the dashed lines were obtained from a zero-dimensional model [270].

5.2.2. *Theoretical modelling*

Several analytical classical transport studies have been made, on the basis of the elliptical Hill's Vortex [373, 397] or other [343, 398] equilibria. These studies yield valuable qualitative information, but they impose zero pressure (and sometimes temperature) at the separatrix, do not satisfy the $\langle\beta\rangle$ condition of Eq. (10) and therefore differ significantly from the experimental FRC profiles. Resistive decay of plasmas similar to FRCs has also been studied qualitatively in slab geometry [399, 320, 215].

A simple approach, which has yielded more quantitative results, is to assume quasi-steady radial profiles based on the simple properties of elongated FRC equilibria described in Section 3.1.1. The most elementary models are zero-dimensional and assume rigid rotor profiles [375, 400] or more general radial profiles [401, 270]. These models have proved particularly useful for establishing a rough power balance for present FRC experiments.

More detailed (but still relatively simple) transport studies are possible using 1-D quasi-steady profile models. This approach was first applied in a steady-state particle transport model [57], with radial particle losses balanced by axial length contraction. Assuming radially uniform temperatures, the density profile was constrained by Eq. (10) and by continuity of the particle flux at the separatrix. The only free choice in this numerical calculation was the resistivity model (classical or LHD). Later on, Hoffman and Milroy [393] extracted from the same model a convenient analytical formula for τ_N, which also showed explicitly the influence of the edge layer for present low values of s. For the particular choice of LHD resistivity, one derives $\tau_N \sim \tau_\parallel^{3/4}\tau_\perp^{1/4}$ for low s values, which suggests a greater edge layer influence than that mentioned in Section 5.1.3.

Flux loss can be included in a simple manner by either assuming quasi-steady profiles [40] or looking for self-similar solutions [402]. Both of these models also admit of an arbitrary choice of the resistivity model. The quasi-steady profile model [40] was used to develop relationships describing the gross resistivity profile in terms of experimentally measurable quantities. A quasi-steady model for axial rather than radial variation has also been implemented [403].

Steady-state 1-D models have also been used to address thermal conduction losses [388] and neutral particle effects [396]. However, the steady-state approach is limited because it rules out flux loss. Steady-state models adequately address energy losses for FRC cases with $\tau_\phi > \tau_E$, but can be misleading when applied to cases with $\tau_\phi \lesssim \tau_E$ [404].

Numerical 1-D (r,t) models can also be used, with more accuracy and complexity than in the above approaches. Some early FRC transport computations were performed [374, 51] that included an edge layer but lacked 2-D effects such as Eq. (10). Later on, Hamasaki added such 2-D effects to his code [327]. Similar 1 1/4-D codes, numerically more efficient, have been recently constructed [269, 405, 406]. Finally, even more accurate and complex 1 1/2-D numerical calculations have been developed, using an alternation of 2-D FRC equilibria and 1-D (flux-averaged) transport [246, 407].

5.3. Confinement results

5.3.1. *Particle transport*

Most FRC confinement studies have been devoted to particle transport, perhaps because it is simplest to characterize and also because it proves experimentally to be the most important energy loss mechanism. The values of τ_N measured in various devices are shown in

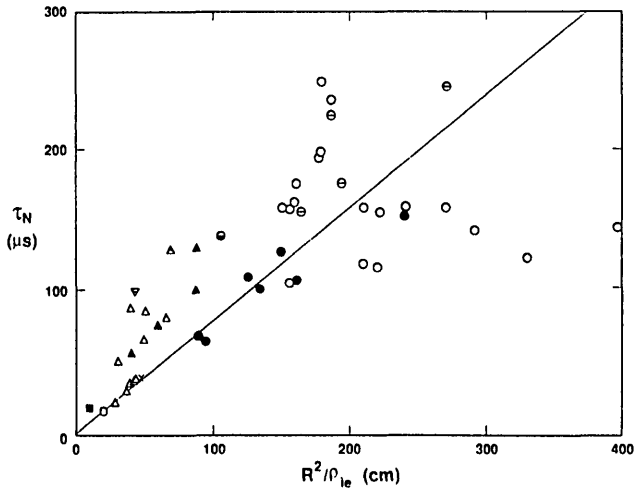

FIG. 35. Measured particle confinement times τ_N as functions of R^2/ρ_{ie}. The symbols are explained in Table III.

Fig. 35 as function of the parameter R^2/ρ_{ie}. This peculiar scaling is an often used yardstick, first proposed by Hamasaki and Krall [327] when some FRX-B data were modelled with the wave energy bound LHD resistivity. This scaling was then adopted experimentally [19, 326]. Later, a more complete LHD scaling was obtained [57] which allowed prediction of the performance of the FRX-C device [273]. Figure 35 suggests some saturation of the values of τ_N for the largest values of R^2/ρ_{ie} achieved in the FRX-C/LSM device. These data correspond to values of s around 2. Further analysis and data from other devices are required to assess the generality of this apparent saturation.

Several empirical and theoretical τ_N scaling laws, written as $\tau_N \sim \ell_s^a x_s^b r_c^c n^d T^e$, are gathered in Table VII (radial pressure balance is used to eliminate B_e and $T \sim T_e \sim T_i$ is assumed). From Table VII, it can be seen that R^2/ρ_{ie} is a crude approximation of the LHD theoretical scaling which ignores the dependences on ℓ_s and T and the dependence on x_s in addition to the x_s^2 factor that arises from profile effects. However, the ℓ_s and T dependences appear experimentally to be small and most FRCs have values of x_s close to 0.4 (some values of τ_N in Fig. 35 were obtained for x_s in the range 0.5–0.6). In addition, the ℓ_s, T and x_s dependences of the LHD model often happen to cancel each other, and the computed values of τ_N appear to remain within a factor of two of R^2/ρ_{ie} up to reactor conditions [37, 57, 408, 38].

Most of the empirical τ_N scaling laws [409, 28, 40, 21] in Table VII are similar to R^2/ρ_{ie}. The Ishimura scaling [409] is essentially $x_s R^2/\rho_{ie}$ because the additional factor $(\ell_s/r_c)^{3/4}$ varies little. The recent TRX scaling was obtained at constant r_c (as did the earlier TRX-1 and FRX-C/T scalings), and it was not possible to differentiate between x_s and r_s dependences. This TRX scaling agrees much better with data from larger devices when written as $x_s^{3.6} r_c^2$ rather than the proposed $r_s^{3.6}$ [142]. Most discrepancies between the various empirical scalings presumably come from the limited database or from possible differences in formation and edge layer properties.

The observed ℓ_s and T dependences are consistently weaker than those predicted by the LHD model, although the absence of a dependence on ℓ_s could be due to edge layer physics [275]. Furthermore, the LHD resistivity does not contribute to flux loss (at least in the local version presently used in FRC modelling) and the TRX-2 data did not reveal any LHD-like density fluctuations [377]. Therefore, the FRC particle confinement physics almost certainly involves other processes than just the LHD instability. In fact, part of the success of the LHD model may be fortuitous since the LHD scaling happens to be similar to the Bohm scaling and also to the Krall scaling [410] based on the drift dissipative mode [385].

Table VII reveals a significant discrepancy between the empirical [40, 21] and classical scaling laws: one has approximately $\tau_N/\tau_N(\text{classical}) \sim n^{0.5}/T^{1.5}$. It should be noted that classical scaling involves T_e rather than T, and that the measured values of T_e are mostly

TABLE VII. PARTICLE CONFINEMENT SCALING: $\tau_N \sim \ell_s^a x_s^b r_c^c n^d T^e$

Scaling	Ref.	(a)	(b)	(c)	(d)	(e)
(A) Empirical						
R^2/ρ_{ie}	[273]	0	2	2	0.5	0
$x_s R^2/\rho_{ie}(\ell_s/r_c)^{3/4}$	[409]	0.75	3	1.25	0.5	0
ϕ	[28]	0	3	2	0.5	0.5
TRX-1	[40]	0	2.2		0.6	0.3
FRX-C/T	[21]	0.2	1.4		0.5	0.4
TRX	[142]	0	3.6		0.9	0
(B) Theoretical						
LHD	[57]	0.6	3.3	2	0.5	-0.7
Bohm		0	2	2	0.5	-0.5
Krall	[410]	0	2	2	0.5	-0.5
Classical		0	2	2	0	1.5
VSLS	[62]	0	2.7	1.8	0.2	1.5

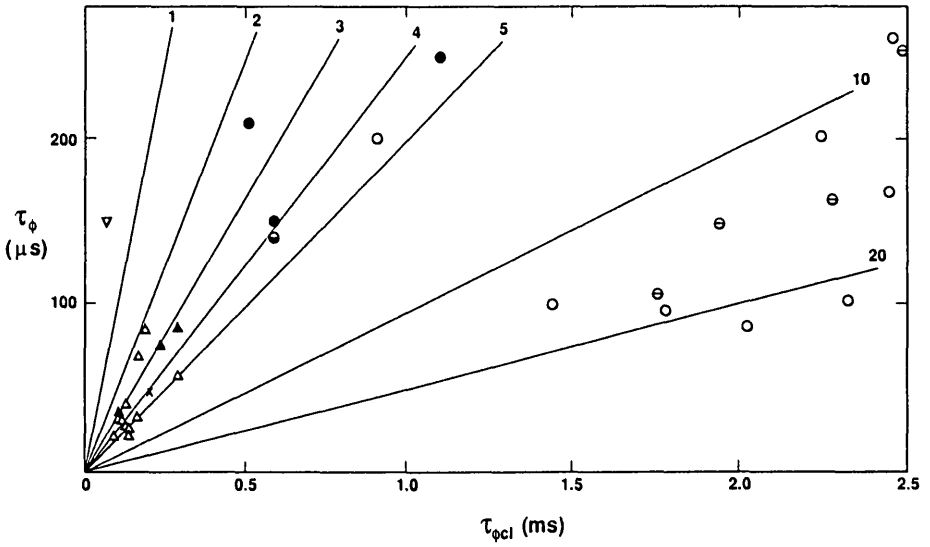

FIG. 36. Measured flux confinement times compared with calculated classical values. The solid lines indicate anomaly factors. The symbols are explained in Table III.

in the range 100–200 eV. Nonetheless, this discrepancy in scaling suggests that the FRC particle transport is anomalous. Various classical estimates (without VSLS losses) gave anomalies as low as 3 (over Spitzer transverse resistivity with $Z_{eff} = 1$) for some data from small devices [373, 397, 57, 400, 343, 40]. These anomalies are not large enough to rule out the possibility of transport by classical processes with a Z_{eff} greater than one [400].

However, the gap between measured and classical values of τ_N tends to increase for low density FRCs formed in larger devices [57]. For such cases, classical estimates yield anomalies of at least 10 which cannot be explained in terms of Z_{eff} [20, 411]. In many cases, the magnitude of τ_N is roughly comparable to the hybrid of the classical and Bohm values. For some FRCs formed with sufficiently high fill pressures, classical processes can be comparable to [20, 253] or even dominate [412] anomalous effects.

The VSLS and classical scalings in Table VII are quite similar, which simply reflects the fact that classical collisions have been assumed to fill the velocity space loss sphere [62]. One would be tempted to rule out a significant contribution of VSLS losses in present FRC experiments on the basis of this discrepancy in scaling. However, if anomalous processes are invoked to explain the FRC τ_N data, anomalous collisions are likely to cause VSLS losses. This loss mechanism should be seriously considered, since its magnitude is consistent with present FRC experiments [62, 322].

5.3.2. Flux decay

The loss of the FRC internal flux during the equilibrium phase is of great importance because, at present, there are no demonstrated techniques that can prevent flux decay. Magnetic flux sustainment based on neutral beam injection is under study [63-65, 18, 413]. Charged fusion products may also contribute to the flux maintenance of future ignited FRCs with advanced fuels [66].

The inferred values of τ_ϕ and $\tau_{\phi cl}$, for various FRC data with good confinement properties, are compared in Fig. 36. The numbered slopes in Fig. 36 indicate the anomaly factors over classical Spitzer diffusivity with $Z_{eff} = 1$, $\eta_\perp/\mu_0$ ($m^2 \cdot s^{-1}$) = $[T_e(eV)/100]^{-3/2}$. For cases without a measurement, T_e was assumed to be either 100 eV or T/2 in the case of $T \leq 200$ eV. Figure 36 suggests moderate flux anomaly factors, mostly in the range 3–5. However, some data from the FRX-C/LSM device [411] show significantly larger anomalies, for reasons yet to be clarified. Flux confinement in the OCT device appears better than classical, but the determination of τ_ϕ was difficult for this case because ϕ did not display a well defined exponential decay [25]. As discussed in Section 5.2.1, there are large uncertainties on these anomaly factors.

As for particle transport, it is more the scaling than the magnitude of τ_ϕ which suggests that the FRC flux confinement is anomalous. Some empirical [40, 21] and theoretical τ_ϕ scaling laws are gathered in

TABLE VIII. FLUX CONFINEMENT SCALING: $\tau_\phi \sim \ell_s^a x_s^b r_c^c n^d T^e$

Scaling	Ref.	(a)	(b)	(c)	(d)	(e)
(A) Empirical						
TRX-1	[40]			2.4	0.4	-0.1
FRX-C/T	[21]	-1		2.0	0.2	0.2
TRX	[142]	0		3.5	0.9	0
(B) Theoretical						
Classical		0	2	2	0	1.5
Krall	[410]	0	2	2	0.5	-0.5

Table VIII; it can be seen that the data do not show the strong $T^{1.5}$ classical dependence. An actual scaling of $\tau_\phi \sim T_e^{0.6}$ was obtained [20]. The empirical τ_ϕ scalings in Table VIII are similar to those of τ_N in Table VII, and are also similar to the Bohm and Krall theoretical scalings. Again, the TRX scaling is more likely to be $\tau_\phi \sim x_s^{3.5} r_c^2$ rather than the proposed $\tau_\phi \sim r_s^{3.5}$ [142]. The peculiar inverse ℓ_s dependence on τ_ϕ inferred in FRX-C/T is not understood and requires further confirmation [21].

The cause of the possible flux confinement anomaly remains obscure. Impurities are unlikely to explain it (see Section 5.3.3) and present models predict a negligible LHD contribution at the field null, although this is still an open question [383]. The theory recently proposed by Krall [385] appears promising, but it does not consider the neighbourhood of the field null. Low-frequency MHD instabilities could also cause a degradation of the FRC flux confinement: it is somewhat puzzling that all FRC data with good confinement properties have been obtained with values of s less than about 2. Values of s around 1.5 have been obtained for some time in small devices [326, 28, 25], but little increase in s was later achieved, in spite of increases in r_c by factors of three to six. It is not clear at the present time whether this possible s limit is the result of formation (see Section 2.5.4) or stability problems.

Some information on the FRC radial resistivity profiles can be obtained by combining τ_N and τ_ϕ data with some theoretical modelling [40]: the values of $\eta(R)$ and $\eta(r_s)$ can be estimated, with many assumptions [253]. Roughly uniform resistivity radial profiles are inferred for most FRCs, for which $\tau_\phi \sim \tau_N$ [28, 40]. This is by no means a general result, and ratios of τ_ϕ/τ_N of about three have been obtained in several devices [239, 20, 42]. Furthermore, ratios of $\eta(R)/\eta(r_s)$ anywhere from 1/5 to 5 have been inferred [40, 21, 253]. The resistivity profile appears to be peaked around R for small values of x_s and around r_s for large values of x_s, a trend that remains unexplained. One difficulty in estimating the ratios $\eta(R)/\eta(r_s)$ is that flux loss actually reflects the average FRC resistivity rather than just $\eta(R)$. In the limit $\eta(R) \to 0$, there is still finite flux decay because of increasingly large currents near the field null [399, 320, 402, 414].

5.3.3. *Energy losses*

Most FRC data in Figs 35 and 36 have ratios of energy to particle confinement times, τ_E/τ_N, of about 0.4. Assuming radially uniform temperatures and taking into account compressional work, it can be shown that each lost electron-ion pair carries away 5T/2 energy [373, 400, 402]. Therefore, particle transport yields a power loss $5NT/2\tau_N$, which is a fraction $5\tau_E/3\tau_N$ of the total power losses $3NT/2\tau_E$. In general, this fraction amounts to 60–80% of the total energy losses [19, 400, 270, 28, 21, 20, 142, 411]. The remaining 20–40% of the total energy losses are essentially due to radiation and thermal conduction.

Radiation losses have been occasionally measured or inferred to be 5–10% of the total energy losses [400, 192, 20]. In the FRX-C/T device, radiative losses of about 8% of total losses were measured by calorimetry, and complementary spectroscopy suggested that these radiative losses could be due to a 0.6% oxygen concentration [192]. Hence, radiation appears to be a small energy loss mechanism in most FRCs, probably from modest ($\lesssim 1\%$) concentrations of oxygen or carbon which result in Z_{eff} values in the range of 1–1.5. Since quartz discharge tubes are generally used, significant radiation from small amounts of silicon could be expected [270, 28]; this is, however, not observed, presumably because wall contact is very transient during FRTP formation. Energy losses associated with neutrals have also been estimated to be negligible [396].

Once radiation has been accounted for, thermal conduction appears to cause 10–30% of the total energy losses. In many cases, such as those presented in Fig. 34, T_e is about constant in time while $T_e + T_i$ drops, suggesting that substantial electron losses balance the large input power from the ions [19, 270, 400, 20]. Furthermore, the measured radial T_e profiles are almost flat up to the separatrix [19, 276]. Zero-dimensional analysis [375, 270, 20] and more detailed modelling [388, 403, 406, 407] have quantified these

electron thermal losses. An anomaly factor over classical (perpendicular) electron thermal diffusivity of about 35 has been inferred for some 5 mtorr FRX-C data [406, 407] from the measured values of τ_E and T_e.

The cause of the electron thermal conduction anomaly is yet to be identified. Around the field null, where gradients are small, one cannot easily explain the fact that T_e remains constant in time without invoking some disturbance of the magnetic structure. Such disturbance could result either from electromagnetic microinstabilities [385, 387] or from more macroscopic low-frequency modes. Krall [385] proposed a scaling law, $\tau_E \sim r_s^3 n T^{0.5}$, based on the drift dissipative electromagnetic mode, in rough agreement with the empirical TRX scaling $\tau_E \sim r_s^{2.7} n^{0.7}$ [410].

In present FRC experiments, electromagnetic modes may be active through the entire separatrix volume (see Section 5.1.3), and heat could be easily conducted up to the edge layer, where parallel thermal conduction is a large energy sink. For such cases, Newton [415] proposed a simple model for the edge layer temperature and obtained a scaling $T_e \sim B_e^{2/3} \ell_s^{1/3}$. The $B_e^{2/3}$ portion of this scaling is consistent with some early [79] and recent [20] measurements, but is also similar to the adiabatic scaling $T_e \sim B_e^{4/5}$. Values of T_e up to 1 keV have indeed been obtained in experiments with $B_e \sim$ 50–100 kG [79, 102], while present values of T_e remain in the range of 100–200 eV for $B_e \sim$ 5–10 kG [19, 276, 400, 28].

Future FRCs with large values of s may have improved heat insulation from low beta values near the separatrix (see Section 5.1.3). For such cases, the values of T_e in the edge layer may be substantially lower than those inside the separatrix, and parallel thermal conduction on open field lines may become unimportant. Hence, a definitive assessment of thermal losses will require FRCs with large values of s.

In most cases, calculations indicate that ion thermal losses are small, presumably because FRCs are well removed from cold radial boundaries and also because parallel ion thermal conduction on open field lines is a moderate heat sink. However, substantial ion losses could occur for cases with r_s close to r_t. Values of $(r_t - r_s)/\rho_{ie}$ of about 10 appear to be required to prevent wall contact, owing to the fairly thick edge layers. There are indications of significant ion thermal losses in some FRC data which did not meet this requirement [25].

Figure 37 gives a comparison of the global FRC confinement properties with those of some tokamak experiments. Values of $n\tau_E$ of about 10^{11} cm^{-3}·s have been achieved in FRCs with $T_i \sim$ 0.7 keV. The next generation of FRC experiments should produce a significant step forward: values of $n\tau_E$ around 10^{12} cm^{-3}·s are projected for compressed FRCs in FRX-C/LSM [42] and for FRCs formed in LSX [39]. These two experiments have different but complementary goals. With $B_e \sim$ 20 kG, FRX-C/LSM will investigate flux loss and electron thermal conduction issues at higher values of T_e (300–500 eV) than in present experiments, but presumably still with $s \lesssim 2$. The LSX device has been designed to operate with $s \lesssim 8$ and may therefore access the regime of possibly improved confinement, as discussed in Section 5.1.3.

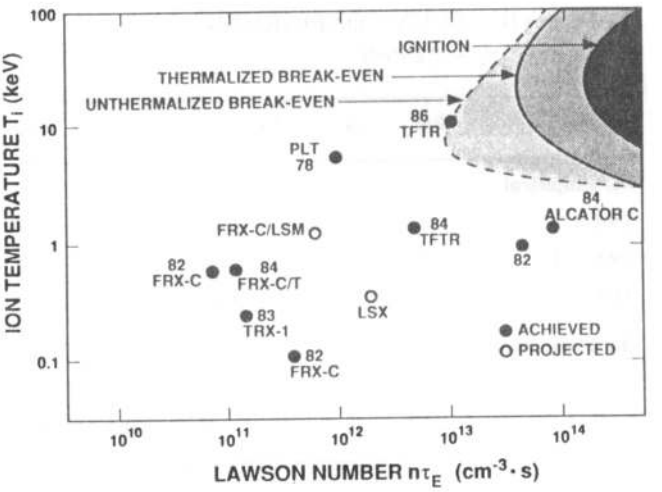

FIG. 37. Achieved and projected values of $n\tau_E$ as functions of T_i for several FRC and tokamak experiments.

Assuming $\tau_E \sim \tau_N/2$, some studies [37, 38] suggest that about an order of magnitude improvement in confinement over the R^2/ρ_{ie} scaling of Fig. 35 is a desirable goal for an attractive FRC reactor. Increased values of x_s and of s are expected to be beneficial for FRC confinement, provided macroscopic stability is retained [416]. Another possibility for improved FRC confinement is to maintain a substantial edge layer in some mirror/FRC hybrid [54, 57]. A factor of two increase in τ_E has been observed when FRCs were translated into a plasma of comparable density [21].

6. CONCLUSIONS

Field reversed configurations have been known since the beginning of fusion research. These elongated CTs were discovered in theta pinches with a reversed bias magnetic field and were at first plagued by tearing and rotational instabilities, which caused a loss of interest

in such plasmas. However, interest revived as experiments with lower radial compression demonstrated long, tearing-free, stable periods before the onset of the n = 2 rotational mode. This instability has been suppressed by multipole fields [22, 23, 20] and present FRCs appear completely grossly stable. The renewed interest in FRCs is partly due to their significant reactor potential: simple and compact geometry including a natural divertor, demonstrated translatability and very high beta values give promise for development to an economical fusion reactor system, make the FRC an ideal candidate for the possible use of advanced fuels [18, 62] and fully justify the present FRC research effort. These attractive attributes should not hide the fact that many physics issues remain to be investigated.

FRC formation still mostly relies on the original field reversed theta pinch method. Although significantly improved over three decades of research, in particular with improved field line connection techniques [27, 28], formation remains poorly controlled and highly dynamic. Hot and clean FRCs can be produced, but their confinement properties appear to depend on many obscure formation details, in particular those concerning preionization. FRC formation also proves to be increasingly difficult in larger devices, for reasons yet to be clarified. The general consensus is that a new FRC formation method on slower timescales is not only desirable but also an increasingly urgent necessity. The Coaxial Slow Source, the Rotamak, the Extrap and the field reversed mirror are candidates for slow FRC formation, and research has been initiated in each of these areas.

FRC equilibrium is relatively well understood. For elongated FRCs inside a flux conserver, one can derive useful, general properties such as those given by Eqs (8)–(12) and the compression laws of Table V. Although based on the MHD model, these properties have been verified within experimental errors for present, highly kinetic FRCs. The most useful relation in FRC physics is perhaps the $\langle\beta\rangle$ condition of Eq. (10) which clearly illustrates the high beta nature of the FRC. It is also the strong constraint on the radial pressure profiles that is partly responsible for steep gradients near the separatrix. In fact, somewhat ironically, reducing $\langle\beta\rangle$ has become a desirable feature and a major goal of FRC research. One way to achieve this goal is to translate FRCs into a flux conserver of smaller radius. Translation has proved a very useful and versatile tool in present experiments and in reactor studies.

FRC stability remains the most intriguing issue. A cursory examination reveals that FRCs are topologically similar to unstabilized Z-pinches and should therefore be violently unstable with regard to MHD. Indeed, MHD theory identified several ideal modes, in particular the global internal tilt instability. Nonetheless, present FRCs are observed to be free of gross instabilities. One might quickly point to the highly kinetic nature of present FRCs as the explanation for this apparent paradox: present values of s (the average number of ion gyroradii across the pressure gradient) are in the range of 1–2, while values of 20–40 appear to be required for reactor conditions [37, 38, 393].

However, detailed studies continue to uncover various stabilizing factors: high beta compressibility, stable edge layer, axial flow in the jet, conducting boundary, elongation, profile effects, FLR effects, rotation and Hall currents may all contribute to the surprising robustness of present FRCs. These factors suggest that there may always be more than just kinetic effects that contribute to FRC stability. Meanwhile, the analytical and numerical tools developed for FRC kinetic studies [29, 365, 337] have raised the level of such calculations and are of general interest for magnetic fusion. Additional stabilizing techniques such as high energy particle injection may be required for future FRCs and are actively investigated [18, 69, 367–372].

FRC confinement is poorly understood at the present time, for various reasons. First, confinement studies are relatively new, with a correspondingly limited database and limited diagnostics and theoretical tools. Second, formation inhibits transport studies, with short lived and unsteady discharges and substantial data scatter. Third, present FRC confinement requires the detailed characterization of not one but two distinct regions: the inside torus and the outside edge layer, whose intrinsic confinement properties are coupled in present FRCs. FRC confinement appears somewhat anomalous in scaling, with a magnitude intermediate between Bohm scaling and classical scaling. Some confinement data from FRX-C/LSM (the largest operating FRC device) reveal somewhat larger anomalies. A strong effort should be devoted in the near future to understanding the cause of this apparent confinement degradation. Particle transport is the dominant energy loss mechanism, and there is evidence for some anomalous electron heat transport as in tokamaks. Future FRC compression in the FRX-C/LSM device [42] will further explore these issues, for higher electron temperatures than in present experiments.

Increasing the values of x_s and of s in order to improve FRC confinement is an often quoted research goal. Numerous theoretical and experimental studies

show that larger values of x_s result in more diffuse pressure profiles, with gentler gradients near the separatrix. Seeking larger values of x_s also extends the trend towards radial compression which helped to eliminate tearing and rotational instabilities. This trend should be continued in future FRC research as much as is allowed by possible ion thermal conduction and impurity effects. In principle, larger values of s also yield improved confinement properties by increasing the number of diffusive radial steps. In addition, a qualitatively new confinement regime may occur for large values of s, with more localized micro-instabilities.

It should be noted that larger values of x_s and of s may conflict with gross stability requirements. As they become more MHD-like, FRCs may lose some of their present stabilizing factors. Forming FRCs with large values of s, with simultaneous good confinement properties and stability properties, has been identified as the most critical issue and the primary thrust of FRC research. The LSX device [39] has been specifically designed to investigate this issue. In the last few years, for unclear reasons, which perhaps involve formation rather than stability, there is a certain lack of success in producing FRCs with good confinement and with values of s greater than about 2 [20, 41, 141, 411]. Future research is required to clarify this point.

The importance of the edge layer and the potential benefits of high energy particle injection have been often brought up in this review. Both relate to some aspects of mirror research and deserve increased experimental and theoretical attention in future FRC research. The edge layer is a crucial component of FRCs rather than merely an exhaust region outside the separatrix. It is the portion of the FRC that is MHD stable, and it may influence the unstable portion of the FRC, in particular for large separatrix pressures and axial flows near the ends. The edge layer may be the key to the origin and, therefore, the control of FRC rotation [318, 352, 331]. The edge layer also strongly influences the confinement properties of present FRCs. Its physics remained largely unexplored, but there are indications of possible beneficial effects from electrostatic potentials [275] and from reduced pressure gradients [54, 57, 21]. These effects, which may be related to the H-mode regime of improved tokamak confinement, suggest the desirability of further research regarding FRC/mirror hybrids. Finally, as a natural divertor, the edge layer may provide impurity control and permit direct energy conversion [18].

High energy particle injection could become another important ingredient of FRC research. Slow FRC formation may be possible by using neutral beams. This FRM approach came close to success a decade ago [15], and later studies [14, 63–65, 174, 172] suggest that it may be worth further consideration. High energy particles from neutral beams could help to achieve stable FRCs with large values of s by maintaining strong kinetic effects. A similar result might also be obtained by mixing ion layers with FRCs [368, 369]. In addition, high energy particles may provide heating, refuelling, rotation control, flux sustainment, and possibly steady state operation [62–65, 18, 413]. Clearly, such a variety of possibly simultaneous benefits presents an opportunity for FRC research that should be actively explored soon.

ACKNOWLEDGEMENTS

The author wishes to thank R.E. Siemon and A.R. Sherwood for suggesting this project. The material gathered in this review greatly benefitted from comments and conversations with H.R. Lewis, L.C. Steinhauer and D.C. Barnes, and with many other colleagues from the Compact Torus community. Special thanks are also due to H.R. Lewis for carefully reading the manuscript and for his encouragement.

This work was supported by the United States Department of Energy.

LIST OF SYMBOLS AND ACRONYMS

A_i	ion atomic mass
B, B_z	poloidal (magnetic) field
B_b	reversed bias field
B_c	crowbarred field
B_e	external (equilibrium) field
B_{LO}	lift-off reversed field
B_M	maximum external field
B_0	initial reversed field
B_o	translation vacuum guide field
B_{th}	threshold stabilization field
B_θ	toroidal field
B_*	Green-Newton field
CT	compact torus
CSS	Coaxial Slow Source
$D_\perp$	perpendicular diffusion coefficient
$e_s = \ell_s/2r_s$	separatrix elongation
E_{BV}	vacuum magnetic energy
E_p	plasma thermal energy within separatrix
E_θ	azimuthal tube electric field
FKR	Furth-Killeen-Rosenbluth

FLR	Finite Larmor Radius
FRC	field reversed configuration
FRM	field reversed mirror
FRTP	field reversed theta pinch
$G_{LO} = B_{LO}/B_*$	normalized lift-off reversed field
HFSB	high flux sharp boundary
k	Boltzmann constant
k_z	axial mode number
ℓ	(half) multipole order
ℓ_c	coil length
ℓ_s	separatrix length
$L_\perp$	perpendicular density gradient length
LHD	lower hybrid drift
LFSB	low flux sharp boundary
m	poloidal mode number
m_i	ion mass
MHD	magneto-hydro-dynamic
n	density, toroidal mode number
n_M	maximum density
n_0	preionized density
N	particle inventory within separatrix
N_0	initial line density
N_*	critical line density
p	plasma pressure
p_M	maximum plasma pressure
p_0	gas fill pressure
PI	preionization
r_c	coil radius
r_ℓ	flux loop radius
r_s	separatrix radius
r_t	discharge tube radius
$r_{\Delta\phi}$	excluded flux radius
R	major (field null) radius
RMF	rotating magnetic field
s	number of ion gyroradii from R to r_s
$S = R/\rho_{ie}$	normalized major radius
t_{LO}	lift-off time
$T = T_e+T_i$	total plasma temperature
$T_{e,i}$	electron, ion temperature
T_I	ideal implosion temperature
v_A	Alfvén velocity
v_D	diamagnetic drift velocity
$v_i = (T_i/m_i)^{1/2}$	ion thermal velocity
V	separatrix volume
VSLS	velocity space loss sphere
$w = \delta/\rho_{ie}$	normalized edge layer thickness
$x_s = r_s/r_c$	ratio of seraratrix to coil radii
Z_{eff}	effective ion charge
$\alpha = \Omega/\Omega_{Di}$	normalized plasma rotation
$\beta = 2\mu_0 p/B_e^2$	(external) plasma beta
$\langle\beta\rangle$	average beta within separatrix
β_s	separatrix beta
γ	instability growth rate
δ	separatrix density gradient length
$\Delta\phi$	plasma diamagnetism
ϵ	pressure profile parameter
η	plasma resistivity
μ	entropy variable
μ_0	permeability of free space
ν	flux relaxation parameter
ρ_i	ion gyroradius
ρ_{ie}	external ion gyroradius
τ_f	formation time
τ_ℓ	configuration lifetime
τ_r	reversal time
τ_s	stable period
τ_A	Alfvén formation time
τ_E	global energy confinement time
τ_N	particle confinement time
τ_ϕ	flux confinement time
$\tau_\parallel$	edge layer particle loss time
$\tau_\perp$	closed-lines particle loss time
ϕ	internal magnetic flux
ϕ_b	reversed bias flux
ϕ_e	equilibrium flux
ϕ_{LO}	lift-off flux
ϕ_0	initial flux
ϕ_*	Green-Newton flux
ψ	flux variable
ψ_M	maximum flux value
ω_r	real part of mode frequency
ω_{LH}	lower hybrid frequency
Ω	plasma rotational frequency
Ω_{Di}	ion diamagnetic frequency

REFERENCES

[1] ALFVÉN, H., in Peaceful Uses of Atomic Energy (Proc. 2nd Int. Conf. Geneva, 1958), Vol. 31, United Nations, New York (1958) 3.

[2] CHRISTOFILOS, N., ibid., **32** (1958) 279.

[3] KOLB, A.C., DOBBIE, C.B., GRIEM, H.R., Phys. Rev. Lett. **3** (1959) 5.

[4] GREEN, T.S., Phys. Rev. Lett. **5** (1960) 297.

[5] ES'KOV, A.G., KURTMULLAEV, R.Kh., KRESHCHUK, A.P., et al., in Plasma Physics and Controlled Nuclear Fusion Research 1978 (Proc. 7th Int. Conf. Innsbruck, 1978), Vol. 2, IAEA, Vienna (1979) 187.

[6] FURTH, H., in Compact Toruses and Energetic Particle Injection (Proc. US-Japan Joint Symp. Princeton, NJ, 1979), Princeton Plasma Physics Laboratory, Princeton University (1979) 3.

[7] JARBOE, T.R., Spheromak research, to be submitted to Nucl. Fusion (1989).

[8] FINN, J.M., SUDAN, R.N., Nucl. Fusion **22** (1982) 1443.

[9] HUGRASS, W.N., JONES, I.R., McKENNA, K.F., PHILLIPS, M.G.R., STORER, R.G., TUCZEK, H., Phys. Rev. Lett. **44** (1980) 1676;
JONES, I.R., KNIGHT, A., in Controlled Fusion and Plasma Physics (Proc. 12th Eur. Conf. Budapest, 1985), Vol. 1, European Physical Society (1985) 647;
DURANCE, G., HOGG, G.R., TENDYS, J., WATTERSON, P.A., Plasma Phys. Controll. Fusion **29** (1987) 227.

[10] PIETRZYK, Z.A., VLASES, G.C., BROOKS, R.D., HAHN, K.D., RAMAN, R., Nucl. Fusion **27** (1987) 1478.

[11] GOLDENBAUM, G.C., IRBY, J.H., CHONG, Y.P., HART, G.W., Phys. Rev. Lett. **44** (1980) 393.

[12] NOGI, Y., OGURA, H., OSANAI, Y., SAITO, K., SHIINA, S., YOSHIMURA, H., J. Phys. Soc. Jpn. **49** (1980) 710.

[13] JONES, W.B., MILLER, R.D., Phys. Fluids **11** (1968) 1550;
WELLS, D.R., NOLTING, E., COOKE, F., Jr., TUNSTALL, J., JINDRA, P., HIRSCHBERG, J., Phys. Rev. Lett. **33** (1974) 1203;
KAWAI, K., PIETRZYK, Z.A., HUNTER, H. T., Phys. Fluids **30** (1987) 2561.

[14] PEARLSTEIN, L.D., ANDERSON, D.V., BALDWIN, D.E., et al., in Plasma Physics and Controlled Nuclear Fusion Research (Proc. 7th Int. Conf. Innsbruck, 1978), Vol. 2, IAEA, Vienna (1979) 457.

[15] SIMONEN, T.C., CLAUSER, J.F., COENSGEN, F.H., et al., ibid., 389.

[16] TURNER, W.C., GOLDENBAUM, G.C., GRANNEMAN, E.H.A., et al., Phys. Fluids **26** (1983) 1965.

[17] GORMEZANO, C., Nucl. Fusion **19** (1979) 1085.

[18] MOMOTA, H., OKAMOTO, M., NOMURA, Y., et al., Fusion Technol. **11** (1987) 436; Plasma Physics and Controlled Nuclear Fusion Research 1986 (Proc. 11th Int. Conf. Kyoto, 1986), Vol. 2, IAEA, Vienna (1987) 719.

[19] ARMSTRONG, W.T., LINFORD, R.K., LIPSON, J., PLATTS, D.A., SHERWOOD, E.G., Phys. Fluids **24** (1981) 2068.

[20] SIEMON, R.E., ARMSTRONG, W.T., BARNES, D.C., et al., Fusion Technol. **9** (1986) 13.

[21] TUSZEWSKI, M., ARMSTRONG, W.T., CHRIEN, R.E., et al., Phys. Fluids **29** (1986) 863.

[22] OHI, S., MINATO, T., KAWAKAMI, Y., et al., Phys. Rev. Lett. **51** (1983) 1042.

[23] HOFFMAN, A.L., SLOUGH, J.T., HARDING, D.G., Phys. Fluids **26** (1983) 1626.

[24] ALIKHANOV, S.G., BAKHTIN, V.P., ES'KOV, A.G., et al., in Plasma Physics and Controlled Nuclear Fusion Research 1982 (Proc. 9th Int. Conf. Baltimore, 1982), Vol. 3, IAEA, Vienna (1983) 319.

[25] TANJYO, M., OKADA, S., ITO, Y., et al., in Plasma Physics and Controlled Nuclear Fusion Research 1984 (Proc. 10th Int. Conf. London, 1984), Vol. 2, IAEA, Vienna (1985) 523.

[26] REJ, D.J., ARMSTRONG, W.T., CHRIEN, R.E., et al., Phys. Fluids **29** (1986) 852.

[27] BELIKOV, V.V., GOLOVIZNIN, V.M., KORSHUNOV, V.K., et al., in Plasma Physics and Controlled Nuclear Fusion Research 1982 (Proc. 9th Int. Conf. Baltimore, 1982), Vol. 2, IAEA, Vienna (1983) 343.

[28] SLOUGH, J.T., HOFFMAN, A.L., MILROY, R.D., HARDING, D.G., STEINHAUER, L.C., Nucl. Fusion **24** (1984) 1537.

[29] BARNES, D.C., SCHWARZMEIER, J.L., LEWIS, H.R., SEYLER, C.E., Phys. Fluids **29** (1986) 2616.

[30] SEMENOV, V.N., SOSNIN, N.V., Sov. J. Plasma Phys. **7** (1981) 180.

[31] HEWETT, D.W., SPENCER, R.L., Phys. Fluids **26** (1983) 1299.

[32] KAKO, M., ISHIMURA, T., AMANO, T., J. Phys. Soc. Jpn. **52** (1983) 3056.

[33] SUZUKI, K., HAMADA, S., J. Phys. Soc. Jpn. **53** (1984) 16.

[34] SHUMAKER, D.E., Fusion Technol. **9** (1986) 75.

[35] MILROY, R.D., BRACKBILL, J.U., Phys. Fluids **25** (1982) 775.

[36] BELIKOV, V.V., GOLOVIZNIN, V.M., KORSHUNOV, V.K., MALYUTIN, A.I., SEMENOV, V.N., in Controlled Fusion and Plasma Physics (Proc. 10th Eur. Conf. Moscow, 1981), European Physical Society (1981) paper L-13.

[37] HAGENSON, R.L., KRAKOWSKI, R.A., A Compact Toroid Fusion Reactor Based on the Reversed Field θ-Pinch, Rep. LA-8758-MS, Los Alamos Scientific Laboratory (1981).*

[38] VLASES, G.C., ROWE, D. S., and the FIREBIRD DESIGN TEAM, Fusion Technol. **9** (1986) 116.

[39] HOFFMAN, A.L., DEHART, T.E., MILROY, R.D., SLOUGH, J.T., in US-Japan Workshop on Compact Toroids (Proc. 8th Symp. Osaka, 1986), Osaka University (1986) 73.

[40] STEINHAUER, L.C., MILROY, R.D., SLOUGH, J.T., Phys. Fluids **28** (1985) 888.

[41] TUSZEWSKI, M., in Physics and Technology of Compact Toroids (Proc. 7th Symp. Santa Fe, 1985), Rep. LA-10830-C, Los Alamos National Laboratory (1986) 142;
TUSZEWSKI, M., CHRIEN, R.E., HUGRASS, W.N., REJ, D.J., SIEMON, R.E., WRIGHT, B.L., in Physics and Technology of Compact Toroids (Proc. 8th Symp. Univ. Maryland, 1987), University of Maryland (1987) 191.

[42] REJ, D.J., CHRIEN, R.E., BARNES, G.A., et al., in Physics and Technology of Compact Toroids (Proc. 8th Symp. Univ. Maryland, 1987), University of Maryland (1987) 167.

[43] SHEFFIELD, J., Nucl. Fusion **25** (1985) 1733.

[44] FLEISCHMANN, H.H., KAMMASH, T., Nucl. Fusion **15** (1975) 1143.

[45] TERRY, W. K., PAPERMAN, E. B., Fusion Technol. **9** (1986) 171.

[46] ARMSTRONG, W.T., MORGAN, J.A., in Megagauss Technology and Pulsed Power Applications (Fowler, C.M., Caird, R.S., Erickson, D.J., Eds), Plenum Press, New York and London (1987) 683.

[47] WILLENBERG, H.J., HOFFMAN, A.L., STEINHAUER, L.C., ROSE, P.H., in Compact Toruses and Energetic Particle Injection (Proc. US-Japan Joint Symp. Princeton, NJ, 1979), Princeton Plasma Physics Laboratory, Princeton University (1979) 233.

---

* Los Alamos Reports can be obtained from P. Lang, OS-6 Group, Mail Stop F674, Los Alamos National Laboratory, Los Alamos, NM 87545, USA.

[48] WILLENBERG, H.J., STEINHAUER, L.C., HOFFMAN, A.L., CHURCHILL, T.L., ROSE, P.H., in Technology of Controlled Nuclear Fusion (Proc. 4th ANS Topical Meeting, King of Prussia, PA, 1980), CONF-801011, Electric Power Research Institute, Palo Alto, CA (1981) 894.
[49] ROBSON, A.E., in Megagauss Physics and Technology (TURCHI, P.J., Ed.), Plenum Press, New York (1980) 425.
[50] MILLER, R.L., KRAKOWSKI, R.A., in Technology of Controlled Nuclear Fusion (Proc. 4th ANS Topical Meeting, King of Prussia, PA, 1980), CONF-801011, Electric Power Research Institute, Palo Alto, CA (1981) 825.
[51] QUIMBY, D.C., HOFFMAN, A.L., VLASES, G.C., Nucl. Fusion **21** (1981) 553.
[52] ARTIUGINA I.M., ZHELTOV, V.A., KANTAN, V.V., et al., Voprosy Atomnoi Nauki i Techniki, Seriia: Termoiadernyi Sintez **1** 3 (1979) 62 (available as Los Alamos Scientific Laboratory Translation LA-TR-79-42, 1979).
[53] KRAKOWSKI, R.A., MILLER, R.L., BATHKE, C.G., et al., in Plasma Physics and Controlled Nuclear Fusion Research 1980 (Proc. 8th Int. Conf. Brussels, 1980), Vol. 2, IAEA, Vienna (1981) 607.
[54] SEYLER, C.E., GROSSMANN, W., STEINHAUER, L.C., Comments Plasma Phys. Controll. Fusion **4** (1978) 21.
[55] LOGAN, B.G., LICHTENBERG, A.J., LIEBERMAN, M.A., MAKHIJANI, A., Phys. Rev. Lett. **28** (1972) 144.
[56] LICHTENBERG, A.J., LIEBERMAN, M.A., Nucl. Fusion **16** (1976) 532.
[57] TUSZEWSKI, M., LINFORD, R.K., Phys. Fluids **25** (1982) 765.
[58] DREICER, H., Proposal for FRX-C and Multiple-Cell Compact Torus Experiments, Rep. LA-8045-P, Los Alamos Scientific Laboratory (1979).
[59] SEVILLANO, E., RIBE, F.L., in Magnetic Reconnection in Space and Laboratory Plasmas, Geophysical Monograph 30, American Geophysical Union, Washington, DC (1984) 313.
[60] BURTSEV, V.A., KOZHEVIN, V.M., MAKHANKOV, A.N., in Fusion Reactor Design and Technology (Proc. 4th IAEA Technical Committee Meeting and Workshop, Yalta, 1986), Vol. 1, IAEA, Vienna (1987) 413.
[61] GILLIGAN, J.G., MILEY, G.H., DRIEMEYER, D., in Technology of Controlled Nuclear Fusion (Proc. 4th ANS Topical Meeting, King of Prussia, PA, 1980), CONF-801011, Electric Power Research Institute, Palo Alto, CA (1981) 840.
[62] MILEY, G.H., Nucl. Instrum. Methods **207** (1983) 111.
[63] HIRANO, K., Nucl. Fusion **24** (1984) 1159.
[64] HIRANO, K., A Self-Consistent Modeling of a Quasi-Steady State Compact Torus Evolving to Ignition, Rep. IPPJ-801, Nagoya University (1986).
[65] HIRANO, K., Ignition of Deuterium Based Fuel Cycles in a High Beta System, Rep. IPPJ-810, Nagoya University (1987).
[66] BERK, H.L., MOMOTA, H., TAJIMA, T., Phys. Fluids **30** (1987) 3548.
[67] OHNISHI, M., OHI, S., OKAMOTO, M., MOMOTA, H., WAKABAYASHI, J., Fusion Technol. **12** (1987) 249.
[68] OHNISHI, M., KURANAGA, H., OKAMOTO, M., Nucl. Fusion **28** (1988) 1427.
[69] NOMURA, Y., J. Phys. Soc. Jpn. **54** (1985) 1369.
[70] POST, R.F., The Physics of Field-Reversed Mirrors, Rep. UCRL-81586, Lawrence Livermore Laboratory (1978).
[71] KOLB, A.C., in Peaceful Uses of Atomic Energy (Proc. 2nd Int. Conf. Geneva, 1958), Vol. 31, United Nations, New York (1958) 328.
[72] KOLB, A.C., GRIEM, H.R., FAUST, W.R., in Ionization Phenomena in Gases (Proc. 4th Int. Conf. Uppsala, 1959), Vol. 2, North-Holland, Amsterdam (1959) 1037.
[73] ROSTOKER, N., KOLB, A.C., Phys. Rev. **124** (1961) 965.
[74] GRIEM, H.R., KOLB, A.C., LUPTON, W.H., PHILLIPS, D.T., in Plasma Physics and Controlled Nuclear Fusion Research (Proc. 1st Int. Conf. Salzburg, 1961), Nucl. Fusion Suppl., Part 2, IAEA, Vienna (1962) 543.
[75] KOLB, A.C., GRIEM, H.R., LUPTON, W.H., et al., ibid., 553; HAIN, K., KOLB, A.C., ibid., 561.
[76] BOYER, K., ELMORE, W.C., LITTLE, E.M., QUINN, W.E., TUCK, J.L., Phys. Rev. **119** (1960) 831.
[77] MATHER, J.W., Nucl. Fusion **1** (1961) 233.
[78] LITTLE, E.M., QUINN, W.E., RIBE, F.L., Phys. Fluids **4** (1961) 711.
[79] LITTLE, E.M., QUINN, W.E., RIBE, F.L., SAWYER, G.A., in Plasma Physics and Controlled Nuclear Fusion Research (Proc. 1st Int. Conf. Salzburg, 1961), Nucl. Fusion Suppl., Part 2, IAEA, Vienna (1962) 497.
[80] LITTLE, E.M., QUINN, W.E., Phys. Fluids **6** (1963) 875.
[81] JAHODA, F.C., SAWYER, G.A., Phys. Fluids **6** (1963) 1195.
[82] JAHODA, F.C., RIBE, F.L., SAWYER, G.A., Phys. Rev. **131** (1963) 24.
[83] BODIN, H.A.B., GREEN, T.S., NIBLETT, G.B.F., PEACOCK, N.J., in Ionization Phenomena in Gases (Proc. 4th Int. Conf., Uppsala, 1959), Vol. 2, North-Holland, Amsterdam (1959) 1065.
[84] NIBLETT, G.B.F., GREEN, T.S., Proc. Phys. Soc. London **74** (1959) 737.
[85] BODIN, H.A.B., NEWTON, A.A., PEACOCK, N.J., Nucl. Fusion **1** (1961) 139.
[86] BODIN, H.A.B., GREEN, T.S., NIBLETT, G.B.F., et al., in Plasma Physics and Controlled Nuclear Fusion Research (Proc. 1st Int. Conf. Salzburg, 1961), Nucl. Fusion Suppl., Part 2, IAEA, Vienna (1962) 511.
[87] BODIN, H.A.B., GREEN, T.S., NIBLETT, G.B.F., PEACOCK, N.J., QUINN, J.M.P., REYNOLDS, J.A., ibid., 521.
[88] GREEN, T.S., Nucl. Fusion **2** (1962) 92.
[89] GREEN, T.S., Phys. Fluids **6** (1963) 864.
[90] GREEN, T.S., Nucl. Fusion **3** (1963) 57.
[91] BODIN, H.A.B., Nucl. Fusion **3** (1963) 215.
[92] BODIN, H.A.B., NEWTON, A.A., Phys. Fluids **6** (1963) 1338.
[93] JORDAN, H.L., in Plasma Physics and Controlled Nuclear Fusion Research (Proc. 1st Int. Conf. Salzburg, 1961), Nucl. Fusion Suppl., Part 2, IAEA, Vienna (1962) 589.
[94] BEERWALD, H., BOGEN, P., EL-KHALAFAWY, T., FAY, H., HINTZ, E., KEVER, H., ibid., 595.
[95] HINTZ, E., ibid., 601.
[96] BOGEN, P., HINTZ., E., ibid., 607.
[97] KEVER, H., ibid., 613.
[98] BOGEN, P., HINTZ, E., SCHLÜTER, J., Nucl. Fusion **4** (1964) 131.

[99] KEILHACKER, M., Nucl. Fusion **4** (1964) 287.
[100] EBERHAGEN, A., GLASER, H., Nucl. Fusion **4** (1964) 296.
[101] EBERHAGEN, A., GLASER, H., Z. Naturforschung **20a** (1965) 1268.
[102] HINTZ, E., KOLB, A.C., LUPTON, W.H., GRIEM, H.R., Phys.Fluids **7** (1964) 153.
[103] KOLB, A.C., THONEMANN, P.C., HINTZ, E., Phys. Fluids **8** (1965) 1005.
[104] HINTZ, E., KOLB, A.C., Phys. Fluids **8** (1965) 1347.
[105] KOLB, A.C., LUPTON, W.H., ELTON, R.C., et al., in Plasma Physics and Controlled Nuclear Fusion Research (Proc. 2nd Int. Conf. Culham, 1965), Vol. 1, IAEA, Vienna (1966) 261.
[106] McLEAN, E.A., ANDERSON, A.D., GRIEM, H.R., in Topical Conference on High Beta Plasma (Proc. Conf. Los Alamos, NM, 1967), Rep. LA-3770, Los Alamos Scientific Laboratory (1967) paper A5.
[107] KOLB, A.C., YOUNG , M.P., McLEAN, E.A., ibid., paper G5;
KOLB, A.C., DIXON, R.H., DÜCHS, D., ELTON, R.C., YOUNG, M.P., in Plasma Physics and Controlled Nuclear Fusion Research 1968 (Proc. 3rd Int. Conf. Novosibirsk, 1968), Vol. 2, IAEA, Vienna (1969) 567;
DÜCHS, D.F., DIXON, R.H., ELTON, R.C., Phys. Fluids **17** (1974) 124.
[108] JAHODA, F.C., LITTLE, E.M., QUINN, W.E., RIBE, F.L., SAWYER, G.A., J. Appl. Phys. **35** (1964) 2351;
LITTLE, E.M., QUINN, W.E., SAWYER, G.A., Phys. Fluids **8** (1965) 1168;
SAWYER, G.A., FINLAYSON, V.A., JAHODA, F.C., THOMAS, K.S., Phys. Fluids **10** (1967) 1564.
[109] GREEN, T.S., NEWTON, A.A., Phys. Fluids **9** (1966) 1386.
[110] ALLEN, T.K., COXELL, H., HILL, M., SPALDING, I.J., in Topical Conference on High Beta Plasma (Proc. Conf. Los Alamos, NM, 1967), Rep. LA-3770, Los Alamos Scientific Laboratory (1967) paper G4.
[111] KALECK, A., KEVER, H., KÖNEN, L., et al., ibid., paper A4.
[112] KALECK, A., KÖNEN, L., NOLL, P., et al., in Plasma Physics and Controlled Nuclear Fusion Research 1968 (Proc. 3rd Int. Conf. Novosibirsk, 1968), Vol. 2, IAEA, Vienna (1969) 581.
[113] KÖNEN, L., NOLL, P., WAELBROECK, F., WITULSKI, H., in Controlled Fusion and Plasma Physics (Proc. 4th Eur. Conf. Rome, 1970), European Physical Society (1970) 41.
[114] KEILHACKER, M., HEROLD, H., COOPER, J., ROBERTS, D.E., in Plasma Physics and Controlled Nuclear Fusion Research (Proc. 2nd Int. Conf. Culham, 1965), Vol. 1, IAEA, Vienna (1966) 315.
[115] EBERHAGEN, A., GROSSMAN, W., Z. Phys. **248** (1971) 130.
[116] TAYLOR, J.B., J. Nucl. Energy C **4** (1962) 401.
[117] SCHMIDT, G., Phys. Fluids **5** (1962) 636;
ROSTOKER, N., KOLB, A.C., Phys. Fluids **5** (1962) 741.
[118] ROBERTS, K.V., TAYLOR, J.B., Phys. Rev. Lett. **8** (1962) 197.
[119] HAINES, M.G., Phys. Lett. **6** (1963) 313;
HAINES, M.G., in Ionization Phenomena in Gases (Proc. 6th Int. Conf. Paris, 1963), Vol. 4, S.E.R.M.A., Paris (1964) 477.
[120] JENSEN, T.H., VOORHIES, H.G., On Angular Momentum of a Theta Pinch Plasma, Rep. GA-4202, General Atomic Co., San Diego, CA (1963).
[121] KVARTSKHAVA, I.F., KERVALIDZE, K.N., ZUKAKISHVILI, G.G., GVALADZE, Yu.S., Nucl. Fusion **3** (1963) 285.
[122] BOSTICK, W.H., WELLS, D.R., Phys. Fluids **6** (1963) 1325.
[123] VELIKHOV, E.P., J. Nucl. Energy C **6** (1964) 203.
[124] THONEMANN, P.C., KOLB, A.C., Phys. Fluids **7** (1964) 1455.
[125] HAINES, M.G., Adv. Phys. **14** (1965) 167.
[126] MORSE, R.L., Equilibria of Collisionless Plasmas, Rep. LA-3844-MS, Los Alamos Scientific Laboratory (1968).
[127] DÜCHS, D., Phys. Fluids **11** (1968) 2010.
[128] ES'KOV, A.G., KURTMULLAEV, R.Kh., MALYUTIN, A.I., SEMENOV, V.N., CHERNYAKOV, A.L., in Controlled Fusion and Plasma Physics (Proc. 6th Eur. Conf. Moscow, 1973), European Physical Society (1973) 595.
[129] ES'KOV, A.G., ZOLOTOVSKY, O.A., KURTMULLAEV, R.Kh., et al., ibid., 599.
[130] LINFORD, R.K., ARMSTRONG, W.T., PLATTS, D.A., SHERWOOD, E.G., in Plasma Physics and Controlled Nuclear Fusion Research 1978 (Proc. 7th Int. Conf. Innsbruck, 1978), Vol. 2, IAEA, Vienna (1979) 447.
[131] ARMSTRONG, W.T., HARDING, D.G., CRAWFORD, E.A., HOFFMAN, A.L., Phys. Fluids **25** (1982) 2121.
[132] SATO, K.I., OSANAI, Y., AIZAWA, T., Nucl. Fusion **20** (1980) 1173.
[133] SATO, K.I., AKIYAMA, R., OSANAI, Y., AIZAWA, T., KAWAKAMI, I., Nucl. Fusion **21** (1981) 1015.
[134] ANDELFINGER, C., DECKER, G., FUNFER, E., et al., in Plasma Physics and Controlled Nuclear Fusion Research (Proc. 2nd Int. Conf. Culham, 1965), Vol. 1, IAEA, Vienna (1966) 249.
[135] SHIMAMURA, S., NOGI, Y., Fusion Technol. **9** (1986) 69.
[136] COMMISSO, R.J., ARMSTRONG, W.T., COCHRANE, J.C., et al., in Physics and Technology of Compact Toroids (Proc. 3rd Symp. Los Alamos, NM, 1980), Rep. LA-8700-C, Los Alamos Scientific Laboratory (1981) 184.
[137] OHI, S., OKADA, S., TANJYO, M., ITO, Y., ISHIMURA, T., ITO, H., ibid., 192.
[138] NAKATA, S., SEKIGUCHI, T., ISAKA, M., Phys. Fluids **28** (1985) 445.
[139] TANJYO, M., OKADA, S., ITO, Y., et al., Translation Experiment of a Plasma with Field Reversed Configuration, Technol. Rep. Osaka Univ. **34** (1984) 201.
[140] WANG, G., WANG, S., CUI, H., LIAO, J., Nucl. Fusion Plasma Phys. (China) **4** (1984) 36.
[141] SLOUGH, J.T., HOFFMAN, A.L., Nucl. Fusion **28** (1988) 1121.
[142] HOFFMAN, A.L., SLOUGH, J.T., Nucl. Fusion **26** (1986) 1693.

[143] SIEMON, R.E., ARMSTRONG, W.T., BARTSCH, R.R., et al., in Plasma Physics and Controlled Nuclear Fusion Research 1982 (Proc. 9th Int. Conf. Baltimore, 1982), Vol. 2, IAEA, Vienna (1983) 283.
[144] BARNES, D.C., ARMSTRONG, W.T., CARAMANA, E.J., et al., in Plasma Physics and Controlled Nuclear Fusion Research 1986 (Proc. 11th Int. Conf. Kyoto, 1986), Vol. 2, IAEA, Vienna (1987) 673.
[145] SLOUGH, J.T., MILROY, R.D., HARDING, D.G., HOFFMAN, A.L., in Physics and Technology of Compact Toroids (Proc. 7th Symp. Santa Fe, NM, 1985), Rep. LA-10830-C, Los Alamos Scientific Laboratory (1986) 106.
[146] SEVILLANO, E., RIBE, F.L., Phys. Fluids **28** (1985) 3142.
[147] OGI, S., SHIRATANI, M., TAKAMATSU, M., WATANABE, Y., AKAZAKI, M., Jpn. J. Appl. Phys. **25** (1986) 762.
[148] MILROY, R.D., in Sherwood Theory Meeting (Proc. Mtg. Arlington, VA, 1983), University of Maryland (1983) paper 2R6.
[149] HOFFMAN, A.L., MILROY, R.D., SLOUGH, J.T., STEINHAUER, L.C., Fusion Technol. **9** (1986) 48.
[150] BARNES, D.C., SCHNACK, D.D., Bull. Am. Phys. Soc. **29** (1984) 1360.
[151] PHILLIPS, J.A., Proposal to Produce Large Compact Toroids, Rep. LA-8711-P, Los Alamos National Laboratory (1981).
[152] ALIDIERES, M., AYMAR, R., JOURDAN, P., KOECHLIN, F., Plasma Phys. **10** (1968) 841.
[153] McKENNA, K.F., REJ, D.J., TUSZEWSKI, M., Nucl. Fusion **23** (1983) 1319.
[154] EBERHAGEN, A., Verh. Dtsch. Phys. Ges. (VI) **10** (1975) 244.
[155] BECKER, G., EBERHAGEN, A., GRUBER, O., et al., in Plasma Physics and Controlled Nuclear Fusion Research 1974 (Proc. 5th Int. Conf. Tokyo, 1974), Vol. 3, IAEA, Vienna (1975) 47.
[156] KONDOH, Y., OKAMURA, S., NAGAO, S., J. Phys. Soc. Jpn. **37** (1974) 200;
KONDOH, Y., NAGAO, S., FUTAWARI, N., ITOH, K., Jpn. J. Appl. Phys. **13** (1974) 1037;
KONDOH, Y., ITOH, K., NAGAO, S., J. Phys. Soc. Jpn. **41** (1976) 1356;
ITOH, K., KONDOH, Y., NAGAO, S., Nucl. Fusion **18** (1978) 769.
[157] McKENNA, K.F., GRIBBLE, R.F., in Physics and Technology of Compact Toroids (Proc. 6th Symp. Princeton, NJ, 1984), Princeton Plasma Physics Laboratory, Princeton University (1985) 202.
[158] JONES, I.R., The Rotamak Concept, Rep. FUPH-R-151, Flinders University of South Australia (1979).
[159] BLEVIN, H.A., THONEMANN, P.C., in Plasma Physics and Controlled Nuclear Fusion Research (Proc. 1st Int. Conf. Salzburg, 1961), Nucl. Fusion Suppl., Part 1, IAEA, Vienna (1962) 55.
[160] JONES, I.R., HUGRASS, W.N., J. Plasma Phys. **26** (1981) 441;
HUGRASS, W.N., GRIMM, R.C., ibid., 455;
HUGRASS, W.N., JONES, I.R., PHILLIPS, M.G.R., ibid., 465;
HUGRASS, W.N., J. Plasma Phys. **28** (1982) 369.
[161] HUGRASS, W.N., Austr. J. Phys. **37** (1984) 509.
[162] KÜHNAPFEL, M., STAMPA, A., TABERSKY, R., TUCZEK, H., in Physics and Technology of Compact Toroids (Proc. 8th Symp. Univ. Maryland, 1987), University of Maryland (1987) 218.
[163] DURANCE, G., JESSUP, B.L., JONES, I.R., TENDYS, J., Phys. Rev. Lett. **48** (1982) 1252.
[164] DURANCE, G., JONES, I.R., Phys. Fluids **29** (1986) 1196.
[165] JONES, I.R., TURLEY, M.D.E., WEDDING, J.E., DURANCE, G., HOGG, G.R., TENDYS, J., Austr. J. Phys. **40** (1987) 157.
[166] McKENNA, K.F., Equilibrium Constraints Applied to RMF-Driven Compact Toroid Devices, Rep. LA-9024-MS, Los Alamos National Laboratory (1981).
[167] LEHNERT, B., Phys. Scr. **10** (1974) 139, **13** (1976) 250, and **16** (1977) 147.
[168] DRAKE, J.R., HELLSTEN, T., LANDBERG, R., LEHNERT, B., WILNER, B., in Plasma Physics and Controlled Nuclear Fusion Research 1980 (Proc. 8th Int. Conf. Brussels, 1980), Vol 2, IAEA, Vienna (1981) 717;
BONNEVIER, B., DALHED, H.E., DRAKE, J.R., et al., in Plasma Physics and Controlled Nuclear Fusion Research 1982 (Proc. 9th Int. Conf. Baltimore, 1982), Vol. 2, IAEA, Vienna (1983) 135.
[169] LEHNERT, B., in Unconventional Approaches to Fusion (BRUNELLI, B., LEOTTA, G.G., Eds), Vol. 13, Plenum Press, New York and London (1982) 135.
[170] LEHNERT, B., Nucl. Instrum. Methods **207** (1983) 223.
[171] HUGRASS, W.N., McKENNA, K.F., SIEMON, R.E., Application for Support for the RMF EXTRAP, Rep. LA-UR-85-3038, Los Alamos National Laboratory (1985).
[172] STARK, R.A., MILEY, G.H., in Physics and Technology of Compact Toroids (Proc. 8th Symp. Univ. Maryland, 1987), University of Maryland (1987) 179.
[173] OHKAWA, T., Nucl. Fusion **10** (1970) 185;
BALDWIN, D.E., RENSINK, M.E., Comments Plasma Phys. Controll. Fusion **4** (1978) 55.
[174] HAMMER, J.H., BERK, H.L., Nucl. Fusion **22** (1982) 89.
[175] HIRANO, K., Nucl. Fusion **28** (1988) 207.
[176] TUSZEWSKI, M., MOMOTA, H., in Plasma Science (Proc. IEEE Int. Conf. Seattle, WA, 1988), IEEE, New York (1988) 89.
[177] BARR, W.L., J. Appl. Phys. **42** (1971) 5411.
[178] IRBY, J.H., DRAKE, J.F., GRIEM, H.R., Phys. Rev. Lett. **42** (1979) 228.
[179] COCHRANE, J.C., ARMSTRONG, W.T., LIPSON, J., TUSZEWSKI, M., Observations of Separatrix Motion during the Formation of an FRC, Rep. LA-8716-MS, Los Alamos Scientific Laboratory (1981).
[180] ARMSTRONG, W.T., COCHRANE, J.C., LIPSON, J., et al., in Physics and Technology of Compact Toroids (Proc. 3rd Symp. Los Alamos, NM, 1980), Rep. LA-8700-C, Los Alamos Scientific Laboratory (1981) 180.
[181] ARMSTRONG, W.T., COCHRANE, J.C., LIPSON, J., TUSZEWSKI, M., Observations of Plasma Tearing Instabilities and Associated Axial Translation in Field-Reversed Experiments, Rep. LA-8729-MS, Los Alamos Scientific Laboratory (1981).

[182] GREVE, P., HAUMANN, J., KUNZE, H.J., ULLRICH, L.K., Phys. Fluids **25** (1982) 452;
KÖNIG, R., KOLK, K.H., KUNZE, H.J., Phys. Fluids **30** (1987) 3579.
[183] SATO, T., HAYASHI, T., Phys. Fluids **22** (1979) 1189.
[184] PIETRZYK, Z.A., J. Appl. Phys. **52** (1981) 183.
[185] PIETRZYK, Z.A., in Physics and Technology of Compact Toroids (Proc. 3rd Symp. Los Alamos, NM, 1980), Rep. LA-8700-C, Los Alamos Scientific Laboratory (1981) 165.
[186] BRUNEL, F., TAJIMA, T., DAWSON, J.M., Phys. Rev. Lett. **49** (1982) 323.
[187] HEWETT, D.W., SEYLER, C.E., Phys. Rev. Lett. **46** (1981) 1519.
[188] FURTH, H.P., KILLEEN, J., ROSENBLUTH, M.N., Phys. Fluids **6** (1963) 459.
[189] LEBOEUF, J.N., TAJIMA, T., DAWSON, J.M., Phys. Fluids **25** (1982) 784.
[190] FINN, J.M., KAW, P.K., Phys. Fluids **20** (1977) 72;
PRITCHETT, P.L., WU, C.C., Phys. Fluids **22** (1979) 2140;
BISKAMP, D., WELTER, H., Phys. Rev. Lett. **44** (1980) 1069.
[191] ARMSTRONG, W.T., CHRIEN, R.E., McKENNA, K.F., et al., in Physics and Technology of Compact Toroids (Proc. 6th Symp. Princeton, NJ, 1984), Princeton Plasma Physics Laboratory, Princeton University (1985) 218.
[192] SIEMON, R.E., ARMSTRONG, W.T., CHRIEN, R.E., et al., in Plasma Physics and Controlled Nuclear Fusion Research 1984 (Proc. 10th Int. Conf. London, 1984), Vol. 2, IAEA, Vienna (1985) 511.
[193] HEWETT, D.W., Nucl. Fusion **24** (1984) 349.
[194] MILROY, R.D., BRACKBILL, J.U., Phys. Fluids **29** (1986) 1184.
[195] ES'KOV, A.G., KITAEV, M.I., KURTMULLAEV, R.Kh., NOVIKOV, V.M., SEMENOV, V.N., STRIZHOV, V.F., in Controlled Fusion and Plasma Physics (Proc. 10th Eur. Conf. Moscow, 1981), European Physical Society (1981) paper L-5.
[196] SIEMON, R.E., BARTSCH, R.R., in Physics and Technology of Compact Toroids (Proc. 3rd Symp. Los Alamos, NM, 1980), Rep. LA-8700-C, Los Alamos Scientific Laboratory (1981) 172.
[197] STEINHAUER, L.C., Phys. Fluids **26** (1983) 254.
[198] FREIDBERG, J.P., MORSE, R.L., RIBE, F.L., in Technology of Controlled Thermonuclear Fusion Experiments and the Engineering Aspects of Fusion Reactors, Rep. CONF-721111, United States Atomic Energy Commission (1972) 812.
[199] KOLB, A.C., Rev. Mod. Phys. **32** (1960) 748.
[200] SGRO, A.G., ARMSTRONG, W.T., LIPSON, J., TUSZEWSKI, M., COCHRANE, J.C., Phys. Rev., A **26** (1982) 3564.
[201] ES'KOV, A.G., KURTMULLAEV, R.Kh., LAUKHIN, Ya.N., et al., in Controlled Fusion and Plasma Physics (Proc. 10th Eur. Conf. Moscow, 1981), European Physical Society (1981) paper L-1.
[202] TUSZEWSKI, M., A semi-empirical formation model for field-reversed configurations, to be published in Phys. Fluids (1988).
[203] ARMSTRONG, W.T., COCHRANE, J.C., COMMISSO, R.J., LIPSON, J., TUSZEWSKI, M., Appl. Phys. Lett. **38** (1981) 680.
[204] XU, Q., ZHAO, H., Nucl. Fusion Plasma Phys. (China) **7** (1987) 37.
[205] KNOX, S.O., MEUTH, H., RIBE, F.L., SEVILLANO, E., Phys. Fluids **25** (1982) 262.
[206] REJ, D.J., HUGRASS, W.N., BARNES, G.A., SIEMON, R.E., FRC Formation Experiments with Tearing Reconnection on the FRX-C/LSM Device, Rep. LA-10818-MS, Los Alamos National Laboratory (1986).
[207] MILROY, R.D., SLOUGH, J.T., Phys. Fluids **30** (1987) 3566.
[208] ES'KOV, A.G., ZOLOTOVSKY, O.A., KALYGIN, A.G., et al., in Controlled Fusion and Plasma Physics (Proc. 7th Eur. Conf. Lausanne, 1975), European Physical Society (1975) 55.
[209] ES'KOV, A.G., KALYGIN, A.G., KURTMULLAEV, R.Kh., MALYUTIN, A.I., PROSHLETSOV, A.P., SEMENOV, V.N., in Controlled Fusion and Plasma Physics (Proc. 9th Eur. Conf. Oxford, 1979), European Physical Society (1979) 128.
[210] KUTUZOV, M.I., SEMENOV, V.N., STRIZHOV, V.F., Sov. J. Plasma Phys. **7** (1981) 520.
[211] MILROY, R.D., SLOUGH, J.T., HOFFMAN, A.L., Phys. Fluids **27** (1984) 1545.
[212] VEKSTEIN, G.E., Sov. Phys. Dokl. **271** (1983) 98.
[213] STEINHAUER, L.C., Phys. Fluids **28** (1985) 3333.
[214] SEMENOV, V.N., STRIZHOV, V.F., Sov. J. Plasma Phys. **9** (1983) 235.
[215] VEKSTEIN, G.E., Sov. Phys. — JETP Lett. **37** (1983) 84.
[216] WU, Ch., ASO, Y., HIMENO, S., YAMAGUCHI, S., OKAMOTO, M., HIRANO, K., J. Phys. Soc. Jpn. **52** (1983) 1215.
[217] DRAKE, J.F., LEE, T.T., Phys. Fluids **24** (1981) 1115.
[218] DAVIDSON, R.C., GLADD, N.T., WU, C.S., HUBA, J.D., Phys. Fluids **20** (1977) 301.
[219] SGRO, A.G., NIELSON, C.W., Phys. Fluids **19** (1976) 126.
[220] CHODURA, R., Nucl. Fusion **15** (1975) 55.
[221] HAMEIRI, E., HAMMER, J.H., Phys. Fluids **25** (1982) 1855.
[222] KALYGIN, A.G., KRESHCHUK, A.P., KURTMULLAEV, R.Kh., MALYUTIN, A.I., PROSHLETSOV, A.P., in Controlled Fusion and Plasma Physics (Proc. 10th Eur. Conf. Moscow, 1981), European Physical Society (1981) paper L-6.
[223] SLOUGH, J.T., HARDING, D.G., HOFFMAN, A.L., in Physics and Technology of Compact Toroids (Proc. 5th Symp. Bellevue, WA, 1982), Mathematical Sciences Northwest, Inc., Bellevue (1983) 16.
[224] ALIDIERES, M., AYMAR, R., ETIEVANT, C., JOURDAN, P., SAMAIN, A., in Ionization Phenomena in Gases (Proc. 4th Int. Conf. Uppsala, 1959), Vol. 2, North-Holland, Amsterdam (1959) 1042.
[225] JOSEPHSON, V., Phys. Rev. Lett. **5** (1960) 416.
[226] ARMSTRONG, W.T., CHRIEN, R.E., HUGRASS, W.N., et al., Bull. Am. Phys. Soc. **30** (1985) 1457.
[227] CLARK, G.L., WUERKER, R.F., Phys. Fluids **5** (1962) 1503.

[228] BARTOLI, C., GREEN, T.S., Nucl. Fusion **3** (1963) 84.
[229] TUSZEWSKI, M., SIEMON, R.E., in Physics and Technology of Compact Toroids (Proc. 6th Symp. Princeton, NJ, 1984), Princeton Plasma Physics Laboratory, Princeton University (1985) 210;
The Los Alamos FRC Group, Proposal for the FRX-D Large s Adiabatic-Compression Experiment, Rep. LA-UR-84-3371, Los Alamos National Laboratory (1985).
[230] ARMSTRONG, W.T., CHRIEN, R.E., HUGRASS, W., et al., in Physics and Technology of Compact Toroids (Proc. 7th Symp. Santa Fe, NM, 1985), Rep. LA-10830-C, Los Alamos Scientific Laboratory (1986) 137.
[231] ES'KOV, A.G., ZOLOTOVSKIJ, O.A., KALYGIN, A.G., KURTMULLAEV, R.Kh., LAUKHIN, Ya.N., in Plasma Physics and Controlled Nuclear Fusion Research 1974 (Proc. 5th Int. Conf. Tokyo, 1974), IAEA, Vienna (1975) 155.
[232] KALYGIN, A.G., KOCHAN, W.J., KRESHCHUK, A.P., KURTMULLAEV, R.Kh., PROSHLETSOV, A.P., in Controlled Fusion and Plasma Physics (Proc. 11th Eur. Conf. Aachen, 1983), European Physical Society (1983) 167.
[233] OKADA, S., ITO, Y., KAKO, M., et al., in Plasma Physics and Controlled Nuclear Fusion Research 1986 (Proc. 11th Int. Conf. Kyoto, 1986), Vol. 2, IAEA, Vienna (1987) 551.
[234] KADISH, A., STEVENS, D.C., Nucl. Fusion **14** (1974) 821;
BECKER, G., Nucl. Fusion **14** (1974) 319;
LI, G., Nucl. Fusion Plasma Phys. (China) **4** (1984) 53.
[235] WRIGHT, J.K., MEDFORD, R.D., CHAMBERS, B., J. Nucl. Energy C **3** (1961) 242.
[236] KADISH, A., Phys. Fluids **22** (1979) 2248.
[237] BARNES, D.C., SEYLER, C.E., ANDERSON, D.V., in Compact Toruses and Energetic Particle Injection (Proc. US-Japan Joint Symp. Princeton, NJ, 1979), Princeton Plasma Physics Laboratory, Princeton University (1979) 110.
[238] ARMSTRONG, W.T., BARNES, D.C., BARTSCH, R.R., et al., in Plasma Physics and Controlled Nuclear Fusion Research 1980 (Proc. 8th Int. Conf. Brussels, 1980), Vol. 1, IAEA, Vienna (1981) 481.
[239] TUSZEWSKI, M., ARMSTRONG, W.T., BARTSCH, R.R., et al., Phys. Fluids **25** (1982) 1696.
[240] SOKOLOV, E.P., Sov.J. Plasma Phys. **12** (1986) 832.
[241] SPENCER, R.L., TUSZEWSKI, M., LINFORD, R.K., Phys. Fluids **26** (1983) 1564.
[242] SHUMAKER, D.E., Bull. Am. Phys. Soc. **31** (1986) 1607.
[243] WEBSTER, R.B., SCHWARTZMEIER, J.L., LEWIS, H.R., CHOI, C.K., Bull. Am. Phys. Soc. **32** (1987) 1728.
[244] GROSSMAN, W., SALTZMAN, J., in Megagauss Physics and Technology (TURCHI, P.J., Ed.), Plenum Press, New York (1980) 403.
[245] HAMEIRI, E., GROSSMAN, W., in Compact Toruses and Energetic Particle Injection (Proc. US-Japan Joint Symp. Princeton, NJ, 1979), Princeton Plasma Physics Laboratory, Princeton University (1979) 118.
[246] BYRNE, R.N., GROSSMANN, W., in Physics and Technology of Compact Toroids (Proc. 3rd Symp. Los Alamos, NM, 1980), Rep. LA-8700-C, Los Alamos Scientific Laboratory (1981) 138.
[247] SPENCER, R.L., HEWETT, D.W., Phys. Fluids **25** (1982) 1365.
[248] SPENCER, R.L., TUSZEWSKI, M., Phys. Fluids **28** (1985) 1810.
[249] TUSZEWSKI, M., SPENCER, R.L., Phys. Fluids **29** (1986) 3711.
[250] CLEMENTE, R.A., Phys. Fluids **26** (1983) 1877.
[251] SUZUKI, K., J. Phys. Soc. Jpn. **54** (1985) 2155, and **55** (1986) 158.
[252] WEBSTER, R.B., SPENCER, R.L., CHOI, C.K., et al., High flux field-reversed configurations, to be submitted to Phys. Fluids (1988).
[253] CHRIEN, R.E., OKADA, S., Phys. Fluids **30** (1987) 3574.
[254] HILL, M.J., Philos. Trans. R. Soc. Lond., Ser. A., Pt 1, C/XXXV 213 (1894); SHAFRANOV, V.D., Sov. Phys. — JETP **6** (1958) 545.
[255] BERK, H.L., HAMMER, J.H., WEITZNER, H., Phys. Fluids **24** (1981) 1758.
[256] WANG, M.Y., MILEY, G.H., Nucl. Fusion **19** (1979) 39.
[257] KANEKO, S., CHIYODA, K., HIROTA, I., J. Phys. Soc. Jpn. **50** (1981) 359.
[258] BYERS, J.A., Phys. Rev. Lett. **39** (1977) 1476.
[259] ANDERSON, D.V., HAMMER, J.H., BARNES, D.C., in Physics and Technology of Compact Toroids (Proc. 4th Symp. Livermore, CA, 1981), CONF-811087, Lawrence Livermore National Laboratory (1981) 15.
[260] VABISHCHEVICH, D.N., DEGTYAREV, L.M., DROZDOV, V.V., PROSHEKHONOV, Yu.Yu., SHAFRANOV, V.D., Sov. J. Plasma Phys. **7** (1981) 536.
[261] MASCHKE, E.K., PERRIN, H., Plasma Phys. **22** (1980) 579.
[262] CLEMENTE, R.A., FARENGO, R., Phys. Fluids **27** (1984) 776.
[263] MEUTH, H., RIBE, F.L., in Compact Toruses and Energetic Particle Injection (Proc. US-Japan Joint Symp. Princeton, NJ, 1979), Princeton Plasma Physics Laboratory, Princeton University (1979) 130.
[264] ISHIMURA, T., Phys. Fluids **27** (1984) 2139.
[265] HARNED, D.S., Phys. Fluids **27** (1984) 554.
[266] SPENCER, R.L., TUSZEWSKI, M., Phys. Fluids **28** (1985) 2510.
[267] TUSZEWSKI, M., ARMSTRONG, W.T., Rev. Sci. Instrum. **54** (1983) 1611.
[268] TUSZEWSKI, M., Phys. Fluids **24** (1981) 2126.
[269] HOFFMAN, A.L., MILROY, R.D., STEINHAUER, L.C., Appl. Phys. Lett. **41** (1982) 31.
[270] REJ, D.J., TUSZEWSKI, M., Phys. Fluids **27** (1984) 1514.
[271] TUSZEWSKI, M., Plasma Phys. Controll. Fusion **26** (1984) 991.
[272] OKADA, S., KISO, Y., GOTO, S., ISHIMURA, T., Density profile measurements for evaluation of FRC plasma transport, submitted to J. Appl. Phys. (1988).
[273] McKENNA, K.F., ARMSTRONG, W.T., BARTSCH, R.R., et al., Phys. Rev. Lett. **50** (1983) 1787.
[274] TUSZEWSKI, M., McKENNA, K.F., Phys. Fluids **27** (1984) 1058.
[275] STEINHAUER, L.C., Phys. Fluids **29** (1986) 3379.
[276] REJ, D.J., ARMSTRONG, W.T., Nucl. Fusion **24** (1984) 177.
[277] ES'KOV, A.G., KOZLOV, N.P., KURTMULLAEV, R.Kh., SEMENOV, V.N., KHVESYUK, V.I, YAMINSKII, A.V, Sov. Tech. Phys. Lett. **9** (1983) 16.

[278] GOLOVIZNIN, V.M., KURTMULLAEV, R.Kh., SEMENOV, V.N., GASILOV, V.A., FAVORSKY, A.P., SHASHKOV, M.Yu., in Megagauss Physics and Technology (TURCHI, P.J., Ed.), Plenum Press, New York (1980) 415.
[279] BELLAN, P.M., Phys. Rev. Lett. **43** (1979) 858.
[280] CAYTON, T.E., LEWIS, H.R., Phys. Fluids **23** (1980) 109;
SANCHEZ, R., Phys. Fluids **24** (1981) 40.
[281] SANCHEZ, R., MEUTH, H., in RF Heating in Plasmas (4th Top. Conf. Austin, TX, 1981), University of Texas, Austin (1981) paper A22/1-5.
[282] CARSON, R.S., VLASES, G.C., in Physics and Technology of Compact Toroids (Proc. 5th Symp. Bellevue, WA, 1982), Mathematical Sciences Northwest, Inc., Bellevue (1983) 4.
[283] HUGRASS, W.N., CHRIEN, R.E., REJ, D.J., SIEMON, R.E., TUSZEWSKI, M., WRIGHT, B.L., in Physics and Technology of Compact Toroids (Proc. 8th Symp. Univ. Maryland, 1987), University of Maryland (1987) 143.
[284] MINATO, T., TANJYO, M., OKADA, S., et al., in US-Japan Joint Workshop on Compact Toroids (Proc. 4th Workshop Osaka, 1982), Osaka University (1982) 191.
[285] WANG, G., WANG, S., CHANG, Q., Nucl. Fusion Plasma Phys. (China) **7** (1987) 202.
[286] SPENCER, R.L., in Sherwood Theory Meeting (Proc. Mtg. Madison, WI, 1985), University of Wisconsin, Madison (1985) paper 1Q-8.
[287] ES'KOV, A.G., KORSHUNOV, V.K., KRYLOV, S.F., et al., in Controlled Fusion and Plasma Physics (Proc. 11th Eur. Conf. Aachen, 1983), Vol. 1, European Physical Society (1983) 171.
[288] ITO, Y., TANJYO, M., OHI, S., GOTO, S., ISHIMURA, T., Phys. Fluids **30** (1987) 168.
[289] CHRIEN, R.E., Phys. Fluids **28** (1985) 3426.
[290] GRAD, H., Proc. Natl. Acad. Sci. USA **70** (1973) 3277.
[291] BARNES, D.C., SEYLER, C.E., Ideal MHD Stability of a Field Reversed Theta Pinch, Rep. LA-UR-79-13, Los Alamos Scientific Laboratory (1979).
[292] BERK, H.L., ROSLYAKOV, G.V., Phys. Fluids **30** (1987) 478.
[293] BERNSTEIN, I.B., FRIEMAN, E.A., KRUSKAL, M.D., KULSRUD, R.M., Proc. R. Soc. London, Ser. A **244** (1958) 17.
[294] SPARKS, L., FINN, J.M., SUDAN, R.N., Phys. Fluids **23** (1980) 611.
[295] CHIYODA, K., J. Phys. Soc. Jpn. **54** (1985) 2160.
[296] NEWCOMB, W.A., Phys. Fluids **23** (1980) 2296.
[297] ANDERSON, D.V., BERK, H.L., HAMMER, J.H., in Physics and Technology of Compact Toroids (Proc. 3rd Symp. Los Alamos, NM, 1980), Rep. LA-8700-C, Los Alamos Scientific Laboratory (1981) 130.
[298] FINN, J.M., Phys. Fluids **24** (1981) 274;
PRITCHETT, P.L., Phys. Fluids **24** (1981) 864;
CARY, J.R., Phys. Fluids **24** (1981) 2239.
[299] ANDERSON, D.V., AUERBACH, S.P., BERK, H.L., et al., in Plasma Physics and Controlled Nuclear Fusion Research 1980 (Proc. 8th Int. Conf. Brussels, 1980), Vol. 1, IAEA, Vienna (1981) 469.
[300] ANDERSON, D.V., BARNES, D.C., J. Comput. Phys. **42** (1981) 288.
[301] NELSON, D.B., SPIES, G.O., Phys. Fluids **17** (1974) 2133;
HAMEIRI, E., Phys. Fluids **23** (1980) 889;
GROSSMANN, W., HAMEIRI, E., WEITZNER, H., Phys. Fluids **26** (1983) 508;
CHIYODA, K., J. Phys. Soc. Jpn. **53** (1984) 2536.
[302] DIXON, R.H., DÜCHS, D.F., ELTON, R.C., Phys. Fluids **16** (1973) 1762.
[303] WESSON, J.A., Nucl. Fusion **6** (1966) 130.
[304] KAPPRAFF, J., GROSSMANN, W., KRESS, M., J. Plasma Phys. **25** (1981) 111.
[305] BERK, H.L., SCHNACK, D.D., SAYER, J.M., Phys. Fluids **25** (1982) 473.
[306] BISKAMP, D., SAGDEEV, R.Z., SCHINDLER, K., Cosmic Electrodynamics **1** (1970) 297.
[307] KALECK, A., in Controlled Fusion and Plasma Physics (Proc. 5th Eur. Conf. Grenoble, 1972), European Physical Society (1972) 30.
[308] FREIDBERG, J.P., PEARLSTEIN, L.D., Phys. Fluids **21** (1978) 1207.
[309] EKDAHL, C., BARTSCH, R.R., COMMISSO, R.J., et al., Phys. Fluids **23** (1980) 1832.
[310] SEYLER, C.E., Phys. Fluids **22** (1979) 2324.
[311] BARNES, D.C., ANDERSON, D.V., Phys. Rev. Lett. **46** (1981) 1337.
[312] HARNED, D.S., Phys. Fluids **26** (1983) 1320.
[313] REJ, D.J., ARMSTRONG, W.T., BARNES, G.A., et al., Phys. Fluids **29** (1986) 2648.
[314] NAKATA, S., SEKIGUCHI, T., SEKI, H., YAMAMOTO, K., Phys. Fluids **29** (1986) 871.
[315] BECKNER, E.H., BANISTER, J.R., Phys. Lett. **10** (1964) 56.
[316] THOMAS, K.S., Phys. Rev. Lett. **23** (1969) 746.
[317] KADISH, A., Phys. Fluids **19** (1976) 141.
[318] STEINHAUER, L.C., Phys. Fluids **24** (1981) 328.
[319] KAYE, A.S., J. Plasma Phys. **11** (1974) 77.
[320] MANHEIMER, W.M., FINN, J.M., Phys. Fluids **24** (1981) 1865.
[321] HARNED, D.S., HEWETT, D.W., Nucl. Fusion **24** (1984) 201.
[322] HSIAO, M.-Y., MILEY, G.H., Phys. Fluids **28** (1985) 1440.
[323] HSIAO, M.-Y., MILEY, G.H., Nucl. Fusion **24** (1984) 1029.
[324] HORTON, W., TAJIMA, T., KAMIMURA, T., Phys. Fluids **30** (1987) 3485.
[325] MINATO, T., TANJYO, M., OKADA, S., et al., in Plasma Physics and Controlled Nuclear Fusion Research 1982 (Proc. 9th Int. Conf. Baltimore, 1982), Vol. 2, IAEA, Vienna (1983) 303.
[326] LIPSON, J., ARMSTRONG, W.T., COCHRANE, J.C., et al., Appl. Phys. Lett. **39** (1981) 43.
[327] HAMASAKI, S., KRALL, N.A., in Plasma Science (Proc. IEEE Int. Conf. Montreal, 1979), IEEE, New York (1979) 143.
[328] CLEMENTE, R.A., Can plasma spin-up in FRCs be reduced, to be published in Comments Plasma Phys. Controll. Fusion (1988).
[329] ASO, Y., WU, Ch., HIMENO, S., HIRANO, K., Nucl. Fusion **22** (1982) 843;
ASO, Y., HIRANO, K., J. Phys. Soc. Jpn. **52** (1983) 1095.

[330] ASO, Y., Nucl. Fusion **28** (1988) 809.
[331] TUSZEWSKI, M., BARNES, G.A., CHRIEN, R.E., et al., Phys. Fluids **31** (1988) 946.
[332] HAMEIRI, E., Phys. Fluids **22** (1979) 89.
[333] ISHIMURA, T., in US-Japan Workshop on Compact Toroids (Proc. 8th Workshop Osaka, 1986), Osaka University (1986) 69.
[334] ITO, Y., CHRIEN, R.E., SUGIMOTO, S., et al., ibid., 47; CHRIEN, R.E., ITO, Y., Bull. Am. Phys. Soc. **32** (1987) 1726.
[335] McCOLL, D.B., MORSE, E.C., HAMMER, J., BERK, H.L., Nuclear Technol./Fusion **2** (1982) 80.
[336] FURTH, H.P., LUDESCHER, C., Sov. J. Plasma Phys. **11** (1985) 2.
[337] HOROWITZ, E.J., A 3-D Quasi-Neutral Hybrid Particle-In-Cell Code with Applications to the Tilt Mode Instability in FRCs: QN3D, PhD Thesis, Rep. UCRL-53808, Lawrence Livermore National Laboratory (1987).
[338] ROSENBLUTH, M.N., BUSSAC, M.N., Nucl. Fusion **19** (1979) 489.
[339] HAMMER, J.H., Nucl. Fusion **21** (1981) 488.
[340] JARBOE, T.R., HENINS, I., HOIDA, H.W., et al., Phys. Rev. Lett. **45** (1980) 1264.
[341] SHESTAKOV, A.I., SCHNACK, D.D., KILLEEN, J., in Compact Toruses and Energetic Particle Injection (Proc. US-Japan Joint Symp. Princeton, NJ, 1979), Princeton Plasma Physics Laboratory, Princeton University (1979) 126.
[342] CLEMENTE, R.A., MILOVICH, J.L., Phys. Lett., A **85** (1981) 148.
[343] CLEMENTE, R.A., GRILLO, C.E., Phys. Fluids **27** (1984) 658.
[344] SCHWARZMEIER, J.L., BARNES, D.C., HEWETT, D.W., SEYLER, C.E., SHESTAKOV, A.I., SPENCER, R.L., Phys. Fluids **26** (1983) 1295.
[345] BARNES, D.C., AYDEMIR, A.Y., ANDERSON, D.V., SHESTAKOV, A.I., SCHNACK, D.D., in Physics and Technology of Compact Toroids (Proc. 3rd Symp. Los Alamos, NM, 1980), Rep. LA-8700-C, Los Alamos Scientific Laboratory (1981) 134.
[346] MILROY, R.D., BARNES, D.C., SCHNACK, D.D., BISHOP, R., in Physics and Technology of Compact Toroids (Proc. 8th Symp. Univ. Maryland, 1987), University of Maryland (1987) 155.
[347] BRUNEL, F., TAJIMA, T., Phys. Fluids **26** (1983) 535.
[348] DREIZIN, Yu.A., SOKOLOV, E.P., Sov. J. Plasma Phys. **7** (1981) 516.
[349] CLEMENTE, R.A., MILOVICH, J.L., Phys. Fluids **26** (1983) 1874.
[350] FRIEMAN, E., ROTENBERG, M., Rev. Mod. Phys. **32** (1960) 898.
[351] ISHIDA, A., MOMOTA, H., STEINHAUER, L.C., Variational formulation for a multi-fluid flowing plasma with application to the internal tilt mode of a field-reversed configuration, to be published in Phys. Fluids (1988).
[352] IKUTA, K., Jpn. J. Appl. Phys. **22** (1983) 706.
[353] SEYLER, C.E., Jr., BARNES, D.C., Phys. Fluids **24** (1981) 1989.
[354] FREIDBERG, J.P., Phys. Fluids **15** (1972) 1102.
[355] SCHWARZMEIER, J.L., SEYLER, C.E., Phys. Fluids **27** (1984) 2151.
[356] KIM, J.-S., CARY, J.R., Phys. Fluids **26** (1983) 2167.
[357] BERK, H.L., WONG, H.V., TSANG, K.T., Phys. Fluids **30** (1987) 2681.
[358] MORSE, E.C., MILEY, G.H., Nucl. Fusion **21** (1981) 473.
[359] FINN, J.M., Phys. Fluids **24** (1981) 274.
[360] FINN, J.M., SUDAN, R.N., Phys. Rev. Lett. **41** (1978) 695.
[361] KIM, J.-S., Vlasov-Fluid Stability of a 2-D Plasma with a Linear Magnetic Field Null, PhD Thesis, University of California, Berkeley (1984).
[362] LEWIS, H.R., BARNES, D.C., SCHWARZMEIER, J.L., SEYLER, C.E., Phys. Fluids **28** (1985) 3546.
[363] SCHWARZMEIER, J.L., LEWIS, H.R., STAUDENMEIER, J.L., WEBSTER, R., BARNES, D.C., Bull. Am. Phys. Soc. **32** (1987) 1728.
[364] STAUDENMEIER, J.L., LEWIS, H.R., BARNES, D.C., SCHWARZMEIER, J.L., in Sherwood Theory Meeting (Proc. Gatlinburg, TN, 1988), Oak Ridge National Laboratory (1988) paper 3C33.
[365] MIKIC, Z., MORSE, E.C., Phys. Fluids **30** (1987) 2806.
[366] MIKIC, Z., BARNES, D.C., in Physics and Technology of Compact Toroids (Proc. 8th Symp. Univ. Maryland, 1987), University of Maryland (1987) 151.
[367] ISHIDA, A., KOBAYASHI, S., KITAO, K., J. Phys. Soc. Jpn. **52** (1983) 885;
ISHIDA, A., KITAO, K., J. Phys. Soc. Jpn. **52** (1983) 1251;
RUCHTI, C.B., LOVELACE, R.V., Phys. Fluids **27** (1984) 1789.
[368] FLEISCHMANN, H.H., in Physics and Technology of Compact Toroids (Proc. 3rd Symp. Los Alamos, NM, 1980), Rep. LA-8700-C, Los Alamos Scientific Laboratory (1981) 31.
[369] SUDAN, R.N., in Unconventional Approaches to Fusion (BRUNELLI, B., LEOTTA, G.G., Eds), Vol. 13, Plenum Press, New York and London (1982) 311.
[370] SCHAMILOGLU, E., GREENLY, J.B., HAMMER, D.A., in Physics and Technology of Compact Toroids (Proc. 8th Symp. Univ. Maryland, 1987), University of Maryland (1987) 171;
PODULKA, W., et al., ibid., paper P3-18.
[371] SPARKS, L., SUDAN, R.N., Phys. Fluids **27** (1984) 626; TURNBULL, A.D., SUDAN, R.N., Phys. Fluids **29** (1986) 1923;
MEHANIAN, C., LOVELACE, R.V.E., Phys. Fluids **31** (1988) 1681.
[372] SUDAN, R.N., LYSTER, P.M., Comments Plasma Phys. Controll. Fusion **9** (1984) 23 and 35.
[373] AUERBACH, S.P., CONDIT, W.C., Nucl. Fusion **21** (1981) 927.
[374] HAMASAKI, S., BOOK, D.L., Nucl. Fusion **20** (1980) 289.
[375] KLEVANS, E.H., in Compact Toruses and Energetic Particle Injection (Proc. US-Japan Joint Symp. Princeton, NJ, 1979), Princeton Plasma Physics Laboratory, Princeton University (1979) 135.
[376] DAVIDSON, R.C., KRALL, N.A., Nucl. Fusion **17** (1977) 1313.
[377] CARLSON, A.W., Phys. Fluids **30** (1987) 1497.
[378] WINSKE, D., LIEWER, P.C., Phys. Fluids **21** (1978) 1017.

[379] BRACKBILL, J.U., FORSLUND, D.W., QUEST, K.B., WINSKE, D., Phys. Fluids **27** (1984) 2682.
[380] GLADD, N.T., SGRO, A.G., HEWETT, D.W., Phys. Fluids **28** (1985) 2222.
[381] FAHRBACH, H.U., KÖPPENDÖRFER, W., MÜNICH, M., et al., Nucl. Fusion **21** (1981) 257.
[382] HAMASAKI, S., GLADD, N.T., KRALL, N.A., Phys. Fluids **29** (1986) 4131.
[383] SGRO, A.G., Magnetic flux loss in an FRC, to be submitted to Phys. Fluids (1988).
[384] GERWIN, R., Anomalous Resistivity at the Field Null of the FRC: A Quasi-Linear Expression Based Upon Flute-Type Modes, Rep. LA-9892-MS, Los Alamos National Laboratory (1983).
[385] KRALL, N.A., Phys. Fluids **30** (1987) 878.
[386] KRALL, N.A., HAMASAKI, S., Bull. Am. Phys. Soc. **32** (1987) 1728.
[387] GLADD, N.T., DRAKE, J.F., CHANG, C.L., LIU, S.C., Phys. Fluids **23** (1980) 1182.
[388] TUSZEWSKI, M., in Sherwood Theory Meeting (Proc. Mtg. Arlington, VA, 1983), University of Maryland (1983) paper 1Q4.
[389] MJOLSNESS, R.C., RIBE, F.L., RIESENFELD, W.B., Phys. Fluids **4** (1961) 730.
[390] FANG, Q.T., MILEY, G.H., in Physics and Technology of Compact Toroids (Proc. 3rd Symp. Los Alamos, NM, 1980), Los Alamos Scientific Laboratory (1981) 144.
[391] HSIAO, M.-Y., STAUDENMEIER, J.L., CHIANG, P.R., Electric fields due to velocity space particle loss in field-reversed configurations, submitted to Phys. Fluids (1988).
[392] LINFORD, R.K., in Unconventional Approaches to Fusion (BRUNELLI, B., LEOTTA, G.G., Eds), Vol. 13, Plenum Press, New York and London (1982) 463.
[393] HOFFMAN, A.L., MILROY, R.D., Phys. Fluids **26** (1983) 3170.
[394] STEINHAUER, L.C., in Sherwood Theory Meeting (Proc. Mount Pocono, PA, 1979), Princeton Plasma Physics Laboratory, Princeton University (1979) paper 1B28.
[395] PARKER, S.E., TEILHABER, K., BIRDSALL, C.K., Bull. Am. Phys. Soc. **31** (1986) 1488.
[396] REJ, D.J., in Physics and Technology of Compact Toroids (Proc. 6th Symp. Princeton, NJ, 1984), Princeton Plasma Physics Laboratory, Princeton University (1985) 214.
[397] NGUYEN, K., KAMMASH, T., Plasma Phys. **24** (1982) 177.
[398] CLEMENTE, R.A., FREIRE, E.M., Plasma Phys. Controll. Fusion **28** (1986) 951.
[399] DRAKE, J.F., GLADD, N.T., HUBA, J.D., Phys. Fluids **24** (1981) 78.
[400] ASO, Y., HIMENO, S., HIRANO, K., Nucl. Fusion **23** (1983) 751.
[401] STEINHAUER, L.C., in Plasma Science (Proc. IEEE Int. Conf. Santa Fe, NM, 1981) IEEE, New York (1981) 137.
[402] HAMADA, S., Nucl. Fusion **26** (1986) 729.
[403] SHIEH, D.R., YORK, T.M., in Physics and Technology of Compact Toroids (Proc. 6th Symp. Princeton, NJ, 1984), Princeton Plasma Physics Laboratory, Princeton University (1985) 182.
[404] TUSZEWSKI, M., Comments Plasma Phys. Controll. Fusion **8** (1984) 237.
[405] CARAMANA, E.J., Phys. Fluids **28** (1985) 3557.
[406] WERLEY, K.A., Phys. Fluids **30** (1987) 2129; HSIAO, M.-Y., WERLEY, K.A., LING, K.-M., A One-and-a-Quarter-Dimensional Transport Code for Field-Reversed-Configuration Studies, Rep. LA-11212-MS, Los Alamos National Laboratory (1988).
[407] SHUMAKER, D.E., Fusion Technol. **13** (1988) 555.
[408] TUSZEWSKI, M., in Physics and Technology of Compact Toroids (Proc. 6th Symp. Princeton, NJ, 1984), Princeton Plasma Physics Laboratory, Princeton University (1985) 145.
[409] ISHIMURA, T., in US-Japan Workshop on Compact Toroids (Proc. 6th Symp. Hiroshima, 1984), Hiroshima University (1984) 47.
[410] HOFFMAN, A.L., SLOUGH, J.T., STEINHAUER, L.C., KRALL, N.A., HAMASAKI, S., in Plasma Physics and Controlled Nuclear Fusion Research 1986 (Proc. 11th Int. Conf. Kyoto, 1986), Vol. 2, IAEA, Vienna (1987) 541.
[411] SIEMON, R.E., CHRIEN, R.E., HUGRASS, W.N., et al., "Field-reversed configuration (FRC) experiments", presented at Plasma Physics and Controlled Nuclear Fusion Research, 12th Int. Conf. Nice, 1988, paper CN-50/C-4-1.
[412] YORK, T.M., MEAD, F.B., in Physics and Technology of Compact Toroids (Proc. 6th Symp. Princeton, NJ, 1984), Princeton Plasma Physics Laboratory, Princeton University (1985) 170.
[413] OKAMOTO, M., Nucl. Fusion **27** (1987) 833.
[414] HAMADA, S., AZEVEDO, M.T., J. Phys. Soc. Jpn. **57** (1988) 1255.
[415] NEWTON, A.A., Nucl. Fusion **26** (1986) 779.
[416] HOFFMAN, A.L., HARDING, D.G., MILROY, R.D., SLOUGH, J.T., STEINHAUER, L.C., VLASES, G.C., in Plasma Physics and Controlled Nuclear Fusion Research 1984 (Proc. 10th Int. Conf. London, 1984), Vol. 2, IAEA, Vienna (1985) 601.